

# NUCLEAR MAGNETIC RESONANCE IMAGING STUDIES OF ASPHALTENE PRECIPITATION IN AGED AND UNAGED ASPHALTS

Francis P. Miknis and Adam T. Pauli  
Western Research Institute  
365 N. 9th Street  
Laramie, WY 82070-3380

Keywords: magnetic resonance imaging, asphalt, asphaltenes, aging

## INTRODUCTION

Nuclear magnetic resonance (NMR) imaging is a powerful, relatively new technique that can be used for noninvasive chemical and physical characterization of local regions in the interior of intact samples. One of the more promising aspects of the technique is its ability to characterize chemical and physical processes noninvasively over time. Because of this ability and the optical opacity of asphalt systems, the potential of NMR imaging in the study of asphalts is being investigated [1]. The work reported here is an exploratory application of NMR imaging to study asphaltene precipitation in oxidatively aged asphalts. Although NMR imaging has been used mostly in medical applications, nonmedical applications are increasing and have recently been reviewed [2].

Historically, asphalts have been modeled as dispersions of associated molecules, referred to as asphaltenes, in an oily solvent phase referred to as maltenes. The asphaltenes are more aromatic and contain more heteroatoms than do the maltenes; therefore, their intermolecular interactions are generally more extensive. Consequently, asphaltenes are largely responsible for the internal structure of asphalts and tend to dominate many of the physical properties of asphalts [3]. The effectiveness by which asphaltenes are dispersed by the maltenes determines the compatibility of an asphalt. Compatible asphalts have smaller amounts of asphaltenes than incompatible asphalts. Thus, a measurement of the amount of asphaltenes in an asphalt is a measure of its compatibility.

The standard method to determine asphalt compatibility is the Heithaus test [4]. In this procedure, samples of asphalt are dissolved in an aromatic solvent, such as toluene, and titrated with an aliphatic solvent, such as n-heptane. The compatibility properties of an asphalt are then determined by measuring the onset of flocculation brought about by the addition of the titrating solvent to solutions of the dissolved asphalt at different concentrations. The Heithaus procedure is somewhat operator dependent. Recently, an automated Heithaus method has been developed to test neat asphalts, cross blended materials, and oxidatively aged asphalts that eliminates the operator dependency [5].

The compatibility of an asphalt is important for practical reasons because the degree of asphalt compatibility affects *inter alia* rutting propensities and oxidative age hardening. The effects of asphalt composition on these and other roadway failure mechanisms are currently being investigated at Western Research Institute under contract with the Federal Highway Administration. As part of that study, nuclear magnetic resonance (NMR) imaging methods are being explored to study asphaltene dispersion and aggregate behavior, and compatibility in oxidatively aged asphalts. Some results of this study are the subject of this paper.

## EXPERIMENTAL

The asphalts studied are part of the Strategic Highway Research Program (SHRP) Core asphalts [6]. Their chemical properties have been characterized [7] and some are listed in Table 1. The asphalts were aged using a combination of thin film oven (TFO) and pressure aging vessel (PAV) aging [8]. NMRI measurements were made on asphalts AAB-1, AAD-1, AAK-1, AAM-1, and ABM-1 that were PAV aged for 12 hrs @ 100°C. Additional NMRI measurements were made on asphalts AAE and AAS-1 that were both PAV aged for 144 and 400 hrs at 60°C. In one set of experiments, asphalt

AAD-1 was aged using a combination of TFO aging only, and TFO aging followed by PAV aging. This produced a set of 4 samples consisting of unaged, TFO aged, and TFO followed by PAV aging for 4 and 12 hrs at 100°C.

Samples were prepared for NMRI imaging experiments in the following way: Aged and unaged asphalt samples were dissolved in toluene. To this mixture, isooctane was added to cause flocculation and asphaltene precipitation. The amount of isooctane needed to cause maximum flocculation was calculated from previous work on the development of an automated Heithaus method [5]. Two samples were prepared for each asphalt. In one case, the samples were stirred after the addition of the isooctane, and in the other case, the isooctane was added slowly to the asphalt-toluene solution to minimize mixing at the solvent interface. Images were acquired after the addition of the isooctane and for different times afterwards to observe settling of the asphaltenes.

NMR imaging experiments were carried out at a nominal proton resonance frequency of 200 MHz using a Chemagnetics/Otsuka Electronics microimaging probe. Samples for NMR imaging experiments were placed in 23 mm (OD) glass vials, which were then placed in 25 mm (OD) glass tubes. The tubes were inserted into the MRI probe and were positioned in the probe using O-rings such that the cross sections to be imaged were contained in the experimental field of view (FOV).

NMR images of asphaltene precipitation were made using the spin echo method. Images were acquired using a pulse delay of 1 s, a free induction decay size of 256 data points, 128 phase encodes, and a gradient strength of 34 G/cm. The echo time was varied from 40 to 80 ms. Eight slices, 1 mm thick and separated by 1 mm were obtained. The time required to obtain a set of images was about 35 minutes using these parameters.

## RESULTS AND DISCUSSION

The effects of aging (oxidation) and stirring on asphaltene precipitation, as viewed with NMR imaging, are illustrated in Figure 1. In these images, and in the images in subsequent figures, only the 4th slice of an image set of 8 slices is shown. The 4th slice corresponds closely to the longitudinal cross section across the center of the sample vial. The times listed in Figure 1 are settling times and refer to the time elapsed between addition of isooctane and the time when the image was recorded. Also, in Figure 1 and in all other figures, the different contrasts represent regions of different molecular mobility. Thus, the lightest areas of contrast in Figure 1 are due to the hydrogens in molecules that have a fair degree of molecular mobility such as the dissolved asphalt, toluene and isooctane. The darker regions in the images are due to hydrogens in molecules having a greater degree of molecular association (hence less molecular mobility) such as the asphaltenes.

When isooctane was added to the unaged AAD-1 asphalt and the mixture stirred, the asphaltenes settled to the bottom of the vial in a normal fashion (Figure 1a). When isooctane was added to the sample of AAD-1 asphalt that was aged for 12 hrs at 100°C and the mixture stirred, the asphaltenes settled to the bottom of the vial also in a normal fashion (Figure 1b). However, when isooctane was added to the top of the aged AAD-1 asphalt/toluene solution without stirring, an additional layer of material formed at the isooctane-toluene/asphalt interface that appeared to have experienced different solvent interactions than did the asphaltenes. This is illustrated by the dark band in Figure 1c that formed at about the level of the original isooctane-toluene/asphalt interface and which appeared to be quite stable upon setting for some periods of time. As these are cross sectional images, the dark band is actually a layer at the interface.

The time evolution of the interface layer is shown in Figure 2a-d by the images taken at different settling times after addition of the isooctane. The first image (Figure 2a) shows the asphalt dissolved in toluene before addition of the isooctane. Figure 2b was taken after isooctane was added, unstirred to the sample vial, and before the asphaltenes could settle to the bottom. In this image a thin layer of additional

material, which also contains spherical globules, can already be seen forming at the solvent interface. After one day of undisturbed settling, (Figure 2c) the layer is becoming more prominent and additional globules can be seen forming near the interface layer. The precipitation of asphaltenes is also noted by the darker diffuse band developing below the interface (Figure 2b). After one week (168 hrs) of settling, the interface layer is still apparent and the asphaltenes can be seen settling to the bottom of the vial (Figure 2d). On other samples, the layer has been imaged for settling times of up to 648 hrs. A set of radial images, 1 mm thick and separated by 1mm, through the interface layer of Figure 2d is shown in Figure 3a-d. This set of images shows the inhomogeneity of the asphalt solution. The distribution of spherical globules in and near the interface is shown in Figure 3b and c.

The formation of the dark layer appears to be related to the degree of aging. In Figure 4a-d, the asphaltene layer is seen at the bottom of the vial in all images for a settling time of 1 week and no dark layer is visible in the unaged and mildly (TFO) aged samples (Figure 4a and b). However, the dark layer is present at the interface for the PAV aged samples (Figure 4c and d) and is most pronounced for the asphalt sample that was aged the longest.

The formation of the interface layer appears to depend also on the concentration of asphaltenes in the unaged asphalt. In addition to asphalt AAD-1, the layering was observed in asphalts AAB-1, AAK-1 and AAE. All of these asphalts have asphaltene concentrations of about 20% or greater (Table 1). The layering was not observed in asphalts AAM-1 and ABM-1, which have low asphaltene concentrations, nor was it observed in asphalt AAS-1, which has a high asphaltene concentration. The reasons for the anomalous behavior of asphalt AAS-1 are not known at present. Asphalts AAS-1 and AAE were both PAV aged at a lower temperature (60°C), but for longer periods of time (144 and 400 hrs). Both have high concentrations of asphaltenes, but only AAE demonstrated the effect. The effects of time and temperature on asphaltene precipitation are currently under study.

The chemical nature of the material near the isooctane-toluene/asphalt interface is not known. This layer could be due to asphaltenes that are becoming more rigid with time at the isooctane-toluene/asphalt interface. A more rigid system would have shorter relaxation times and would appear darker in the NMR images. The layer could also be due to oxidation of the maltenes, which are then attracted to the highly polar surface of the asphaltenes and form a distinct layer at the interface. Compositional factors such as the amounts of strong and weak acids, bases and neutrals probably also contribute to the extent of oxidation and the associated interactions. Other possibilities exist. Nevertheless, the layer of material at the interface appears to have properties that are different from the asphaltenes and the maltenes. For example, the dark layer appears to be a more rigid material than the asphaltene layer. If the sample is stirred with a spatula the dark layer breaks into pieces. An example is shown in Figure 5. The top two images show the breakup of the interface layer longitudinally across the solvent-asphaltene boundary. The bottom two images show the breakup of the interface layer radially across the solvent-asphaltene boundary. In both types of images, the rigid nature of the interface layer is apparent. This material will need to be characterized in the future to determine how it might affect asphalt compatibility.

## SUMMARY

Applications of magnetic resonance imaging to study various aspects of asphalts are in their infancy. Consequently, a number of imaging methods and instrumental parameters need to be investigated to determine the feasibility of MRI to study asphalts. In this study, exploratory MRI measurements were made on the effects of aging on the flocculation and precipitation of asphaltenes from asphalt. NMR images were obtained on asphalts which were dissolved in toluene and titrated with isooctane to the point of maximum flocculation. When the titrant was added slowly to minimize mixing at the isooctane-asphalt/toluene interface, the images showed that a layer of material formed at the solvent interface which was different from the asphaltenes or the maltenes. The formation of this layer appeared to be dependent on asphaltene

concentration and degree of aging, i.e., the greater the asphaltene content and the degree of aging, the more prominent the layer. These observations suggest that NMR imaging might be used to assess the compatibility of aged asphalts and work is in progress along these lines.

## DISCLAIMER

This document is disseminated under the sponsorship of the Department of Transportation in the interest of information exchange. The United States Government assumes no liability for its contents or use thereof.

The contents of this report reflect the views of WRI which is responsible for the facts and the accuracy of the data presented herein. The contents do not necessarily reflect the official views or the policy of the Department of Transportation.

Mention of specific brand names or models of equipment is for information only and does not imply endorsement of any particular brand to the exclusion of others that may be suitable.

## ACKNOWLEDGMENTS

The authors gratefully acknowledge support of this work by the Federal Highway Administration under Contract No. DTFH61-92C-00170.

## REFERENCES

1. Miknis, F. P.; Netzel, D. A., *Prepr. Pap.-Am. Chem. Soc., Div. Fuel Chem.* **1996**, 41(4), 1327-1331.
2. Komoroski, R. A., *Anal. Chem.*, **1993**, 65, 1068A.
3. Boduszynski, M. M., in *Chemistry of Asphalts*, J. W. Bunger and N. C. Li, eds, *Advances in Chemistry Series*, **195**, Amer. Chem. Soc., Washington, DC, 1981, 119-135.
4. Heithaus J. J., *J. Inst. Petrol.*, **1960**, 48, 45-53.
5. Pauli, A. T., *Prepr. Pap.-Am. Chem. Soc., Div. Fuel Chem.*, **1996**, 41(4), 1327-1331.
6. Cominsky, R. J.; Moulthrop, J. S.; Elmore, W. E.; Kennedy, T. W., *SHRP Materials Reference Library Asphalt Selection Process*; Report No. SHRP-IR-A-89-002; Strategic Highway Research Program, National Research Council, Washington, DC, 1989, 31 pp.
7. Branthaver, J. F., et al., SHRP-A-368, *Binder Characterization and Evaluation, Volume 2: Chemistry*, Strategic Highway Research Program, National Research Council, Washington, DC, 1993, 193 pp.
8. Petersen, J. C., et al., SHRP-A-370, *Binder Characterization and Evaluation, Volume 4: Test Methods*, Strategic Highway Research Program, National Research Council, Washington, DC, 1994, 479 pp.

Table 1. Summary of Chemical Properties of Selected Asphalts

Property	AAB-1	AAD-1	AAE	AAK-1	AAM-1	ABM-1	AAS-1
Asphalt Grade	AC-10	AR-4000	60/70	AC-30	AC-20	AR-4000	AC-20
Crude Source	WY Sour	Calif.	Lloyd- minster air blown	Boscan	West Tex. Intermed.	Calif. Valley	Arab Heavy
<u>Component Analysis, %</u>							
Asphaltenes	19.3	23.9	24.8	22.9	9.4	8.3	21.3
Polar Aromatics	38.3	41.3	30.5	41.8	50.3	52.4	34.1
Napthene Aromatics	33.4	25.1	31.6	30.0	41.9	29.6	39.7
Saturates	8.6	8.6	12.7	5.1	1.9	9.0	5.9
<u>Other Properties</u>							
Carbon Aromaticities	0.32	0.24	0.33	0.32	0.25	--	--
Hydrogen Aromaticities	0.071	0.068	0.087	0.068	0.065	--	--
H/C	1.55	1.59	1.45	1.46	1.55	1.43	1.43
Molecular Weight (in toluene)	840	700	--	860	1300	--	960

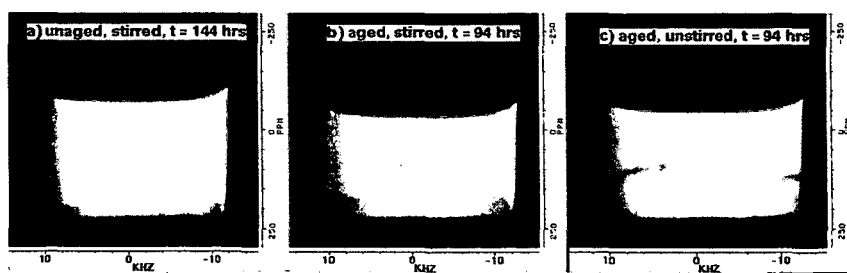


Figure 1. NMR images illustrating effects of aging and stirring on asphaltene precipitation. Times listed are settling times and refer to the time elapsed between addition of isoctane and the time when the image was recorded.

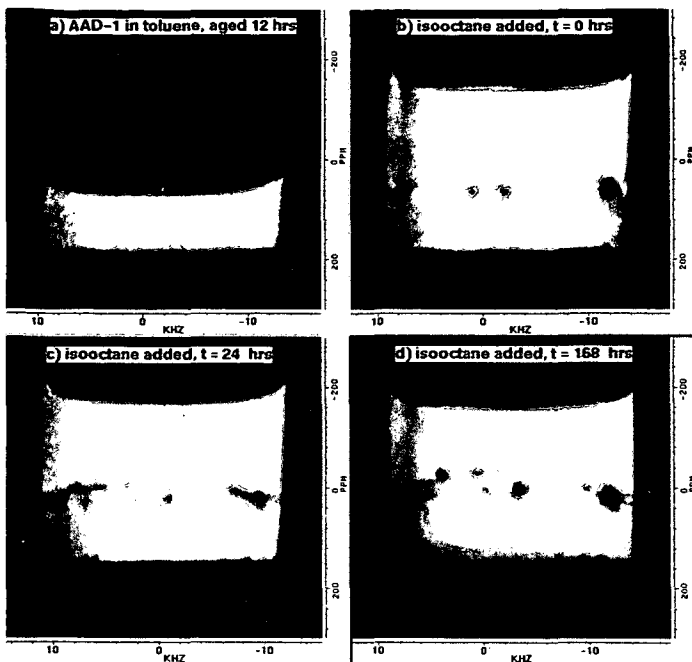


Figure 2. NMR images illustrating time evolution of interface layer in aged asphalt. Times listed are settling times.

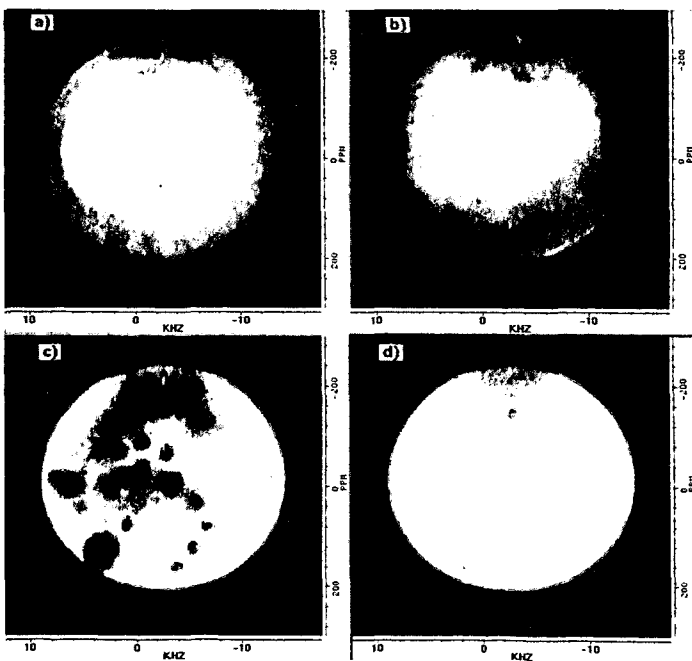


Figure 3. Radial NMR images at different depths illustrating spherical globules in the solvent interface layer.

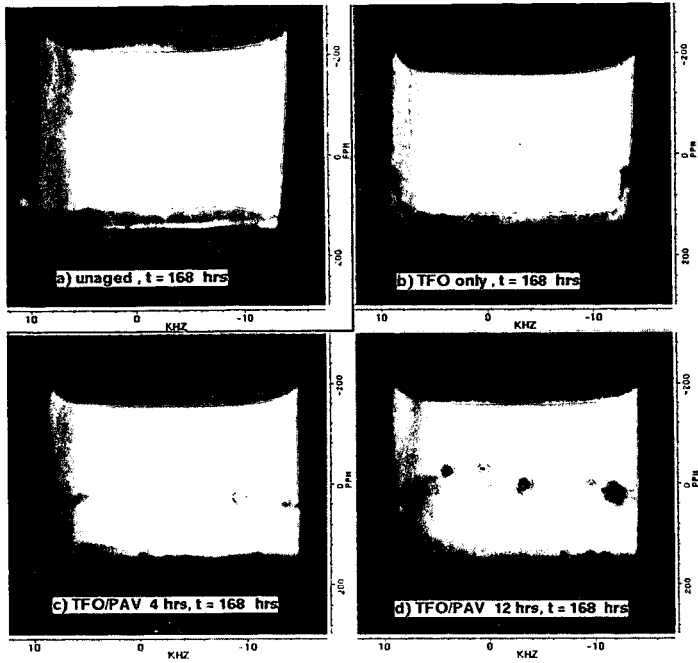


Figure 4. NMR images illustrating the effect of aging on asphaltene settling.

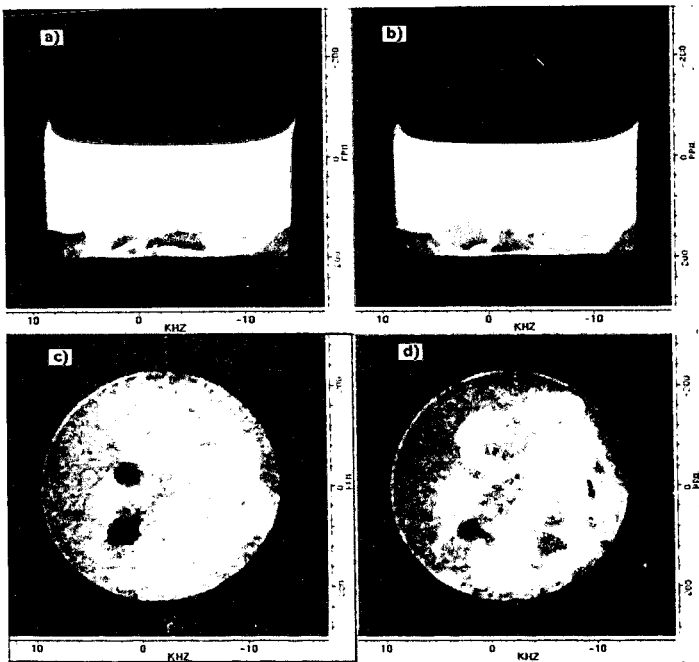


Figure 5. NMR images illustrating breakup of interface layer with stirring. a), b) Longitudinal cross-section images at different positions, c), d) Radial cross-section images at different positions.

# MEASUREMENTS OF VAPOR PRESSURES OF COAL TARS USING THE NON-ISOTHERMAL KNUDSEN EFFUSION METHOD

Vahur Oja and Eric M. Suuberg  
Division of Engineering  
Brown University, Providence, RI, 02912

Keywords: Coal Tars, Coal Pyrolysis, Vapor Pressures

## INTRODUCTION

Vapor pressures of high molecular weight thermal decomposition products of coals (i.e., tars) are sometimes an important parameter in modeling the combustion behavior of the coals. The extent to which the tars can vaporize, before retrograde reactions reincorporate them into a char, plays a key role in determining the flux of combustibles to the flame front. This is reflected in various pyrolysis models [1-8]. There has been a lively debate in the coal pyrolysis literature concerning what values to assume for the vapor pressures of coal tars, since there have never been actual measurements of this property. What relevant data have been available have come from highly hydrogenated coal liquids [9] or from pure model compounds, and uncertainties of an order of magnitude have not been uncommon. The significance is that models of the coal pyrolysis tar yield are quite sensitive to this input parameter. Comparisons of the behavior of various proposed correlations are offered elsewhere [5,10].

In this study, the vapor pressures of primary coal tars have been examined using the Knudsen Effusion method, modified for application to mixtures containing components with a wide range of volatilities. The Knudsen effusion technique was selected because of the thermally labile nature of the primary tars (those that have not undergone secondary cracking). This requires that the vapor pressures be determined at temperatures well below those of pyrolysis, i.e., below 250 °C. This, in turn, means that the vapor pressures will be very low, because the tars have molecular weights of several hundred dalton.

## EXPERIMENTAL

### *The Knudsen Effusion Technique for Vapor Pressure Measurement*

The vapor pressures of actual coal tars and model "tars", consisting of mixtures of PAH, are measured, using a molecular effusion/TGA technique. The various so-called "effusion" methods are based on the molecular effusion of a vapor from a surface, or through an orifice [11]. Of these methods, that which has been selected for use here, is the Knudsen method [12,13], in which a substance of interest effuses through a small pinhole of known area, in an otherwise sealed container or cell. The Knudsen method is used for the measurement of low vapor pressures in the range from 1 to 10<sup>-6</sup> torr, under molecular flow conditions. This ideally requires that pressures inside and outside the sample cell are low enough that the frequency of collisions of vapor molecules with gas phase species are low in comparison with the frequency of collisions with the cell. The measurement of vapor pressure involves determining the rate of loss of molecules of the evaporating substance from the effusion cell under these conditions. Measurements are typically made under isothermal conditions, with weight loss from the cell being recorded as a function of time, generally in a TGA-type apparatus. We have, however, modified the technique for non-isothermal operation, as described further below.

The basic theory of the effusion method has been often reviewed in the literature [12-14]. The theory of method is actually based upon the basic kinetic theory of gases. From these classical results, Knudsen derived an expression for the slow isothermal flow out of a cell with a small hole in it. The vapor pressure of a material in the cell can be calculated from Knudsen's original effusion rate result:

$$P_1 - P_2 = \frac{G}{t} \frac{w_1 + w_2}{\sqrt{\rho}}$$

where  $P_1$  is the pressure of saturated vapor inside the cell,  $P_2$  is the pressure outside of the effusion cell,  $w_1$  is the resistance of hole in the cell,  $w_2$  is the resistance of cell containing the

sample,  $G$  is the mass lost by effusion,  $t$  is the effusion time,  $\rho$  is the density of the vapor at the temperature of experiment. The relation simplifies upon applying several simplifying assumptions, including the ideal gas law, that the pinhole leak is the main flow resistance, and assuming  $P_1 \gg P_2$ , yielding:

$$P = \frac{m}{t A_0} \left( \frac{2 \pi R T}{M} \right)^{1/2}$$

The above result is called the ideal Knudsen equation, in which  $P$  is the desired vapor pressure,  $m$  the mass loss during the effusion time interval,  $A_0$  is orifice area,  $M$  the substance molecular weight,  $t$  the effusion time, and  $T$  the absolute temperature of the experiment. It is further assumed when applying this equation to the effusion process that the equilibrium vapor pressure of the effusing species obtains within the cell, that the orifice walls do not intercept and return into the cell an appreciable fraction of molecular current entering the hole, that there is no back flux into the orifice exit and the number of intermolecular collisions in the vapor phase occurring within the orifice is negligible.

In our implementation, the mass loss rate was continuously recorded, using a Cahn 2000 recording electrobalance. The cell containing the pinhole leak was suspended on one arm of the balance, which has nominal sensitivity in the  $\mu\text{g}$  level. The backpressure in the TGA system was maintained at  $10^{-7}$  torr, which has been noted to be sufficient so as to provide accuracy in the  $10^{-6}$  torr range of vapor pressures. The cell itself was maintained inside of a black capsule within the TGA, and was in close proximity to a thermocouple within the capsule. This was necessary in order to achieve the  $0.1^\circ\text{K}$  accuracy in temperature measurement required in vapor pressure work at low temperatures. The temperature measurement issue will be further discussed below.

#### *The Non-Isothermal Knudsen Effusion Technique*

One modification of the Knudsen effusion technique was required in order to apply it to materials as complicated as coal tars. Very complex mixtures, which contain materials exhibiting a wide variety of vapor pressures, cannot be conveniently studied by the traditional Knudsen effusion methods involving increasing temperature in isothermal steps. Typically, mixtures of components exhibiting a wide range of volatility are examined by a non-isothermal distillation procedure, for example ASTM D86, D216, D447, D850 and D 1078. The difficulties in applying these methods have led to various alternative methods, including the well-known "simulated distillation" as performed by gas chromatograph, and thermogravimetric methods [15]. These ordinary distillation techniques are not, however, acceptable in our case. Here, as noted above, the temperatures that would be typically involved in an ambient pressure, or mild vacuum, distillation would still be unacceptably high. We are forced to work at the high vacuums of the Knudsen effusion method in order to keep temperatures below those for decomposition of the tars. In contrast to the ASTM-type procedures, however, the pressure outside of the cell is of no consequence, provided that it is below the vapor pressure of the sample by at least an order of magnitude, and as long as the situation in the pinhole leak approximates collisionless flow.

The non-isothermal Knudsen effusion method was developed in response to the above need. The method allows a very wide range of temperatures to be scanned quickly, and with modest amounts of mass loss. The latter is important in the case of a mixture, in which the properties of the sample will change with mass loss. Reliable measurements using the Knudsen effusion method require particular attention to the problem of the measuring and controlling the temperature of the Knudsen cell. Most discrepancies between the results of the different workers using the Knudsen or related techniques are the result of insufficient attention to temperature measurement. As the sample must receive heat purely by radiation (since the cell is operated in a high vacuum) a long time is required to reach thermal equilibrium in an isothermal experiment. In our case, the main thermal lag is associated with heating of the five gram capsule which surrounds the sample cell. However, the sample cell has a view factor of the capsule which approaches one. Together with the fact that the effusion cell has a much smaller mass, 0.15 grams, it thus tracks the capsule temperature well. Thus a long equilibration time, associated with changing the capsule temperature in isothermal experiments, is avoided if an experiment is carried out non-isothermally.

## **RESULTS AND DISCUSSION**

The performance of the non-isothermal technique was checked using anthracene and naphthacene, since the vapor pressures of these compounds have earlier successfully measured by us, using the standard isothermal Knudsen effusion method. Figure 1 shows the non-isothermal measurement

results for anthracene at heating and cooling rates of 5 °C/min. It is apparent that there is a significant deviation of the results from the isothermal technique data. The fact that the heating data under-predict, and the cooling data over-predict, the real vapor pressures might be anticipated. This performance suggests that the cell temperature is lagging the surrounding capsule temperature, and that the heat transfer limitation has shifted to the capsule-cell transport process. For this reason, it is logical to expect that by decreasing the rate at which the capsule is driven in temperature, this limitation can be minimized. This is borne out by the results obtained at 0.8 °C/min heating rate, shown in Figure 2. There is in this case good agreement between the results obtained from the non-isothermal and isothermal techniques.

Figure 3 shows the results of the isothermal technique applied to naphthalene, in "cooling" mode. As seen in Figure 3, there is again good agreement between the results of isothermal and non-isothermal methods. Thus the reliability of the non-isothermal method appears to be established.

The results of the first application of the non-isothermal method to coal tars is shown in Figure 4. The results were applied to a fresh coal tar in this case. The tar was produced by the pyrolysis of a Bruceton "standard" Pittsburgh No. 8 high volatile bituminous coal, in a fluidized bed at approximately 550°C. The Bruceton coal has the following elemental composition: C-80.4%, H-5.3%, O-6.7%, N-1.6%, S-1.0%, ash 4.6%, all on a dry basis. The tar was collected in THF, and carefully dried prior to measurement.

In the vapor pressure experiments, the temperature of the tar sample was continually raised from an initial value of 60°C to a final temperature of 220 °C, at a rate of 0.5 °C/min. Because the tar changes in composition during evaporative loss of its components, the ability to quickly scan the whole temperature space of interest is of great importance. The results of Figure 4 show that the tars evaporate in a "distillation-like" fashion. More volatile species are lost earlier in the process, leaving behind a progressively less volatile residue. The experiments of Figure 4 involved tracking the vapor pressure during both heatup and cooldown cycles. It can be seen that the trace of each heatup cycle (at a progressively higher total level of mass loss) tracks well the immediately preceding cooldown curve. This is not surprising, because during cooldown, the rates of mass loss fall quite low, and until the temperature is again raised to considerably higher values, little further mass loss occurs. Thus there should be little change in vapor pressure attributable to mass loss during the cooldown and early part of the next heatup cycle.

It can be noted that the vapor pressure remains in the range from about  $7 \times 10^{-5}$  to  $7 \times 10^{-3}$  torr as the temperature of the sample is raised from 60°C to 225°C, as a result of loss of progressively less volatile components. Using an earlier derived correlation for the vapor pressures of coal tars [16]:

$$P [\text{torr}] = 4.45 \times 10^6 \exp(-255M^{0.586}/T)$$

if the mid-range of the pressure and temperatures of Figure 4 are taken to be  $\ln P = -7.5$  (or  $P = 5.5 \times 10^{-4}$  torr) and  $1/T = 0.00255$  (or  $T = 392$  K), then the value of  $M$  would be calculated to be about 430 daltons, which is in good agreement with the measured molecular weight of the middle fractions of the tar, from both present measurements and earlier results [16].

More recently, there has developed a concern about condensation-type reactions influencing the results of the vapor pressure measurements, even at these modest temperatures. Indirect evidence of a problem comes from the decreasing solubility of the tar after the vapor pressure experiments have been carried out. If a non-volatile component were to form during the vapor pressure measurement, then the volume fraction of volatile species would be decreased, and assuming that ideal solution behavior is maintained, the vapor pressure would decrease in proportion to the fraction of non-volatile material. At any given temperature, the shift of vapor pressure with cycling involves many orders of magnitude of pressure. We feel, at this point, that selective distillation of lighter fractions may be the more important effect, because there is an overall upward shift in molecular weight during the experiment, but no evidence of formation of large amounts of condensation products.

The data of Figure 4 allow one to judge that there is little change in the latent heat of vaporization during the experiment. This implies that a relatively narrow range of molecular weight is involved. The tar boiling point curve for an arbitrarily selected pressure of  $10^{-4}$  torr is shown in Figure 5.

## CONCLUSIONS

The non-isothermal Knudsen effusion method has been shown to be a useful and reliable method for measuring the vapor pressures of pure components and complex mixtures. It is considerably faster and more convenient than the conventional isothermal Knudsen effusion method.

## ACKNOWLEDGMENT

The financial support of the U.S. Department of Energy, under grant DE-FG22-92PC92544, is gratefully acknowledged.

## REFERENCES

1. Suuberg, E.M., in *Chemistry of Coal Conversion* (R. Schlosberg, Ed.), Plenum, 1985.
2. Unger, P.E., Suuberg, E.M., *18th Symp. (Int.) on Comb.*, The Comb. Inst., p. 1203, 1981.
3. Niksa, S. *AIChE J.*, **34**, 790 (1988).
4. Niksa, S. and Kerstein, A., *Energy Fuels*, **5**, 647 (1991).
5. Fletcher, T., Kerstein, A., Pugmire, R., Solum, M., Grant, D. *Energy Fuels*, **6**, 414 (1992).
6. Solomon, P.R., Serio, M.A., and Suuberg, E.M., *Prog. Energy Comb. Sci.*, **18**, 133 (1992).
7. Solomon, P.R., Hamblen, D.G., Carangelo, R.M., Serio, M.A., Deshpande, G.V., *Energy Fuels*, **2**, 405 (1988).
8. Oh, M.S., Peters, W.A., and Howard, J.B., *AIChE J.*, **35**, 776 (1989).
9. Tsonopoulos, C., Heidman, J., and Hwang, S.-C., *Thermodynamic and Transport Properties of Coal Liquids*, Wiley, 1986.
10. Oja, V. and Suuberg, E.M., *ACS Div. Fuel Chem. Prepr.*, **41**, 82 (1996).
11. Dushman, S., *Scientific Foundations of Vacuum Technique*, Wiley, 2nd edition, 1962.
12. Knudsen, M., *Ann. Physik.*, **28**, 999, 1909.
13. Knudsen, M., *Ann. Physik.*, **29**, 179, 1909.
14. Hollahan, J., *J. Chem. Educ.*, **39**, 23, 1962.
15. Huang, H., Wang, K., Wang, S., Klein, M. and Calkins, W. H., *ACS Div. Fuel Chem. Prepr.*, **41**, 87 (1996).
16. Suuberg, E.M., Unger, P.E., and Lilly, W.D., *Fuel*, **64**, 956 (1985).

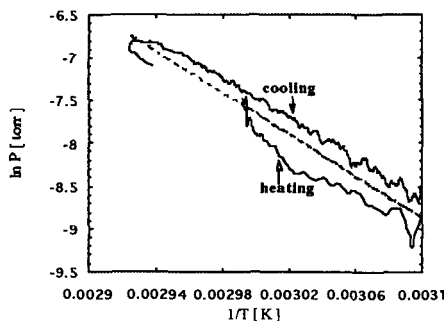


Figure 1. A comparison of vapor pressure results obtained using the non-isothermal and isothermal effusion methods on anthracene. The isothermal data are shown as the dashed line. Heating and cooling rates are 5°C/min.

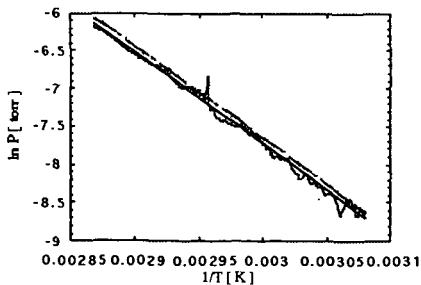


Figure 2. A comparison of the results on anthracene, obtained at 0.8°C/min heating and cooling rates.

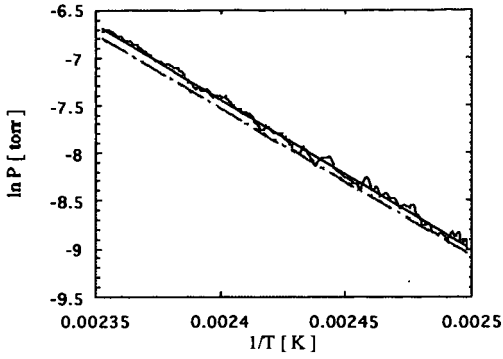


Figure 3. The non-isothermal effusion method applied to measuring the vapor pressure of naphthalene. Cooling rate 0.8°C/min.

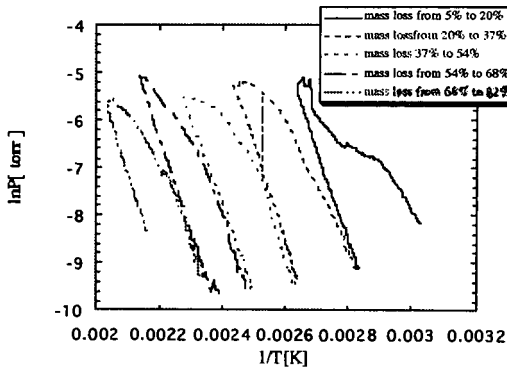


Figure 4. The non-isothermal Knudsen effusion method applied to Bruceton coal tar.

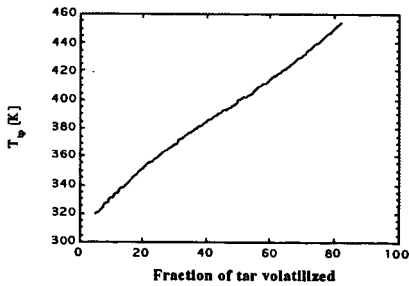


Figure 5. Boiling point distribution of Bruceton coal tar, 0.1 mtorr pressure.

## CORRELATION BETWEEN CARBON RESIDUE AND MOLECULAR WEIGHT

John F. Schabron and James G. Speight  
Western Research Institute,  
365 N. 9th St., Laramie, WY 82070-3380

Key Words: Petroleum Residua, Carbon Residue, Molecular Weight

### INTRODUCTION

Petroleum residua are materials obtained by nondestructive distillation of petroleum, usually below 350°C (660°F) since thermal decomposition can be substantial above this temperature (1). Distillation can be at atmospheric pressure (atmospheric residuum) or reduced pressure (vacuum residuum). Residua are usually tacky (atmospheric) or hard (vacuum) at room temperature. These materials typically have low atomic hydrogen-to-carbon ratios, which require hydrogen addition or carbon rejection (coking) schemes to convert them to liquid fuels. They can be difficult to process because of relatively high concentrations of elements other than carbon and hydrogen, and high viscosities (1).

Simple physical property measurements were once considered adequate to predict feedstock behavior in petroleum refining (1,2). The use of various types of residua available worldwide with different properties has added complexity to these considerations (3). Residua composition and properties must be understood to optimize refining strategies (4). Measurements such as elemental analysis, metals content, asphaltene content, and carbon residue provide some indication of residua behavior, but are not single predictors for upgrading processes (5). More insight is needed about the components of residua that cause specific problems in processing (6). The possibility exists that data from various analyses can be combined in a manner to provide insight into behavior during refining (7).

Molecular weight and molecular size are the most misunderstood parameters of petroleum constituents. There are many reports of high molecular weights (100,000-300,000 Daltons) for asphaltenes (8). True molecular weights for asphaltenes very rarely exceed 3,000. Apparent higher values are due to molecular association effects due to the presence of polar constituents causing inter- and intramolecular interactions.

### EXPERIMENTAL

The samples were vacuum residua and commercial grade asphalt materials from various sources. Asphaltenes were determined by adding n-heptane at a 40:1 volume ratio (9). Microcarbon residue (MCR) values were determined according to ASTM D-4530. This requires less than 1 g of sample and correlates with the Conradson carbon residue (CCR) test, which consumes 5-10 g sample (10). Number average molecular weights were determined by ASTM D-2503 using a Knauer vapor pressure osmometer (VPO) in toluene at 140°F (60°C). Although pyridine would be considered more desirable for breaking up molecular associations between more polar materials, toluene was used in this study since complete solubility could not be achieved in pyridine for residua asphaltenes.

### RESULTS AND DISCUSSION

Ideally, a predictive model can be applied to various feedstocks from different sources and of different types such as waxy, resinous, etc. to predict MCR or CCR values, which are predictors of coke yield. Carbon residue values are related to phase separation and delayed coking tendencies in a refinery (1,7,11). Asphaltene content can be used to provide a rough correlation with carbon residue values (12). For the twelve residua considered in the current study, the correlation between percent asphaltenes and MCR yields a correlation coefficient ( $r$ ) value of only 0.584. Additional refinement is needed to be a useful predictor of residue formation tendencies. This refinement involves including association effects. Residua with relatively low heteroatom contents yield MCR values significantly lower than residua with relatively higher heteroatom contents (13).

A correlation relating asphaltene content, molecular weight and heteroatom content with CCR and MCR of whole residua has been developed (14). Subsequent results suggest that the inclusion of heteroatoms is not necessary, since heteroatom associative affects are already taken into account by measuring the apparent molecular weights of the asphaltenes. In the previous study, the intercept was 8.19 wt.% MCR, which is due to contributions from other aromatic and polar materials in the residua.

The fractional contributions of the various constituents of residua to MCR have been shown to be additive (13). Thus, by considering the contribution of all the fractions, a more universal correlation can be obtained. A new correlation with MCR values and apparent molecular weights in toluene is shown in Figure 1. This consists of twelve residua, six asphaltenes and twelve chromatographic fractions (six aromatics and six polars) considered as whole materials, and the six asphaltenes and the twelve chromatographic fractions considered as fractional contributions

(13,15) Saturate fractions containing no significant aromatic structures and providing no contribution to MCR are not included. The correlation coefficient is 0.943 for 44 points, with a slope of 0.0198 and an intercept of -0.42. This is within experimental error of 0 wt.% MCR. These results suggest a generic universality for residua constituents between molecular weights and residue forming tendencies.

In Figure 1, two asphaltenes fall near the line, while four do not. The four that do not exhibit unrealistically high molecular weights relative to their MCR values. These latter four were not included in the linear equation. The high molecular weights are most likely due to severe associations of these very polar materials in toluene. The two asphaltenes which fell near the line have heteroatom content (N+O+S) of less than 6 wt.%, while the four that are far to the right of the line have heteroatom contents greater than 6 wt.%. The high heteroatom content contributes to polarity and association effects.

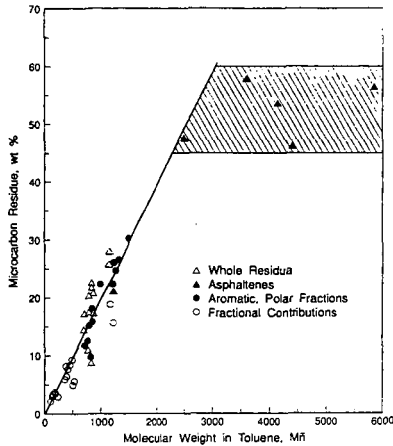


Figure 1. Microcarbon Residue vs. Molecular Weight for Residua Asphaltenes, Chromatographic Fractions, and Fractional Contributions in Toluene.

In an unrelated study (16,17) Athabasca bitumen pentane asphaltenes were separated into four ion exchange chromatography fractions. These materials were fully soluble in pyridine. The MCR values for these materials are plotted against their weights in pyridine. For reference, the toluene correlation line developed in Figure 1 is shown in Figure 2, and also the MCR value of the whole asphaltene plotted against the molecular weight in benzene, which is essentially the same value one would expect in toluene.

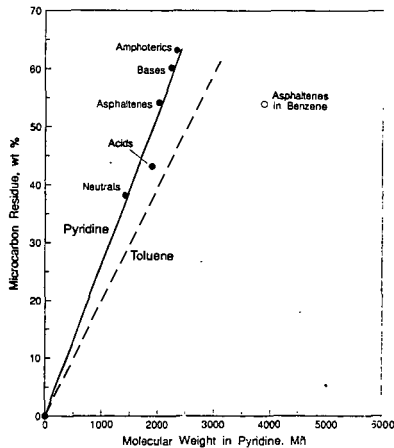


Figure 2. Microcarbon Residue vs. Molecular Weight for Athabasca Asphaltenes and Asphaltene IEC Fractions in Pyridine

The MCR values decrease in the order amphoteric, base, whole asphaltenes, acid, and polar

neutral fractions (16). The point for the original asphaltene molecular weight in benzene falls far to the right of the line, with a MCR value of 54.0 and a molecular weight value of 3,890 Daltons. The pyridine molecular weight for the whole asphaltene is 2,018 Daltons (17). The equation for the pyridine line was calculated by including the origin point (0,0) to obtain a slope of 0.0262 and an intercept of -0.46, with a correlation coefficient of 0.990. The slope of the toluene line (0.0198) is smaller than the slope of the pyridine line, which is due to less association in pyridine.

The correlation lines can be used as a tool to gauge association. For example, to bring the asphaltene with the highest apparent molecular weight of 5,850 Daltons to the toluene line in Figure 1 without changing its MCR value would require a molecular weight of about 2,950 Daltons. Thus, it appears that the association tendency for this material is  $5,850 \div 2,950 = 2.0$  units average in an associative complex in toluene solution. Using the pyridine line in Figure 2, the same MCR value yields a molecular weight value of 2,250, or 2.6 average units in an associative complex in toluene. The associative forming tendencies do not appear to have a direct effect on MCR values. This is suggested by the flattening of the correlation above a molecular weight of 3,000 Daltons in toluene (Figure 1), which appears to be due mainly to associative effects. The associations are broken up by the severe heating conditions involved in carbon residue formation.

A correlation which is more useful for the highly associated species is between carbon residue and H/C atomic ratios (Figure 3). Figure 3 includes points for all the materials in Figures 1 and 2. The correlation coefficient is 0.975, for 33 points with a slope and intercept of -105 and 173, respectively. Two points lying far off the line, correspond to a very waxy residuum and its wax-containing asphaltenes and these were not included in the calculation. The point of intersection at MCR = 0 wt.% occurs at a H/C ratio of 1.65. This implies that for residua constituents that there will be no carbon residue contribution for most species with H/C atomic ratios greater than about 1.65.

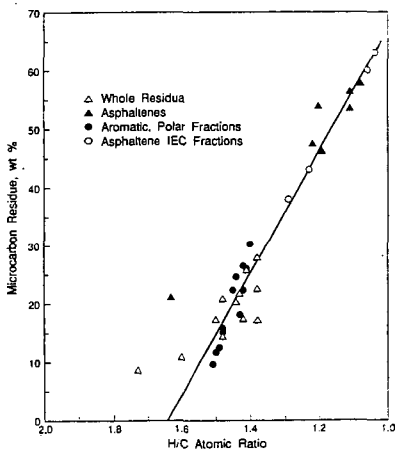


Figure 3. Microcarbon Residue vs. H/C Atomic Ratio for Residua, Asphaltenes, and Chromatographic Fractions

#### LITERATURE CITED

1. Speight, J.G., *The Chemistry and Technology of Petroleum*. 2nd Edition. Marcel Dekker, New York, NY (1991).
2. Speight, J.G., *The Desulfurization of Heavy Oils and Residua*. Marcel Dekker, New York, NY (1981).
3. Dolbear, G., A. Tang, and E. Moorhead, *Upgrading Studies with California, Mexican, and Middle Eastern Heavy Oils*. In *Metal Complexes in Fossil Fuels*, R. Filby and J. Branthaver, eds., American Chemical Society, Washington, DC, 220-232 (1987).
4. Schuetz, B., and H. Hofmann, *Hydrocarbon Proc.*, Feb., 75-82 (1984).
5. Dawson, W.H., E. Chornet, P. Tiwari, and M. Heitz, *PREPRINTS*, Div. Petrol. Chem., Am. Chem. Soc., 34, 384 (1989).
6. Gray, M.R., *AOSTRA J. Res.*, 6, 185 (1990).
7. Gary, J.H., and Handwerk, G.E., *Petroleum Refining: Technology and Economics*. Second Edition. Marcel Dekker Inc., New York (1984).
8. Speight, J.G., D.L. Wernick, K.A. Gould, R.E. Overfield, B.M.L. Rao, and D.W. Savage, *Revue De L'Institut Francais Du Petrole*, 40(1), 51 (1987).
9. Speight, J.G., R.B. Long, and T.D. Trowbridge, *Fuel*, 63, 616 (1984).

10. Long, R.B., and J.G. Speight, *Revue de L'Institut Francais du Petrole*, 44(2), 205 (1989).
11. Speight, J.G., Chemical and Physical Studies of Petroleum Asphaltenes. In *Asphaltenes and Asphalts*, 1, T.F. Yen and G.V. Chilingarian (Editors), Elsevier, Amsterdam, 12, 54 (1994).
12. Wiehe, I.A., PREPRINTS, Div. Petrol. Chem. Am. Chem. Soc., 38(2), 428 (1993).
13. Schabron, J.F, G.W. Gardner, J.K. Hart, N.D. Niss, G. Miyake, and D.A. Netzel, The Characterization of Petroleum Residua, U.S. Department of Energy Report DE/MC/11076-3539 (1993).
14. Schabron, J.F. and J.G. Speight, *Revue de L'Institut Francais du Petrole*, in press (1997).
15. Branthaver, J.F., J.C. Petersen, R.E. Robertson, J.J. Duvall, S.S. Kim, P.M. Harnsberger, T. Mill, E.K. Ensley, F.A. Barbour, and J.F. Schabron, "Binder Characterization and Evaluation", Strategic Highway Research Program Report SHRP-A-368, Volume 2: Chemistry, National Research Council, Washington, D.C. (1993).
16. Speight, J.G., PREPRINTS, Div. Fuel and Ind. Eng. Chem., Am. Chem. Soc., 31(3), 818 (1986).
17. Moschopedis, S.E., J.F. Fryer, and J.G. Speight, *Fuel*, 55, 227 (1976).

## NOVEL CHARACTERIZATION OF PETROLEUM RESIDS BY LIQUID CHROMATOGRAPHY COUPLED WITH MASS SPECTROMETRY

C. S. Hsu

Analytical Sciences Laboratory  
Exxon Research and Engineering Company  
Route 22 East, Clinton Township  
Annandale, NJ 08801

**Keywords:** characterization of petroleum resids and asphaltenes, thermospray, liquid chromatography-mass spectrometry.

The characterization of petroleum resids and asphaltenes has remained a tremendous challenge to mass spectrometry. These fractions contain thousands of heavy molecules that are difficult to separate into individual components or less complex subfractions by distillation or solvent elution due to high intermolecular van der Waals force and dipole-dipole interactions. The molecules usually lack volatility to provide a stable stream of vapor for mass spectrometric analysis. The number of isomers for a given molecular formula can be tremendous, that makes the differentiation of isomers, particularly stereoisomers, impractical and meaningless. High resolution accurate mass measurement is also very difficult because of the large number of possible elemental combinations that would require very high resolving power and mass measurement stability of the mass spectrometer. Mass spectrometric analysis of these fractions are therefore generally for the determination of molecular weight distribution. However, if high mass resolving power by mass spectrometry or molecular class separation by chromatography is achievable, then compound type and carbon number distributions would be useful information for the studies of upgrading these fractions. Due to multitude of molecules present, it would be desirable to ionize these molecule intact without fragmentation to facilitate mass spectral analysis.

Among low energy ionization techniques, field ionization (FI) and field desorption (FD) are commonly used (see Figure 1). In both FI and FD techniques, the molecules are ionized by a fine emitter with a high voltage (ca. 10-13 kilovolts) between the emitter and a counter-electrode at a short distance that creates a high electric field. The only difference between these two techniques is sample introduction. In FI, the sample is volatilized under mass spectrometric vacuum to produce vapor in the vicinity of the emitter for ionization. However, the temperature required for volatilizing resids and asphaltenes can be too high to cause thermal decomposition of the molecules. To avoid thermal decomposition, FD is used in which the sample is deposited onto a fine emitter which is inserted into mass spectrometer via a vacuum lock. When a high electric field is applied on the emitter, molecules are ionized by quantum tunneling to produce low internal energy molecular ions. To provide fluidity of the sample some emitter current is also applied during ionization. Once ions are formed, they are repelled off the emitter by Coulombic repulsion. In FD, therefore, the sample is ionized without volatilization.

The FD technique, however, suffers from two major drawbacks: weak signal and cluster formation. Since only limited surface area is available on the emitter for field ionization and field desorption, the emitter is usually activated in indene, acetonitrile or acetone vapor to grow microneedles (whiskers) to increase high-field sites or area. Nonetheless, the number of molecules accessible to the high-field sites are still limited. In addition, ionization efficiency by quantum tunneling is very low, compared to other ionization techniques, such as electron-impact ionization and chemical ionization. As a result, low ion yield and weak signal are obtained. Due to transient nature of the signal, medium and high resolution mass measurement is difficult to perform. With a somewhat larger sample load, several layers of molecules are present between the surfaces of the emitter and the sample matrix. Ions formed on the surface of the emitter will have to penetrate through these layers before they are expelled out of the source region. Some of them are neutralized, charge transferred, or undergone ion-molecule reactions. Figure 2 shows a 875-1026°F distillate from a Californian crude oil with an average molecular weight near 500. The presence of dimers with molecular weights between 700 and 1300 is also apparent.

We have resolved the difficulties encountered in FD by using thermospray (TSP) ionization, a technique used in liquid chromatography/mass spectrometry (LC/MS). In TSP,

sample is dissolved in a mobile phase that is sprayed out of a heated nebulizer. A heavy duty filament or a discharge electrode is placed near the nebulizer as an ionization means. Excess amounts of solvent (mobile phase) molecules are preferentially ionized by electron bombardment of a heavy duty filament or discharge ionization of a discharge electrode. These solvent ions then ionize sample molecules via protonation, hydride extraction, or charge exchange. Since the sample molecules are not directly heated and ionized by high energy electron beams, intact protonated, hydride-abstracted, or molecular ions are formed in TSP.

The sample molecules are well-separated by an excess amount of solvent so that ion-molecule reaction between sample ions and molecules can be avoided. Thus, cluster formation encountered in FD is eliminated. The same distillate as in the FD experiment mentioned above was dissolved in a mobile phase of 75% methylene chloride and 25% hexane. A discharge electrode is used as an external source for TSP ionization, yielding a TSP spectrum as shown in Figure 3. The most noticeable feature of the TSP spectrum is the absence of dimer cluster in the 700-1300 mass range. The distribution of the ions in TSP is quite similar to that in FD except the absence of peaks corresponding to saturated hydrocarbons. Not being able to ionize saturated hydrocarbons is a major disadvantage of TSP because all of the suitable solvents for TSP experiments have similar or higher proton affinity than saturated hydrocarbons. Hence, saturated hydrocarbons have to be separated from aromatic hydrocarbons and analyzed separately. However, there are many other advantages of using TSP for petroleum resids and asphaltenes to compensate for such limitation.

One advantage of TSP is its stable ion current. Figure 4 compares the TSP and FD spectra of a 1120-1305°F DISTACT distillate of a Middle East crude oil. Both show similar molecular distribution in the mass range of 300-1400 with an average molecular weight of about 800. A much stronger ion current was obtained in TSP, compared to a weak current in FD. With high intensity and stability of ion current, slower scans for medium/high resolution mass measurement can be performed in TSP. Another advantage of TSP is its ability of on-line coupling with liquid chromatography (1). Liquid chromatography (LC) separates aromatic hydrocarbons by increasing polarity into monoaromatic, diaromatic, triaromatic, tetraaromatic, and polar elution regions. It greatly facilitates the differentiation of overlapping aromatic and naphthenoaromatic hydrocarbons (2). Figure 5 shows monoaromatic, diaromatic, triaromatic, and tetraaromatic elution regions of the above DISTACT distillate separated by LC. It can be seen that the average molecular weight gradually decreases with increasing aromaticity. The average molecular weights are about 850 for monoaromatics, 820 for diaromatics, 790 for triaromatics, and 730 for tetraaromatics, respectively. That is, in a given distillation range LC elution regions containing compounds with higher aromaticity have lower average molecular weights.

With increasing resolving power, it is also possible to obtain accurate mass measurement for elemental composition of the compounds (3). Figure 6 shows the compound type distributions obtained from medium resolution (ca. 5000 resolving power) measurement of the monoaromatic, diaromatic, triaromatic, and tetraaromatic elution regions shown in Figure 5. The distributions are shown as relative abundance as a function of the z-number of equivalent hydrocarbon series. For this specific sample, indenenes or dinaphthenobenzenes were found to be the most abundant series in monoaromatics, benzothiophenes in diaromatics, dibenzothiophenes in triaromatics, and pyrene in tetraaromatics. The use of a mass spectrometer with higher resolving power, such as Fourier-transform ion cyclotron resonance mass spectrometry (FT-ICR), would be required for further confirmation of these compound series at high masses (4).

We have demonstrated that petroleum resids and asphaltenes can be characterized in fair details by using thermospray ionization technique. This technique can also be used in on-line liquid chromatography-mass spectrometry to further define the type of molecules present in these heavy high boiling petroleum fractions. To overcome intermolecular interaction between resid and asphaltene molecules for aggregate formation, dispersing the molecules in a solvent medium appears to be a reasonable approach for obtaining molecular information of these fractions. It would be worthwhile to study the behavior of these molecules in other type of LC/MS, such as atmospheric pressure chemical ionization (APCI) and electrospray, for the characterization of petroleum resids and asphaltenes.

- (1) C. S. Hsu and K. Qian, *Energy Fuels*, 7, 268-272 (1993)
- (2) K. Qian and C. S. Hsu, *Anal. Chem.*, 64, 2327-2333 (1992)
- (3) C. S. Hsu, K. Qian and Y. C. Chen, *Anal. Chim. Acta*, 264, 79-89 (1992)
- (4) C. S. Hsu, Z. Liang and J. E. Campana, *Anal. Chem.*, 66, 850-855 (1994)

Figure 1 Simplified schematic diagram of a field ionization/field desorption ion source.

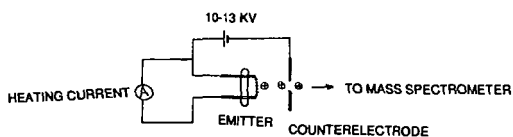


Figure 2 Field desorption mass spectrum of a 875-1026°F distillate from a Californian crude oil, showing the presence of dimers formed during ionization.

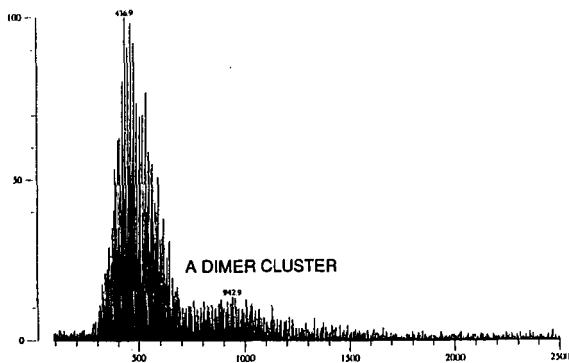


Figure 3 Thermospray ionization mass spectrum of a 875-1026°F distillate from a Californian crude oil, no dimers formed.

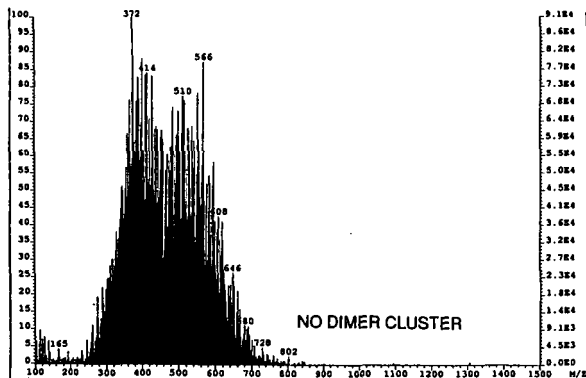


Figure 4 Similar molecular weight distributions are obtained by field desorption and thermospray of a 1120-1305°F DISTACT fraction of a Middle East crude oil.

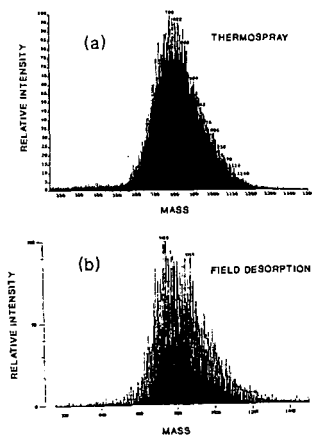


Figure 5 Molecular distributions of a 1120-1305°F DISTACT fraction of a Middle East crude oil in the monoaromatic, diaromatic, triaromatic and tetraaromatic elution regions of normal phase liquid chromatography.

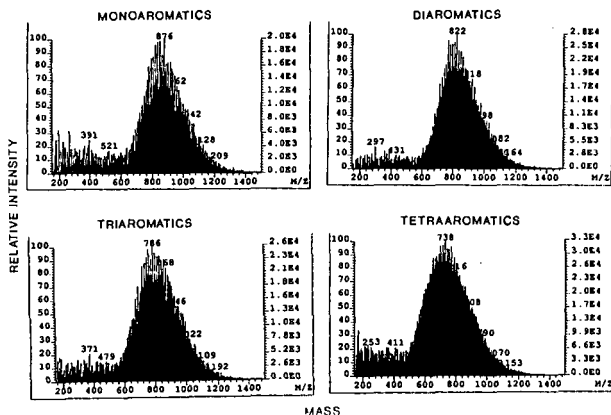
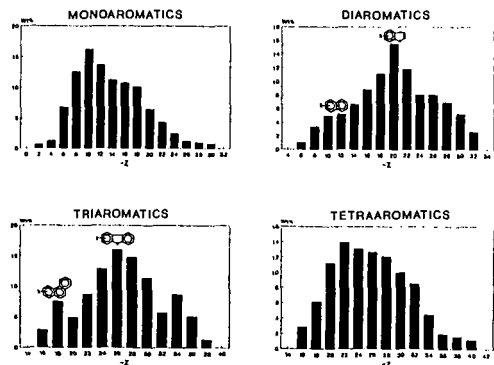


Figure 6 Compound type distributions of a 1120-1305°F DISTACT fraction of a Middle East crude oil in the monoaromatic, diaromatic and tetraaromatic elution regions of normal phase liquid chromatography.



## INTERFACIAL PROPERTIES OF ACID, BASIC AND NEUTRAL FRACTIONS DERIVED FROM ORINOCO BELT CRUDE OIL,

Cesar Ovalles\*, Maria del Carmen Garcia, Eduardo Lujano, Williams Aular, Reinaldo Bermudez, Edgar Cotte, INTEVEP, S. A., P. O. Box 77343, Caracas 1080A, Venezuela.

Key Words: Extraheavy Crude Oil, Interfacial Properties, ABN Separation

### INTRODUCTION

The interfacial properties of acid fractions play an important role in the stabilization of crude/water emulsions mainly because of their behavior as natural surfactants [1-13]. Also, acid compounds are used as biomarkers in geochemical correlations [14]. On the other hand, acid fraction are known to be coke precursor compounds [14], contributed to deactivation of heterogeneous catalysts used in refining operations and to stabilize water/crude oil emulsions making difficult crude dehydration during oil production processes [10-14].

In 1956, Reisherg and Doscher [1] demonstrated that interfacially active components present in Ventura crude oil are of acidic nature, whereas, in 1964, Newman [2] reported that the later fraction is constituted mainly of phenolic compounds for a Eichlingen-Niedersachsen crude. From these studies and for a Rio Bravo crude oil, Bartle and Niederhausen [3] concluded that the interfacially active materials are concentrated principally in the resins and asphaltene fractions.

Schramm and coworkers [4] studied the influence of the concentration of indigenous surfactants on the recovery of Athabasca bitumen using steam at high pH values. The interfacially active components were separated from the crude oil using the tendency of the former substances to concentrate at the interface of a foam. Using this method, the authors proposed [4] a general chemical structure which consists of naphthenic rings with carboxylic acid substituents. The surfactants (R-O<sup>-</sup>) were generated by addition of sodium hydroxide (eq. 1) in order to enhance bitumen separation from the oil sand [4].



Unfortunately, the extraction of the natural surfactant at high pH value (>10) can generate species, via hydrolysis (eq. 2), which were not originally present in the crude oil. These new species may present substantially different interfacial activity than that found for the indigenous compounds [7-8].



Speight and coworkers [5] extracted phenolic and carboxylic acid compounds from Athabasca bitumen using solvents of different polarities and ion-exchange resins. The authors concluded that oxygenated compounds present in the asphaltene fraction have phenolic substituents, whereas resins concentrate the carboxylic acid moieties [6]. No details were given on the interfacial activity of the isolated fractions.

Seifert and Howells [7-8] extracted anionic compounds with NaOH/EtOH from a paraffinic crude oil (Midway-Sunset) and characterized the interfacially active compounds at pH values greater than 10. By comparison of interfacial tension vs pH of the original crude and its acid fractions (strong and weak), the authors concluded that their extraction method was efficient for the isolation of the surface active compounds. However, the authors reported the generation, via hydrolysis (eq. 2), between 40 and 50% of tensoactive materials which was not originally present in the crude oil [7-8].

Acevedo *et al.* [9] studied the interfacial activity of SARA fractions separated from Orinoco Belt crude oils and concluded that natural surfactants were present mainly in the resin fractions. From interfacial tension vs pH determinations for the crude oil and its extracts and the lower molecular weights found for methylated asphaltenes, the author suggested that carboxylic acid species were responsible for the observed interfacial activity. However, no further characterization were reported [9].

Sjoblom and coworkers [10-12] extracted surface active compounds from North Sea crude oil using a consecutive adsorption technique. The interfacial properties of the extracted fractions were evaluated using a decane/water (1:1) model system. It was found that the interfacial tension decreased and the stability of the emulsion w/o formed was higher as the polarity of the fraction increased. Sjoblom *et al.* [13] found a molecular weight for the indigenous surfactants between 900 and 1500 g/mole and, based on spectroscopic methods, proposed an average structure which

contains a long alkylic chain bonded with phenol, nitrogen or carboxylic acid substituents. However, the effects of the presence of strong (carboxylic) and weak (phenols) acids on the surface activity of the indigenous surfactants were not studied in detail.

From the previous literature, it can be concluded that the relationships between chemical structure and surface activity of acid fractions, which in turn at higher pH values behave as natural surfactants, are still widely unknown. Furthermore, the effects of the nature of the hydrocarbon chain, R, on the interfacial properties of these fractions have not been addressed in detail. This R group controls not only the acid strength (pKa) of an anionic surfactant but also its hydrophilic-lipophilic balance.

In this work, acid, basic and neutral fractions from Orinoco Belt Crude Oil (Cerro Negro) were isolated by ion-exchange chromatography and characterized by spectroscopic methods (FTIR, H- and  $^{13}\text{C}$ -NMR), titration with KOH and molecular weight measurements using vapor pressure osmometry (VPO). The ion-exchange chromatography method was chosen because it is based on separation by functional group, induces little changes on the nature of the crude oils and reasonable mass balances can be easily obtained [14-15]. For measuring the interfacial activity, the method reported by Acevedo and coworkers [9] was used.

### EXPERIMENTAL

All reagents were analytical grade and were used without further purification. The Cerro Negro crude oil used in this study came from the Morichal oil field (southeastern part of Venezuela) and has the following characteristics (wt %):  $^{\circ}\text{API} = 8.1^{\circ}$ , % C = 80.32, % H = 9.88, % S = 3.7, % Asphaltenes, = 11.50, [V] = 367 ppm, [Ni] = 95.5 ppm, acidity = 3.7 mg KOH/g, Conradson Carbon = 17.22 %.

FTIR spectra were carried out using  $\text{CH}_2\text{Cl}_2$  as solvent and KBr cells.  $\text{CDCl}_3$  was used as solvent and TMS as reference for H- and  $^{13}\text{C}$ -NMR analysis. VPO molecular weight determinations were carried out in  $\text{CHCl}_3$  as solvent.

For the isolation of the total acid fraction (TAF), a column of quaternary alkylammonium chloride supported on a crosslinked styrene-divinylbenzene resin (Bio Rad AG-1, 200-400 mesh) was used as reported previously by Green and coworkers [14-16]. For the separation of the strong acid fraction (SAF) the method used was developed originally by McCarthy and Duthie [17].

The interfacial tension measurements were carried out using a toluene/water model system was used [9] (Robal Electronics Balance) and the values were reported at equilibrium at room temperature. The samples were dissolved in toluene and the concentrations were calculated with respect to the oleic phase. The pH of the aqueous phase was adjusted with KOH [9, 18].

### RESULTS AND DISCUSSION

Total and strong acid fractions (TAF and SAF) were isolated from the crude oil by ion-exchange chromatography using a styrene-divinylbenzene resin [14-16] and  $\text{KOH}/\text{SiO}_2$  [17] columns, respectively. In general, mass balances were between 90 and 95% with average percentages of extraction of 18% and 4% for TAF and SAT with respect to the original crude oil. The characterization by FTIR showed the presence of a band at  $1710\text{ cm}^{-1}$  which was assigned to the carbonyl groups of the acid moiety [15-16]. Also, other bands were observed which corresponded very well with the reported values for:  $\nu(\phi\text{-OH}) = 3590\text{ cm}^{-1}$ ,  $\nu(\text{N-H})_{\text{arom}} = 3460\text{ cm}^{-1}$ ,  $\nu(\text{C-H})_{\text{arom}} = 3000\text{ cm}^{-1}$ ,  $\nu(\text{C-H})_{\text{aliph}} = 2800\text{ cm}^{-1}$ ,  $\nu(\text{C=C})_{\text{arom}} = 1600\text{ cm}^{-1}$  [15-17]. From the analysis of the absorbance ratio of  $\nu(\text{C=O})/\nu(\text{C=C})$  and  $\nu(\phi\text{-OH})/\nu(\text{NH})$  bands and their total acid Numbers (Table 1) it can be concluded that SAF present higher concentration of carboxylic acid groups than TAF, whereas the later has more phenolic containing compounds than the former.

H-NMR characterization showed, besides the normal signals between 7.2 and 8.5 ppm for aromatic protons and between 0.1 and 3.8 ppm for aliphatic protons, a broad band in the range 9-10 ppm which was attributed to the carboxylic acid proton as reported in the literature [19].  $^{13}\text{C}$ -NMR analysis showed a small signal at 168 ppm which is consistent with the presence of carboxylic acid in TAF and SAF.

The interfacial activity vs pH was evaluated using a toluene/water model system and the results are shown in Fig. 1. As can be seen, this system presents very small interfacial activity in the pH range studied. On the other hand at pH greater than 13, a very small value for the interfacial tension (<1 dynes/cm) was obtained for the original Cerro Negro crude oil (CNC) as it is reported previously in the literature [7-9]. Furthermore, a reconstituted sample of the Cerro Negro Crude oil (prepared by mixing TAF and BNF in the 18/82 ratio) showed similar interfacial

activity than that found for the original CNC (Fig. 1). These results indicate that the separation method induced little changes on the interfacial properties on the crude oil as stated in the Introduction.

The effect of the pH on the interfacial activity of Cerro Negro crude oil and its fractions can be seen in Fig. 2A. It was found that the TAF present lower interfacial tension (2.1 dynes/cm) than those found for the original crude oil (5.3 dynes/cm) and BNT (4.6 dynes/cm) at 1000 mg/l and pH = 12. Similar results were obtained (Fig. 2B) by changing the concentration of the sample in the 100-15000 mg/l range at pH = 12. In general, the interfacial activity decreased in the order TAF > CNC > BNT.

In the same way, SAF showed lower interfacial tension (0.8 dynes/cm) than those determined for CNC (5.3 dynes/cm) and BNF (4.6 dynes/cm) at 1000 mg/l and pH = 12 (Fig. 3A). Also, a similar order of interfacial activity was found, SAF > CNC > BNT (Fig. 3B). From these results can be concluded that interfacially active compounds at high pH values are concentrated mainly in the acid fractions (TAF and SAF) of the crude as expected from the analysis of the literature [1-12].

Chemical characterization (FTIR, total acid number, H-NMR and molecular weight by VPO) and interfacial properties (interfacial tension at pH= 12, interfacial saturation, ISC, and excess,  $\Gamma$ , concentrations and area occupied at interphase) of Cerro Negro crude oil and its acid, basic and neutral fractions can be seen in Table 1. It is important to point out that in case of traditional surfactants, the ISC is better known as critical micellar concentration or CMC. Because the fractions studied in this work are very complex mixtures of a large variety of compounds and formation of micelles in these systems is not confirmed [20], it is preferred to use the term ISC instead of CMC. Therefore, ISC is defined as the concentration in which the interfacial tension remains constant at a given pH value.

As can be seen in Table 1, the interfacially active fractions TAF showed higher concentration of acids and phenols, measured by absorbance ratio of  $\nu(\text{C}=\text{O})/\nu(\text{C}=\text{C})$  and  $\nu(\phi\text{-OH})/\nu(\text{NH})$ , in comparison with the crude oil and its basic and neutral fractions. It is reported that the intensity of these bands increases as the activity of the natural surfactants increases for stabilization of water/crude emulsion [10-12]. Also, it can be observed in Table 1 and Fig. 2 that interfacial activity increases (lower interfacial tension and ISC) as the acidity of the sample increases for TAF, CNC and BNT.

In the same way, H-NMR analysis showed that the percentage of aromatic protons in TAF is higher (7.5%) than those found for the CNC (5.9%) and BNT (5.1%) whereas the molecular weight of TAF is higher (929 g/mol) than CNC (638 g/mol). Therefore, it can be concluded that the hydrophobic portion of the natural surfactants has higher aromatic character and molecular weight whereas the hydrophilic region showed higher acidity and concentration of polar substituents in comparison with the original Cerro Negro crude oil.

As seen in Table 1, the strong acid fraction showed an interfacial tension value (measured above its ISC) similar to the original crude and TAF (0.7, 0.6 and 1.2 dynes/cm, respectively). However, the ISC found for SAF is approximately one fourth of CNC but two fold of TAF (1050, 4000, 650 mg/l, respectively). On the other hand, the molecular weight of SAF is higher (774 g/mol) than that found for CNC (638 g/mol) but smaller with respect to TAF (929 g/mol).

Also, the area occupied at the interface for SAT is greater (156 Å) than those found for CNC and TAF (113 and 132 Å, respectively). These results indicate that SAF has **lower interfacial activity per molecule** than TAF due to higher value of ISC, greater area occupied at interface but lower molecular weight of the former in comparison with the later extract. Therefore, the results can be explained in terms of a better hydrophilic-lipophilic balance of the TAF, (higher molecular weight, lower concentration of polar groups and higher total acid number) in comparison with the SAF. All the results presented in this work constitute an important contribution toward the understanding the chemical structure-surface activity relationships of the natural surfactants present in Venezuelan crude oil.

#### REFERENCES

- 1) Reisberg, J.; Doscher, T. M. *Producers Monthly*, **20**, 46 (1956).
- 2) Neuman, H. J. *Erdon und Khole*, **17**, 346 (1964).
- 3) Bartell, F. E.; Niederhauser, D. O., *Fundamental Research on Occurrence and Recovery of Petroleum*, American Petroleum Institute, N. Y., 57 (1946-7).
- 4) Schramm, L. L.; Smith, R. G.; Stone, J. A., *Aostran Journal of Research*, **1**, 5 (1984).
- 5) Moschopedis, S. E.; Speight, J. G., *Fuel*, **55**, 334 (1976).
- 6) Moschopedis, S. E.; Speight, J. G., *Fuel*, **55**, 187 (1976).

- 7) Seifert, W. K.; Howells, W. G., Amer. Chem. Soc., Div. Pet. Chem. Prepr., **14**, 73 (1969).
- 8) Seifert, W. K., Amer. Chem. Soc., Div. Pet. Chem. Prepr., **14**, 87 (1969).
- 9) Layrisse L.; Rivas, H.; Acevedo, S. J. Disp. Sci. Tech., **5**, 1 (1984).
- 10) Nordli, K. G.; Sjoblom, J.; Kizling, J.; Stenius, P. Colloids. & Surf., **57**, 83 (1991).
- 11) Sjoblom, J.; Mingyuan, L.; Christy, A. A.; Ronningsen, H. P., Coll. & Surf., **96**, 261 (1995).
- 12) Sjoblom, J.; Mingyan, L.; Christy, A. A.; Gu, T. Colloids. & Surf., **66**, 55 (1992).
- 13) Urdahl, O.; Brekke, T.; Sjoblom, J., Fuel, **71**, 739 (1992).
- 14) Green, J. B.; Sturm, G. P., Jr.; Reynolds, J. W.; Thomson, J. S.; Yu, S. K.-T.; Grigsby, R. D.; Tang, S.-Y.; Shay, J. Y.; Hirsh, D. E.; Sanchez, V., U. S. Department of Energy, DE 90000200, Fossil Energy, Niper-161 (1988) and references therein.
- 15) Green, J. B.; Hoff, R. J.; Woodward, P. W.; Stevens, L. L., Fuel, **63** (1984).
- 16) Green, J. B.; Yu, S. K.-T.; Green, J. A.; Doughty, D. A.; Vogh, J. W.; Grigsby, R. D.; Vrana, R. P.; Thomson, J. S.; Carbognani, L., U. S. Department of Energy, DE 90000200, Fossil Energy, Niper-322 (1989).
- 17) McCarthy, R. D.; Suthie, A. H., J. Lipid Research, **3**, 117 (1962).
- 18) Acevedo, S.; Escobar, G.; Gutierrez, L.; Rivas, H.; Fuel, **71**, 619 (1992).
- 19) Silverstein, R. M.; Bassler, G. C.; Morrill, T. C., Spectrometric Identification of Organic Compounds, Wiley, New York, p249 (1981).
- 20) Speight, J. G.; Wernick, D. L.; Gould, K. A.; Overfield, R. E.; Rao, B. M., Savage, D. W. Revue de L'Institut Français du Pétrole, **40**, 51 (1985)

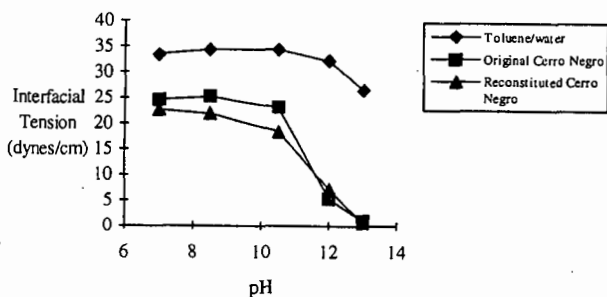


Fig. 1. Interfacial tension vs pH for original and reconstituted Cerro Negro crude oil. Concentration = 1000 mg/l. Toluene/water model system (pH = 12).

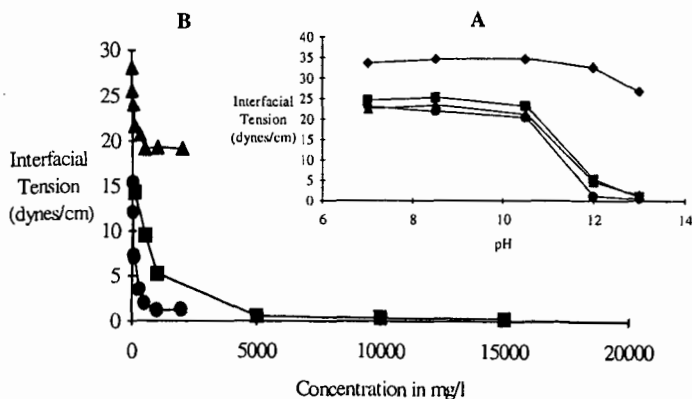


Fig. 2. Effects of (A) pH (at 1000 mg/l) and (B) concentration (at pH = 12) on the interfacial tension for Cerro Negro crude oil (CNC, ■) and its total acid (TAF, ●), basic and neutral (BNT, ▲) fractions using a toluene/water model system (♦).

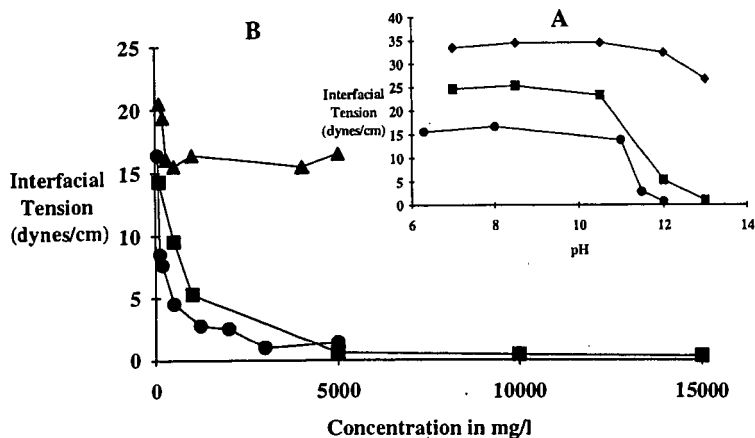


Fig. 3. Effects of (A) pH (at 1000 mg/l) and (B) concentration (at pH = 12) on the interfacial tension for Cerro Negro crude oil (CNC, ■) and its strong acid (SAF, ●), basic and neutral (BNF, ▲) fractions using a toluene/water model system (◆).

Table 1. Chemical and interfacial characterization of Cerro Negro crude oil and its acid, basic and neutral fractions<sup>a</sup>.

Chemical Characterization	Fraction				
	CNC <sup>b</sup> (100%)	TAF <sup>c</sup> (18%)	BNT <sup>d</sup> (82%)	SAF <sup>e</sup> (4%)	BNF <sup>f</sup> (96%)
$v(C=O)/v(C=C)^g$	0.57	0.97	0.37	3.38	0.06
$v(\phi-OH)/v(NH)^h$	0.18	0.64	0.50	0.52	0.77
Total acid No. <sup>i</sup>	3.7	4.1	0.95	71.8	0.2
%H <sub>arom</sub> <sup>j</sup>	5.9	7.5	5.1	7.5	6.9
%H <sub>alif</sub> <sup>k</sup>	93.9	92.5	95.0	92.9	93.1
Mol. Weight. <sup>l</sup>	638	929	477	774	518
Interfacial Properties					
Interf. Tension. <sup>m</sup>	0.6	1.2	11.1	0.7	15.5
ISC <sup>n</sup>	4000	650	500	1050	3700
Interf. Area <sup>p</sup>	113	132	187	156	°
Interf. Conc. ex. (Γ) <sup>q</sup>	1.47	1.26	0.89	1.06	°

<sup>a</sup>The fractions were separated by ion-exchanged chromatography according with the literature [14-17]. Numbers in bracket indicate percentage w/w with respect to Cerro Negro Crude oil. <sup>b</sup>Cerro Negro Crude oil. <sup>c</sup>Total acid fraction. <sup>d</sup>Basic and neutral fraction obtained from TAF separation. <sup>e</sup>Strong basic fraction. <sup>f</sup>Basic and neutral fraction obtained from SAF separation. <sup>g</sup>Absorbance ratio between  $v(C=O)$  at 1700-1710  $cm^{-1}$  and  $v(C=C)$  at 1600  $cm^{-1}$ . <sup>h</sup>Absorbance ratio between phenolic  $v(O-H)$  at 3590  $cm^{-1}$  and aromatic  $v(N-H)$  at 3460  $cm^{-1}$ . <sup>i</sup>Total acid number in mg of KOH/gr of sample. <sup>j</sup>Percentage of aromatic protons determined by H-NMR. <sup>k</sup>Percentage of aliphatic protons determined by H-NMR. <sup>l</sup>Molecular weight determined by VPO. Error  $\pm 5\%$ . <sup>m</sup>Interfacial tension (in dynes/cm  $\pm 1$ ) above its concentration of saturation for a toluene/water model system at room temperature and pH = 12. Interfacial tension without additive = 32.5 dynes/cm. <sup>n</sup>It did not show a typical Gibbs isotherm. <sup>p</sup>Interface saturation concentration in. mg/l. <sup>q</sup>Area occupied at the interface in  $\text{\AA}^2$ . <sup>r</sup>Interfacial concentration in excess  $\times 10^{10}$  moles/cm<sup>2</sup>.

# IDENTIFICATION OF ACIDIC CONSTITUENTS IN A CALIFORNIA HEAVY CRUDE

N.A. Tomczyk, R.E. Winans  
Chemistry Division, Argonne National Laboratory, Argonne IL 60439

J.H. Shinn  
Chevron Research and Technology Company, Richmond, CA 94802-0627

Keywords: Crude, Analysis, Acidic Constituents

## Abstract

Acidic constituents of heavy California crudes cause corrosion in the processing equipment. Many of the smaller acids have been identified, and this paper will focus on the heavier acidic compounds from a San Joaquin Valley crude. The acidic fraction is isolated by base extraction, methylated and analyzed by desorption high resolution mass spectrometry, NMR, and FTIR. The majority of the compound groups have been identified. The effect of mild hydrotreating on the distribution of acidic components will be discussed.

## Introduction

A well known and significant problem in crude oil processing is corrosion due to acidic constituents. It is the goal of this study to first determine the acidic compounds responsible for the corrosion, then develop an online system to treat the crude before it enters the high temperature processes. In this work, we examine the composition of acid fractions in oils before and after mild hydrotreating, a process known to reduce the corrosivity in oils with very little change in composition in other than the acidic fractions. An online system to monitor the process will be the subject of future work.

Samples of pre- and post-treated San Joaquin Valley (SJV) crudes were extracted with base. Prior to methylation, the samples were analyzed by Fourier Transform - Infrared Spectroscopy (FTIR) and by  $C^{13}$  Nuclear Magnetic Resonance (NMR). Then, after methylation, they were analyzed by High Resolution Mass Spectrometry (HRMS); the results of which will be the focus of this paper.

## Description of Samples Used

The oil was sourced from California's San Joaquin Valley, and was desalted in the commercial refinery operation. The hydrotreating consisted of heating the crude to temperatures between 550 and 650 F at hydrogen pressures between 100 and 500 psig over a commercial hydrotreating catalyst in a continuous-flow pilot plant system. Samples were taken throughout the run at various severities.

A common measure of acidity in oils was used to compare samples before and after treatment. This method, known as Neutralization Number or Total Acid Number, involves addition of potassium hydroxide (KOH) to the samples until a neutral pH is achieved, and recording the amount of base required to achieve neutrality as milligrams of base per gram of oil. The Neutralization Numbers for the untreated and treated oils discussed in this paper were 5.18 and 0.87, respectively.

## Extraction

The extraction procedure used is a version of the one developed by Seifert and Howells [1]. It requires a 45 g sample to be dissolved in 67 g of isopentane. The mixture is then extracted ten times with a base solution of 70% ethanol and 1% NaOH, followed by two times with a 70% ethanol solution. The solution is centrifuged after each extraction to separate the layers. Centrifuging often results in three layers, an organic and an aqueous separated by solids, which contain asphaltenes. These solid layers are set off to the side until the extraction of the oil is complete. The solids are then dissolved in xylene and extracted with base. The two base extracts are then combined prior to cleanup and acidification at 0°C. Once acidified, the solution is extracted with ethyl ether. The ether is washed with distilled water to neutrality and dried with  $MgSO_4$ . Approximately 100 mg of

extract is methylated with  $\text{BF}_3$  in MeOH. Percent yields were 4.90% and 2.55% for the crude and the treated oils respectively.

## Results

The samples were analyzed on a 3-sector MS-50 high resolution mass spectrometer [2]. The instrument was run in the electron impact mode. The analysis was performed using low electron voltage (17 eV) at 40,000 resolution. The samples were heated from 200 to 400° C on a probe inserted directly in the source. Mass measurements were a result of averaging the data from all the scans taken throughout the temperature range.

The spectra generated by the HRMS were analyzed by a program written in house. It calculates possible formulas for the masses detected by the instrument and categorizes them according to heteroatom substitution (i.e.  $\text{NO}_x$ ,  $\text{O}_x$ ,  $\text{S}_x$ ...) and hydrogen deficiency. The notation of substitution, such as  $\text{N}_2\text{O}_3$ , only indicates that a compound contains two nitrogen and three oxygen. It is written as such to aid in the ease of presenting the data.

The first change that is evident is the shift in average mass. As can be seen in figure 1, the peak mass in the crude distribution is approximately 580 mass units. In the hydrotreated distribution, the peak mass is around 250 mass units.

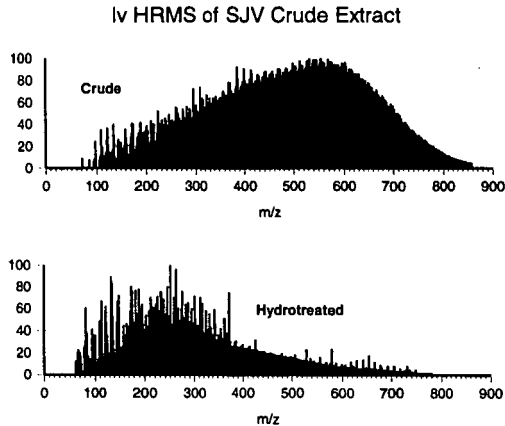


Figure 1. Mass distribution of SJV Crude and most treated product

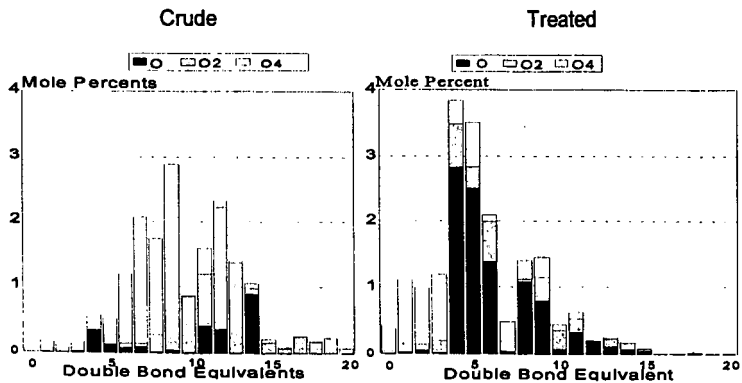


Figure 2. Distribution of oxygen containing species

Looking at figure 2, it is evident that there is a shift in the distribution of the compounds to smaller molecules. There also appears to be a shift from the  $O_4$  functional groups dominating in the crude sample to predominantly single oxygen functional groups in the treated sample without a loss of apparent compound concentration. The groupings of  $O_2$ , and  $O_3$ ,  $O_5$ , and  $O_6$  (not shown in graph) exhibited an overall reduction in concentration and compound size.

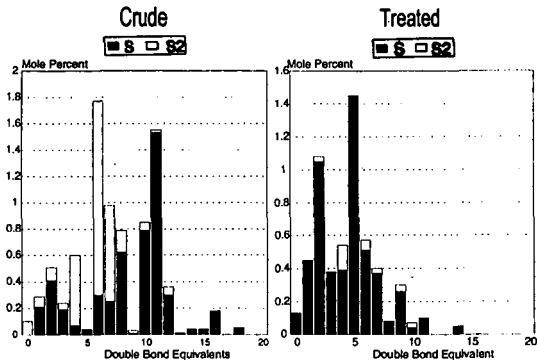


Figure 3. Distribution of sulfur containing species

In figure 3, there is not a significant loss of compounds from the crude to the treated sample. There is, however, an almost complete reduction in  $S_2$  species in the treated sample, thus increasing the concentration of compounds containing one sulfur. There is also a shift towards smaller molecules. In the crude, the compounds are distributed between 0 and 18 DBE, where as, in the treated sample, they are clustered almost entirely below 10 DBE.

Figure 4 shows a significant decrease in the concentration of  $SO_3$  (which designates compounds with a sulfur and three oxygens that are not necessarily together in one functional group) and  $SO_2$  in the treated sample coupled with an increase of  $SO$  containing compounds. There also appears to be a loss of compounds in this group. Though the concentration of the compounds between DBE zero and DBE 10 is not reduced, the compounds above DBE 10 are almost completely gone.

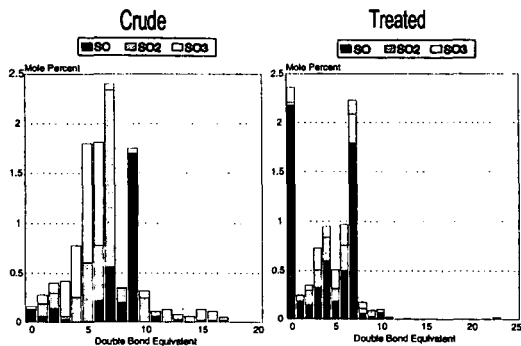


Figure 4. Distribution of  $SO_x$  containing species

For the nitrogen functional groups, in figure 5, there is a sharp reduction in the  $N$  through  $N_2$  moieties coupled with an increase in  $N_3$  groupings in the treated sample. While the distribution across the size of the molecules appears to be intact, there appears to be an overall reduction of compound concentration.

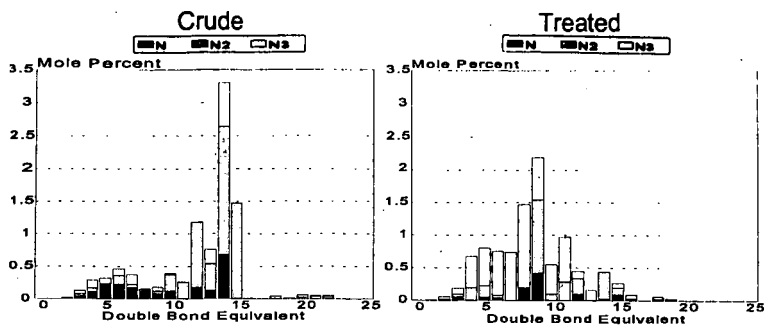


Figure 5. Distribution of nitrogen containing compounds

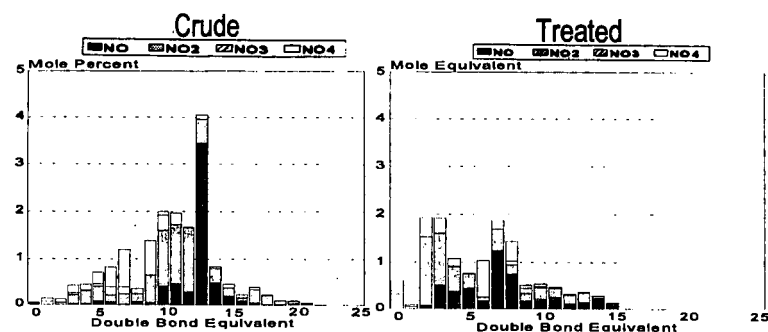


Figure 6. Distribution of  $\text{NO}_x$  containing compounds

Nitrogen-oxygen compounds appear to have had their concentration redistributed (figure 6). In the crude, it appears that the most prevalent class of compounds are those with 13 DBE (mole percent of 3.5), with lesser amounts spread between 3 and 21 DBE. In the treated sample, the distribution shifts to smaller DBE, (i.e. smaller molecule sizes). Looking at the other three  $\text{NO}_x$  moieties, appear to shift to smaller compounds coupled with a slight reduction in overall concentration.

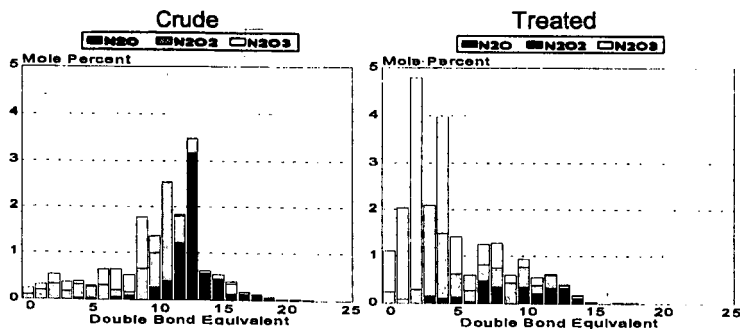


Figure 7. Distribution of  $\text{N}_2\text{O}_x$  containing compounds

The most obvious change in figure 7 is the  $N_2O_3$  grouping. There is a significant increase in the amount of compounds in the treated sample. This change is coupled with a significant a concurrent decrease in  $N_2O$ . The  $N_2O_2$  moieties are only slightly decreased in the treated sample. The redistribution of the entire series is only minor. It is the center of the concentration that is shifted from 13 DBE to 3 DBE.

Not surprisingly, the overall trend appears to be towards smaller compounds. However, while the  $S_x$ ,  $O_x$ , and  $SO_x$  groupings show a tendency towards fewer heteroatoms in the compounds, the  $N_x$  and the  $N_2O_x$  groupings appear to become more complex and keep their larger molecules.

### Conclusions and Future Work

The techniques employed in this study allow us to identify the relative concentrations of various important acidic groups in crude oils and processed products. A broad molecular-weight range of species containing various levels of oxygen, sulfur, and nitrogen are observed. The species identified include aromatic, aliphatic, and phenolic acids. Hydrotreating of acidic crudes to reduce their acid content has different impacts on the different species present. Changes in the number of species with high heteroatom content, and changes in molecular size of certain groups of species have been observed. Our current work applies these techniques to a focused group of samples designed to help understand which components most strongly relate to corrosive behavior in oils, how to facilitate measuring the corrosive species, and how to convert these species to non-corrosive forms.

### Acknowledgement

This work was performed under the auspices of the U.S. Department of Energy, under contract number W-31-109-ENG-38. This work was supported by a CRADA agreement between Chevron Research and Technology Company and Argonne National Laboratory under the U. S. Department of Energy-Bartlesville, Fossil Energy Project.

### References

- 1) Seifert, W.K. and W.G. Howells, "Interfacially Active Acids in a California Crude Oil", *Analytical Chemistry*, 41(4), 554-562 (1968).
- 2) Winans, R.E., "Mass Spectrometric Studies of Coal and Coal Macerals," *Advances in Spectroscopy*, H.L.C. Meuzelaar (ed.), Plenum Press, New York, 1992, 255.

# DYNAMICS OF ASPHALTENES SOLUTIONS IN TOLUENE STUDIED BY MEANS OF THEIR ADSORPTIONS ON GLASS SURFACES

Sócrates Acevedo, Gaston Escobar, María A. Ranaudo,  
Marisol García and Jimmy Castillo  
Universidad Central de Venezuela, Facultad de Ciencias,  
Centro de Química Organica, 47102 Caracas, 1041 Venezuela.

Keywords: asphaltene dynamics, molecular weights, aggregation, thermal lens spectroscopy

Using conventional VPO measurements in toluene and thermal lens spectroscopy (a laser technique) to measure the adsorption of asphaltenes on a glass surface from toluene solutions, the dynamics of Hamaca asphaltene solutions have been studied. The results described below are consistent with two dynamic events occurring at very different rates. In the first one the adsorbed asphaltenes were measured directly by the above laser method. When the signal corresponding to this adsorbed sample was plotted against time (solution concentration: 4000 mg l<sup>-1</sup>) a maximum, near 125 min was observed. A much lower and steady value for the signal was observed after 300 min. A similar experiment was performed with resins and a low and constant signal was observed in this case. The second event was the slow increase of average molecular weight where the number average molecular weight  $M_n$  increased, during a period of two days, from 4230 to 17420 in toluene.

## Experimental.

Two Hamaca asphaltene samples were examined. Sample A<sub>1</sub> were asphaltenes precipitated from extraheavy (8° API) Hamaca crude oil by adding 40 volumes of n-heptane to a 1:1 mixture of crude and toluene as described earlier. This sample contains about 80% asphaltenes and 20% of resins. Sample A<sub>2</sub> was a resin-free asphaltene obtained by washing the above A<sub>1</sub> sample with boiling n-heptane in a soxhlet apparatus during a period of three days.

## M<sub>n</sub> determinations.

These were measured in toluene at 50°C in a concentration range from 1 to 5 g l<sup>-1</sup> as described earlier<sup>1</sup>. Results are shown on Table 1 for Hamaca and for similar samples of asphaltenes obtained from another extraheavy crude oil (Cerro Negro) which are included for comparison. As shown in this table, the  $M_n$  for the A<sub>1</sub> samples could be averaged whereas the values for A<sub>2</sub> increase steadily with time. Due to limitations of the VPO technique it was impossible to measure  $M_n$  values higher than those shown on Table 1.

Hamaca Asphaltenes,							
	Time (hours)						
	0	24	48	72	96	144	216
A <sub>1</sub> <sup>a</sup>	2760	2820	2850	3350	2380	3010	2230
A <sub>2</sub>	4230	4330	17420	b	b	b	b
a: average 2770±375							
Cerro Negro Asphaltenes							
A <sub>1</sub> <sup>c</sup>	2570	3220	2880	2570	-	3500	3100
A <sub>2</sub>	5350	5470	10720	15170	b	b	b
b: M <sub>n</sub> too high to be measured by this method							
c: average 2970±370							

Table 1. M<sub>n</sub> values vs time for asphaltene samples.

## Thermal Lens Spectroscopy.

For thermal lens measurements we have used a home made thermal lens spectrometer with a collinear dual-beam configuration (see Figure 1).

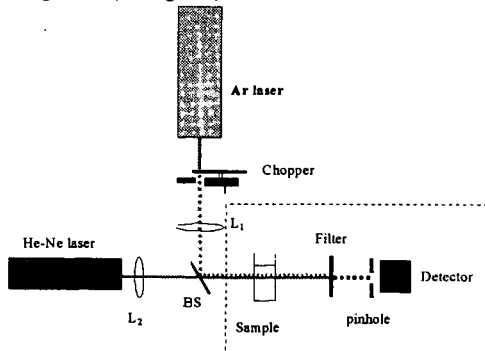


Figure 1. Experimental set-up for thermal lens spectroscopy.

A Coherent Innova 300 argon ion laser (250 mW, 488 nm) was used as a pump or excitation beam whose amplitude was modulated by a chopper and was focused onto the sample with a lens  $L_1$  (200 mm focal length). In the present case, the sample cell was the glass slide described below. A 5 mW He-Ne laser (632.8 nm) was used as probe beam and focused with lens  $L_2$  (200 mm focal length). The probe beam focus is placed 6 cm before the sample cell. A 50% beam splitter (BS) was used in order to direct collinearly the excitation and probe beam through the sample cell. The signal was obtained by sampling the intensity at the center of the probe beam with a precision pinhole and a silicon photodiode. The detector-pinhole system was mounted on a XYZ translator in order to localize the laser beam center.

### Adsorption Measurements.

Toluene solutions of the above  $A_2$  Hamaca samples were prepared as required using an ultrasound apparatus to dissolve the asphaltenes as fast as possible. For diluted solutions ( $< 1 \text{ g l}^{-1}$ ) this required less than a minute whereas for the more concentrated solutions were sonicated for 15 minutes to ensure completed dissolution. Glass slides (4 cm x 1 cm), used as adsorption surfaces, were dipped in the above solutions and stored in stoppered compartments. After the appropriate times, these were withdrawn, dried and analyzed using the above thermal lens spectroscopy. Signal averages were obtained by impinging the beams on different spots on the glass surface. Two types of experiments were performed: In the first, we monitored the signal against the time for a  $4 \text{ g l}^{-1}$  solution of asphaltene in toluene. The results are plotted in Figure 2. In the second type, toluene solutions of different concentrations were prepared, the glass slides were dipped in and measurements were recorded after 78 hours. The results are plotted on Figure 3.

### Discussion.

#### a. Time dependent experiments.

The results shown on Figure 2, could be analyzed in terms of the following considerations: During the first stages of the dissolution process the asphaltenes are present in solution as large particles formed by the association of aggregates.

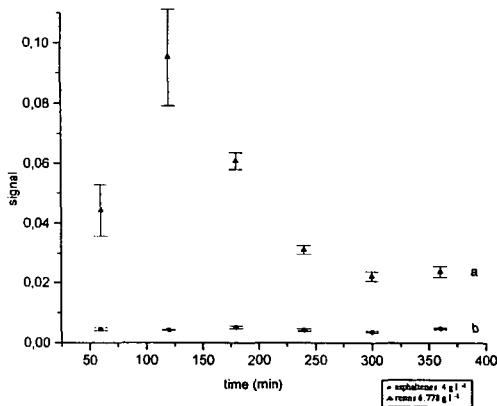


Figure 2. Adsorption of  $A_2$  Type asphaltenes (a) and resins (b) on a glass surface as a function of time.

To simplify the arguments these could be represented as  $A_n$  where each A component is an asphaltene aggregate formed by a range of molecular weight compounds from large ( $A_1$ ) to small ( $A_n$ ) molecular weight components. The  $A_n$  and A macrostructures and composition would depend on the precipitation conditions used to obtain the samples ( $A_1$  type) as well as on any further treatment employed to purify the sample ( $A_2$  type). For instance, in macrostructure A the large components  $A_1$ , formed by aromatic structures bonded through aliphatic chains in a way similar to that suggested by Strausz *et al*<sup>2</sup> would be placed at the periphery of A enclosing smaller molecular weight components. In any case we suggest that during the first stages of the adsorption process, the predominant species present in solution would be the  $A_n$  whose adsorption would account for the increase in the signal  $S(t)$  in Figure 2. After a while, dissociation of  $A_n$  in their A components will set in leading to the observed decrease in  $S(t)$  since in principle adsorption of a lower molecular weight species (A) leads to a decrease in  $S(t)$ . As shown in Figure 2, this process occurs during the first 300 minutes of measurements.

To account for the behaviour of  $M_n$  measured for the  $A_1$  and  $A_2$  samples (see Table 1) we suggest that due to entropic factors, the solvent will enter the A macrostructure breaking internal weak bonds between their components and releasing some of them. Then, the system will move to an equilibrium state consistent with the prevailing conditions of solvent, concentration and temperature. The above dynamic behaviour could be summarized by noting that both  $A_1$  and A macrostructures, as they are in samples  $A_1$  and  $A_2$  are not equilibrium macrostructures in toluene. For instance, the increase in  $M_n$  with time, for samples  $A_2$  is likely due to the removal or resins from asphaltene sites active for molecular interaction when the sample is dissolved in toluene.

## b. Concentration dependent experiments.

The adsorption isotherms of asphaltenes on inorganic surfaces, using conventional UV absorption spectroscopy, have been studied in our labs earlier<sup>3</sup>. However, due to experimental limitations inherent to this technique which leads to errors comparable or larger than the amount of sample adsorbed, the measurements have to be made at very low concentrations, usually below 200 mg l<sup>-1</sup>. Figure 3 shows clearly that use of the above thermal lens technique leads to fairly good results at low and high concentrations, due to the direct measurement of the amount adsorbed and to the high sensitivity of the laser beam. The adsorption isotherm shown in Figure 3 for Hamaca (A<sub>2</sub> sample) is consistent with a Langmuir type adsorption at low concentration. As discussed elsewhere<sup>3</sup>, the "jump" near 1000 mg l<sup>-1</sup> is probably due to the adsorption of aggregates formed after the cmc corresponding to this sample.

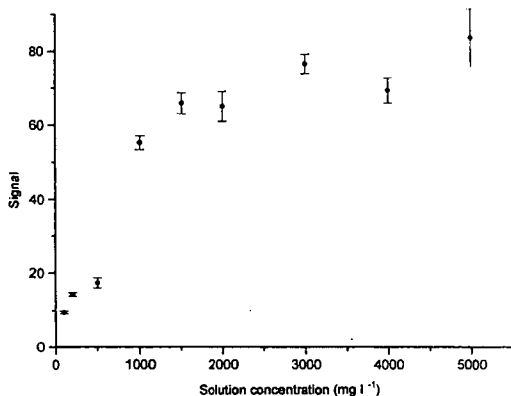


Figure 3. Adsorption isotherm of Hamaca asphaltenes (A<sub>2</sub> Type). Solvent: Toluene. Temperature: 25°C.

## References.

1. Acevedo, S., Mendez, B., Rojas, A., Layrissa, I., and Rivas, H., *Fuel*, **64**, 1741 (1985).
2. Strausz, O. P., Mojelsky, T. W., and Lown, R.M., *Fuel*, **71**, 1355 (1992).
3. Acevedo, S., Ranaudo, M. A., Escobar, G., Gutierrez, L., and Ortega, P., *Fuel*, **74**, 595 (1995).

# SEPARATION OF FRACTIONS EXHIBITING VARIABLE PARAMAGNETISM FROM HEAVY OILS AND THE STUDY OF THEIR PROPERTIES

V.A. Martynova, L.N. Andreyeva, A.A. Velikov, F.G. Unger  
Institute of Petroleum Chemistry, Russian Academy of Sciences,  
634055, Tomsk, RUSSIA

Keywords: asphaltene, resins, paramagnetism

Scanty knowledge of nature of resins and asphaltenes is the main obstacle to effective and complex use of heavy oils. There are many theoretical concepts which consider the nature of supermolecular interactions in oil dispersed systems (ODS) from the positions of electrolytic dissociation, donor-acceptor interaction,  $\pi - \pi$  interactions of polyconjugated systems, exchange (quantum) interaction and etc.

In spite of different views on the nature of resins and asphaltenes the scientists have defined that just the formation and destruction conditions for supermolecular structures in oil dispersions decisively affect the processes of extraction and thermal destruction of the system components as well as predetermine the structure and physico-chemical properties of the end products of oil processing. Based on the researches carried out at the Institute of Petroleum Chemistry RAS concerned with the paramagnetic nature of oil dispersions, asphaltenes have been found to be a concentrate of paramagnetic molecules existing as associates with diamagnetic molecules. Paramagnetic molecules and reversible homolytic transformations of diamagnetic molecules into paramagnetic ones play the main role in the transformation of supermolecular structures in oil dispersed systems and are responsible for thermodynamically unstable equilibrium of the system as a whole [1-4].

Long-term studies of ODS paramagnetic nature made it possible to substantiate theoretically: i) the presence of such molecule types in ODS which under change of external effects rather easily go from diamagnetic to paramagnetic state and if the effect is removed they return to the initial state and ii) extraction of molecule concentrates from high-viscous oils exhibiting variable paramagnetic properties [5-7]. The method developed allows to divide heavy oils into fractions with different paramagnetism. The studies of fraction behaviour by ESR- and IR-spectroscopies and by microcalorimetry during dissolution and heating showed that the level and width of energy slot for a reversible diamagnetic-paramagnetic transitions depend on structure and chemical composition of molecules. Homolytic mechanism of supermolecular structure transformations has been presented based on quantum-mechanic insight into the nature of intermolecular interactions in ODS [8-10].

## EXPERIMENTAL

At the Institute of Petroleum Chemistry RAS a method has been developed to separate fractions with variable paramagnetic properties (FVP) from crude oils and heavy residues. A specially designed device was employed. The method is based on destruction of ODS supermolecular structures from the exposure to external factors (temperature, pressure, solvent type and time delay) and on the sequential selection of concentrates of FVP molecules different in the energy of reversible diamagnetic-paramagnetic transitions, i.e. in their stability to external effects.

Presented are the results on the study of initial petrol deasphaltate obtained from commercial mixture of West Siberian oils and of extracted FVP. FVP-1 and FVP-6 exhibiting different paramagnetism are characterised in Table 1.

Table 1.

Physico-chemical characteristics of ODS

Test sample	Molecular mass (oxy-accopy)	PMS, $n \times 10^{18}$ spin/cm <sup>3</sup>	Elemental composition, wt. %						
			C	H	N	S	O	$n \times 10^2$ V Ni	
Deasphaltate	751	2.76	83.40	9.66	0.65	2.52	1.78	0.90	0.40
FVP -1	693	2.11	85.16	10.00	0.54	2.43	0.96	0.49	0.21
FVP -6	1403	71.40	85.50	8.58	1.05	2.60	2.26	3.14	1.43

FVP properties dependent on external effects (temperature and solvent amount) were studied by ESR-, IR-spectroscopies and by microcalorimetry. The effect of the nature of different solvents on the change in the concentration of paramagnetic sites (PMS, spin/cm<sup>3</sup>) in ODS has been studied previously. In the present work we used chloroform as a solvent.

## I. ESR-SPECTROSCOPY

The changes in PMS concentrations (spin/cm<sup>3</sup>) in ODS dependent on external factors were studied by ESR-spectrometer "SEX-2544" (Poland). Detailed procedure features are described in [4,8]. The results of ESR-studies of the three ODS samples (deasphaltate, FVP-1 and FVP-6) are presented in Figs. 1-4.

Fig. 1 presents the change in paramagnetic properties of the test samples versus the temperature. The test samples were vacuum pretreated and sealed in quartz ampoules. The change in ODS paramagnetism versus the solvent concentrations in chloroform is shown in Fig. 2. The change in FVP-1 paramagnetic properties versus solvent and temperature is given in Fig. 3. As is seen from ESR-spectra presented in Fig. 4, the quantitative view of the spectrum varies because of temperature and solvent effects.

Relative change in the intensity of ESR-signal for ODS versus the temperature

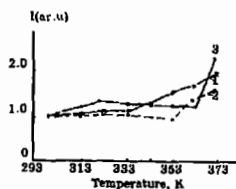


Fig. 1.  
1. desophtalinate  
2. FVP-1  
3. FVP-6

Relative change in the intensity of ESR signal for ODS in chloroform versus the concentration

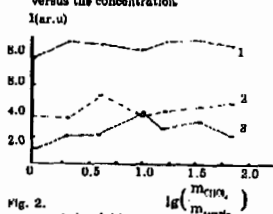


Fig. 2.  
1. desophtalinate  
2. FVP-1  
3. FVP-6

Relative change in the intensity of ESR-signal for FVP-1 in chloroform versus the concentration and temperature

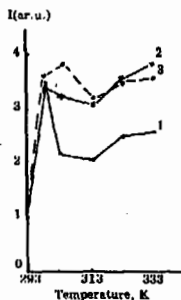


Fig. 3.  
1. FVP-1 : CHCl<sub>3</sub> wt. ratio 1:1  
2. " " " 1:2  
3. " " " 1:10

The results of ESR-studies are expressed in arbitrary units (ar.u.). PMS concentration (spin/cm<sup>3</sup>) of vacuum-treated ODS samples at 298 K is taken as a unit.

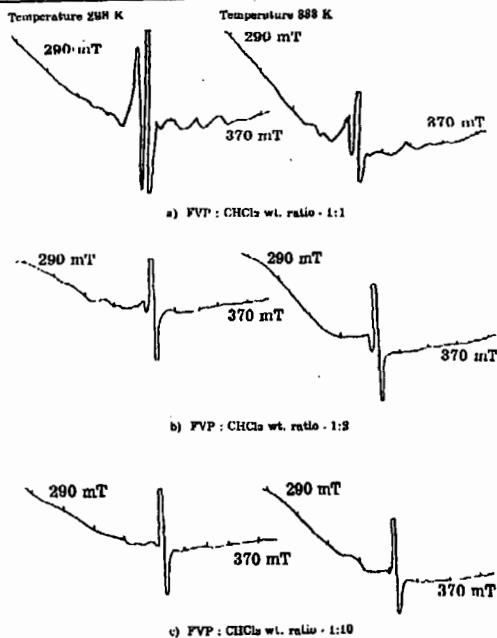


Fig. 4 (a,b,c). ESR-spectra for FVP-1 in chloroform obtained at different concentrations and temperatures

## II. IR-SPECTROSCOPY

IR-spectra were registered by "SPECORD" M-80 (Germany) in sodium chloride cells. Recorded were review solution spectra in chloroform relative to chloroform as well as film spectra of the test samples obtained from chloroform solutions in KBr window relative to air. Detailed procedure features of IR-spectra recording are given in [6,9]. The aims of IR-studies were: i) to reveal structural fragments of the molecules included in FVP and responsible for their behaviour and ii) to study the changes in  $D_{opt}$  characteristic absorption bands under dilution in chloroform.

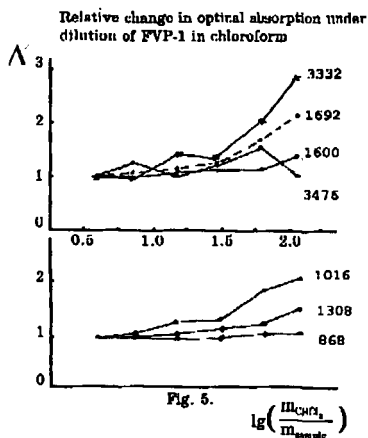
Table 2 and Figure 5 present the results of IR-spectroscopic studies. The analyses of IR-spectra made it possible the observations in the following range of wave numbers: 3600-3200; 1900-1500; 1400-1300 and 1100-800  $\text{cm}^{-1}$ , respectively.

## II. IR - SPECTROSCOPY

Table 2.

Reference of characteristic absorption bands for ODS solutions in chloroform studied by IR-spectroscopy

Wave number, $\text{cm}^{-1}$	Vibrations	Possible structures
3476	$>\text{N} - \text{H}$	pyrrol cycle
3332	$-\text{OH}$	hydroxyl group
1692	$\text{C} = \text{O}$	carbonyl group
1600	$\text{C}=\text{C}(\text{C})$	benzene rings
1308	$\text{S} = \text{O}$	sulfones, sulfonamides
1016	$\text{R} - \text{O} - \text{C} - \text{O} - \text{R}'$	acetoxy-group
868	$\nu\text{C} - \text{N}$ $\sigma\text{C} - \text{H}$ arom	nitro-, amino-groups



## III. MICROCALORIMETRY

Thermodynamic characteristics ( $Q$ ,  $J$  and  $\Delta H$ ,  $\text{kJ/mol}$ ) of ODS samples dilution in chloroform were studied by differential microcalorimeter MKDP-2, designed at the Institute of Petroleum Chemistry RAS. The sensitivity of the device is  $2 \times 10^{-3} \text{ J}$ . Detailed procedure of ODS microcalorimetric studies is given in [4,10]. The results of ODS microcalorimetric studies are given in Figs. 6-7 and in Tables 3-4. They were carried out under the conditions similar to those observed in ESR- and IR-spectroscopies.

### III. MICROCALORIMETRY

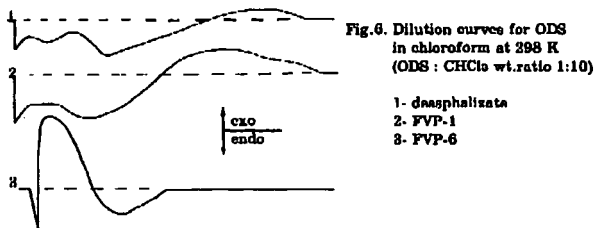


Table 3.

Enthalpies of ODS dilution in chloroform at different concentrations (298 K)

ODS : solvent wt. ratio	ΔH, kJ / mol		
	desasphaltizate	FVP-1	FVP-6
1 : 10	{ + 4.35 - 0.59	{ + 4.59 - 1.16	{ - 6.07 + 2.24
1 : 20	{ + 4.70 - 0.25	{ 4.21	{ - 6.75 + 0.20
1 : 30	{ + 5.66 - 0.59	{ + 3.45	{ - 2.29 + 3.20
1 : 40	{ 5.85	{ + 5.87	{ - 3.35 + 0.54
1 : 100	{ 12.35	{ + 4.28	{ - 4.28 + 1.94

the " + " sign - endothermic process  
the " - " sign - exothermic process

### III. MICROCALORIMETRY

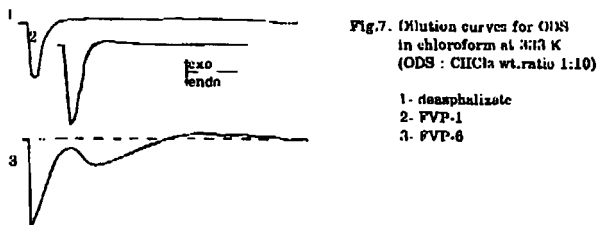


Table 4.

Enthalpies of ODS dilution in chloroform at different temperatures (ODS : CHCl<sub>3</sub> wt.ratio 1:10)

Test sample	Δ H, kJ / mol		
	Temperature, K		
	298	313	333
Desasphaltizate	{ + 4.35 - 0.59	{ + 4.28 - 0.36	{ + 1.13 - 1.04
FVP-1	{ + 4.59 - 1.15	{ + 2.72 - 0.46	{ + 1.08
FVP-6	{ 6.07 + 2.24	{ - 5.08 + 3.37	{ + 10.20 - 2.08

the " + " sign - endothermic process  
the " - " sign - exothermic process

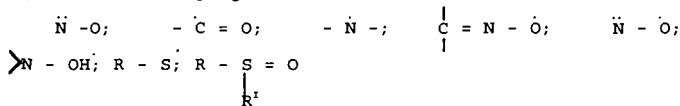
## CONCLUSION

Thus the results of ESR-studies allow to conclude that FVP really differ in their paramagnetism and under external effects exhibit variable paramagnetic properties, i.e. their components are the carriers of ODS labile properties. FVP-1 was found to be the most susceptible to external changes. Under the conditions of separation this fraction had to contain compounds with low energy of diamagnetic-paramagnetic transitions. Biradicals are known to exhibit such paramagnetic properties in the initial state and in the solutions. They are likely included in a concentrate of separated molecules (FVP) and are responsible for their variable paramagnetism as well as for unstable thermodynamic equilibrium of ODS.

IR-studies were carried out to reveal structural fragments responsible for such FVP behaviour. Seven characteristic absorption bands have been identified for all the separated FVP fractions. They differ only in their intensities. The lowest  $D_{osc}$  values were obtained for FVP-1 while the highest ones - for FVP-6. Based on elemental analysis and IR-spectroscopy it has been determined that the presence of cyclic and aromatic compounds of a polyconjugated type with S, N and O-containing fragments is typical for FVP. IR-spectra of FVP are similar and the differences in the elemental compositions are insignificant. Based only on these data it was difficult to explain a great difference in fraction behaviours determined by ESR-spectroscopy. Therefore we carried out IR-studies of FVP relative to solution concentration in chloroform.

The comparison of data obtained by ESR- and IR-spectroscopies allowed: i) to define that for ODS solutions Lambert-Buger-Beer law becomes invalid and ii) to conclude that increasing solvent portion (by  $kT$  change) in the system intensifies intermolecular interactions between solvent molecules and the components of supermolecular ODS structures. It results in the strengthened vibrations of atoms in structural fragments up to the break of separate bonds and/or to transition of a part of ODS molecules into a triple state. ESR- and IR-spectroscopies data indicate the proceeding of homolytic processes in ODS. The specific features of FVP behaviour are caused by biradical state of individual ODS components.

At present nitrite, hydrazile, phenoxy, hydrocarbon and mixed bi- and polyradicals are well known. They include the following fragments:



and etc. corroborated by our studies.

Stable biradicals with similar fragments may be attributed to a group of "biradicals with heteroatoms", the non-paired electron of which is to a great extent located on S, N and O atoms. The presence of biradicals of "metal ketyls" group is also possible.

Microcalorimetric measurements of enthalpies of ODS dilution dependent on external factors (solvent amount, temperature) indicate that these processes proceed at low energies (1-15 kJ/mol). Dilution curves have complex profile of thermal effects of dilution, which can be explained by different rate of dilution for individual ODS components as well as by transformations of supermolecular structures in the solution after a complete dilution. Sign inversion (exo-, endo-) indicates deep character of the phenomena. Comparison of the data on the relative change in PMS concentration in the system and the data on the change in dilution enthalpies ( $\Delta H$ , kJ/mol), obtained under similar conditions, indicates that the processes of dilution associate formation in ODS have a predominant-radical nature (endo-effects), which intensify under external effects (change of  $kT$  system), i.e. depend on the initial concentration of PMS in ODS, different capacity of concentrates of FVP molecules to singlet-triplet changes, on the solvent type and solvent amount and on temperatures.

The authors consider the search for mechanisms intended to control homolytic processes proceeding in ODS to be a key to solve many problems of technological preparation, transportation and processing of high-viscous crude oil and heavy oil residues.

## REFERENCES

# NEUTRON SCATTERING CHARACTERIZATION OF ASPHALTENE PARTICLES

Min Y. Lin  
Reactor Radiation Division, NIST, Gaithersburg, MD 20899  
and

E.B. Sirota and H. Gang  
Exxon Research and Engineering Co., Annandale, NJ 08801

Keywords: Asphaltene; particles; small angle neutron scattering

## 1. Introduction

The question of structure and association of asphaltene molecules in model solutions as well as in crude oils remains largely unanswered. It is however essential to the understanding of behavior of asphaltenes, specifically, their high viscosity. With small angle scattering techniques of neutrons and x-ray (SANS and SAXS), which probes length scales ranging from nanometers to near microns, it is possible to study the structure and aggregation behavior of asphaltene solutions, hence gaining the crucial information about their particle size, shape, physical interaction and phase behavior. Until recently, most such studies have concentrated on the basic asphaltene particles/micelles and their size, shape, while leaving larger size groups and long range correlations untouched, due to the difficulties of probing such long range length scales using SANS or SAXS. As a result, the high viscosity structure correlation of those solutions is still unclear.

In this work, we present first the conventional experimental data (momentum transfer  $Q > 0.01 \text{ \AA}^{-1}$ ) obtained with SANS, which can be interpreted with a model of disk like shape for the basic asphaltene particles. These particles have an average radius of gyration around  $40 \text{ \AA}$ . Even though the size distribution is fairly polydisperse, most of the particles are below  $100 \text{ \AA}$ . At larger length scales ( $Q < 0.01 \text{ \AA}^{-1}$ ), high resolution SANS data show that the scattering profile continue to rise, suggesting large length scale correlation or large particles present. While the large length scale correlation is the popular explanation, we try to interpret it as the signature of the presence of large particles. Unfortunately, those particles are so large that no scattering technique currently can probe their Guinier range to directly measure their size. Indirectly, we estimate their size based upon scaling arguments.

## 2. Basic Particles

Figure 1 shows a typical scattering intensity profile obtained from a dilute asphaltene solution with SANS. The intensity  $I(Q)$  as a function of the momentum transfer  $Q$  is over a "conventional" small angle range, i.e.,  $0.006 < Q < 0.2 \text{ \AA}^{-1}$ . In this range, the data can be fitted with a model for the particles with certain shape and size distribution. While no model is unique[1], we use a model of disk-shape and a Shultz distribution for the radius. Except at the lowest  $Q$ , the fitted curve shown in Fig. 1 is a good representative for the data. The fit results in an average radius (first moment of the radius distribution)  $a = 14 \text{ \AA}$  with a standard deviation of  $\sigma = 92\%$ , and the thickness of the disk is  $l = 20 \text{ \AA}$ .

The radius distribution is shown in Fig. 2. As can be seen, the distribution is rather broad. Indeed, if one uses the first moment to calculate the radius of gyration of the disk, it is

$$\langle R_g \rangle_1 = (a^2/2 + l^2/3)^{1/2} = 11.5 \text{ \AA},$$

which is quite small compared to the radius of gyration  $\langle R_g \rangle_G$  obtained in a Guinier fit for the same data which is close to  $40 \text{ \AA}$ . This is because that the Guinier fit represents a higher, different moment of the distribution.

The Shultz distribution has the following form: it is the product of a power law and an exponential decay:

$$P(r) = A r^{\alpha-1} \exp(-\beta r)$$

where  $\alpha = 1/\sigma^2$ ,  $\beta = \alpha/\langle r \rangle$ , and  $A$  is a normalization constant.  $\langle r \rangle$  is its first moment, and is typically used as the average. It can be shown that the  $n$ th moment is

$$\langle r^n \rangle = \langle r \rangle^n (\alpha+n-1) \dots (\alpha+2)(\alpha+1)/\alpha^n$$

The Guinier radius of gyration is obtained as

$$\langle R_g \rangle_G^2 = -3 \frac{\partial}{\partial(Q^2)} \ln I(Q \rightarrow 0) = \langle m^2 R_g^2 \rangle / \langle m^2 \rangle.$$

For the disk model, it is related to the 6th moment, and therefore is

$$\langle R_g \rangle^2 = \langle r^6 \rangle / 2 \langle r^4 \rangle + l/3 = 47.8 \text{ \AA},$$

which is more than 4 times larger than the first moment.

### 3. Large Size Particles

Even though the size distribution of the "basic" asphaltene particles are fairly broad, a typical particle size is well below 100 Å. The rheological property of the solutions can hardly be understood by the mere existence of these particles, if no further interaction or association of them is considered. However, in the Q range shown in Fig. 1, scattering intensity for concentration below 5% scales with the concentration, suggesting no interaction in the length scales probed[2]. The only interaction shown by SANS is the rise in intensity for  $Q < 0.01 \text{ \AA}^{-1}$ . Unfortunately, this has been largely ignored, mostly due to the limited range it is probed. However, it could be an important clue for the interaction or structure that is responsible for the macroscopic properties.

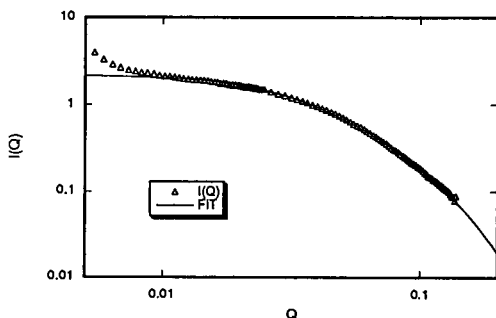


Fig. 1 SANS intensity as a function of Q. It was taken from a 2.5 wt% asphaltene (C7) solution in 1-methyl naphthalene-d10 at temperature 60 °C. The solid line is a fit with a disk-like particle shape. The distribution of the radius of the disk is shown in Fig. 2.

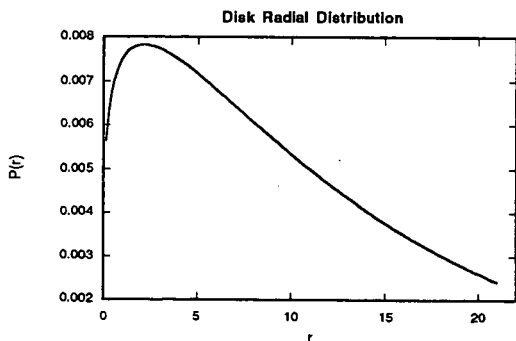


Fig. 2 Shultz distribution of the disk radius used to fit the data in Fig. 1. The average radius is  $\langle r \rangle = 14 \text{ \AA}$ , and standard deviation is  $\sigma = 0.92$ .

In Fig. 3, we show two SANS data sets taken to  $Q$  below  $0.005 \text{ \AA}^{-1}$ . In this extended  $Q$  range, the low- $Q$  rise in intensity is more dominant. A quantitative analysis of the low- $Q$  data in terms of the interactions of the basic particles is still difficult, although a fractal model has been proposed[3]. In our data, however, the slope shown at low  $Q$  is close to  $s = -4$ , the Porod slope, therefore it is not possible for a fractal structure (a mass fractal has  $s > -3$ , where  $-s$  is the fractal dimension). On the other hand, a slope of  $-4$  is typical for a compact object, in a Porod region of scattering intensity, much like those basic particles, which show a similar behavior, but at much larger  $Q$  ( $Q > 0.1 \text{ \AA}^{-1}$ ), as shown also in the Figure. We can speculate that there are very large particles present in the solution, which could be compact aggregates of the basic, much smaller particles discussed above. However, the Guinier range of those large particles are in such a  $Q$  that is too small to measure by today's small angle scattering instruments. Light scattering would provide a right  $Q$  range, but the high absorption of light by those particles makes a light scattering measurement very difficult, if not impossible.

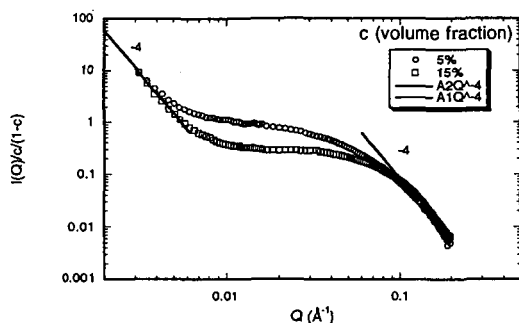


Fig. 3 SANS intensity normalized by the concentration for 5.0 wt% (circles) and 15 wt% (squares) in 1-methylnaphthalene-d10 at room temperature. At both lowest and highest  $Q$  ranges, the data show a  $-4$  slope (Porod scattering).

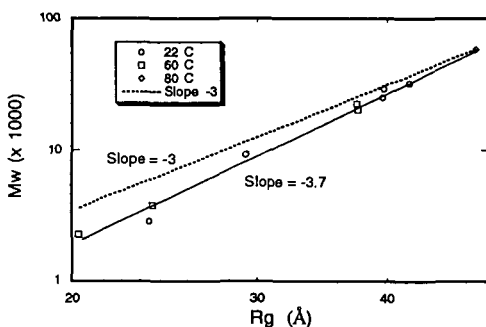


Fig. 4 Molecular weights and radii of gyration obtained from several solutions ranging from 0.5 wt% to 24 wt% at varying temperatures. Each point represents one solution at one temperature.

In Fig. 4, we plot the radius of gyration  $\langle R_g \rangle_G$  as a function of its molecular weight  $M_w$  (particle mass multiplied by the Avogadro constant) of the basic particle obtained for several solutions at different temperatures. While both  $\langle R_g \rangle_G$  and  $M_w$  are obtained from the same curve, they are actually independent. Although some of the solutions are higher than 5%, we assume that there are no interactions between the basic particles for both numbers to be meaningful. This assumption is related to, and consistent with the other assumption that the low  $Q$  behavior of the scattering is due to another group of particles with much larger sizes. Drawing a straight line through the points in the logarithmic plot, we find a slope of  $s = 3.7$ . Since  $M \sim R^d$ , where  $R$  and  $M$  are the size and mass of a particle, we should have  $s = d$ . The dimension  $d$  can never be larger than 3 in 3 dimension space where the asphaltene solutions are, unless the mass is not conserved.

This is actually consistent with the assumption that there are another group of mass present in the solution, and the total mass of the basic particles is indeed not conserved. It flows back and forth to the large size group, as conditions like concentration and temperature change. When concentration is increased or temperature lowered, there are more basic particles aggregated to form larger particles, resulting in a decrease of the total mass for the basic particles. If we assume both groups are compact particles ( $d = 3$ ) as suggested by the slopes of  $-4$  in Fig. 3, we can draw another line in the figure, with a slope of  $s = d = 3$ . The interception of the two lines is at a point taken from a 0.5 wt% solution at 80 C, where the low  $Q$  scattering is almost flat, suggesting no large size group present. The vertical distance between the two lines relative to the height of the upper line gives the percentage of mass missing from the smaller size group, and therefore is the percentage of mass residing in the large size group. Since we know the total concentration of the solution  $c$ , we then know from the graph  $c_1$  and  $c_2$ , the concentrations of each group, as  $c = c_1 + c_2$ , the total mass has to be conserved.

Furthermore, the amplitude of the intensity in a Porod region is proportional to both concentration  $c$  and  $S/V$ , where the surface to volume ratio for most low aspect ratio objects is in turn proportional to  $1/R_g$ , its size inversed. Thus for the two groups in the same solution under certain temperature, we have

$$\frac{A_1}{A_2} = \frac{c_1 R_{g2}}{c_2 R_{g1}}$$

$$\text{or } R_{g2} = \frac{A_1 c_2}{A_2 c_1} R_{g1}.$$

Since we know all the quantities on the right side, we can then calculate the larger size  $R_{g2}$ . For the 15 wt% solution, we obtain  $R_{g2} = 9.7 \mu\text{m}$ . The size is fairly large, and we need independent verification.

#### 4. Conclusion

We present an analysis for asphaltene solution data obtained with SANS that suggest the presence of two distinctive groups of particles, vastly different in their sizes. The "basic" group, while smaller in size, is the majority when the solution is very dilute and temperature is high. Their typical size is about 40 Å and is readily seen by SANS and SAXS. For the other group, the size is larger than 1000 Å and therefore is hard to probe even by high resolution SANS or SAXS. They are mostly results of the aggregation of the smaller-size particles when concentration is high and temperature is low. From thermodynamic point of view, it is not totally unreasonable. However, many questions remain, e.g., one of which is why no particles in the intermediate size range exist.

This analysis is in contradiction to the conventional understanding that the low  $Q$  behavior of the scattering merely reflects the interactions among the basic particles. More recently we performed experiments before and after dilute solutions were filtered with sub-micron filters, partially confirming the results of our analysis.

#### References

1. E.Y. Sheu, and D.A. Storm, in E.Y. Sheu and O.C. Mullins (editors) *Asphaltenes, Fundamentals and Applications*, Plenum Press, New York, (1993).
2. M.Y. Lin et al, unpublished.
3. J. Briant, G. Hotier, *Revue de l'Institut Francais du Petrole*, **38**(1), 83 (1983); and Y.C. Liu, E.Y. Sheu, S.H. Chen and D.A. Storm, *Fuel* **74**, 1352 (1995).

# AN IMPROVED CHROMATOGRAPHIC METHOD FOR THE SEPARATION OF SATURATED HYDROCARBONS, AROMATIC HYDROCARBONS, RESINS AND ASPHALTENES FROM HEAVY CRUDE OILS

Carlos De La Cruz\*, Nelson Márquez, Marcos Escobar and Soraya Segovia

Laboratorio de Espectroscopía Molecular y Atómica, and Laboratorio de Petroquímica y Surfactantes, Departamento de Química, Facultad Experimental de Ciencias, La Universidad del Zulia, Maracaibo-VENEZUELA.

**Keywords:** Heavy crude oils, resins, asphaltenes.

## INTRODUCTION.

Two general chromatographic methods have been used to isolate molecular fractions from heavy crude oils. The first of these involves initially a n-paraffinic extraction of the maltenes (solubles) and asphaltenes (insolubles) from heavy crude oils, and later the liquid-solid chromatographic separation of the maltenes into saturated hydrocarbons and polar compounds such as "polar aromatics" and resins (1). The second chromatographic method involves the direct separation of saturated and aromatic hydrocarbons, resins and asphaltenes from heavy crude oils using appropriate solvents and adsorbents (2,3,4). The main disadvantage of both methods is the lack of reproducible results due to the very complex and similar resin and asphaltene molecular structures (5,6).

We report in this paper an improved chromatographic method for the separation of 5 molecular fractions from a typical heavy crude oil, and study the reproducibility of it. The isolated fractions are characterized using UV-Visible and Atomic Absorption Spectroscopies. The results obtained with this method are compared with those of the standard literature.

## EXPERIMENTAL.

### Sample.

The heavy crude oil (10.3° API gravity) comes from the Boscán Field, near Maracaibo city, Venezuela. It was kindly provided without water and sediments by INPELUZ.

### Chromatographic separation.

The chromatography consists of the extraction of 5 molecular fractions from an activated alumina (Brockman, Activity I, 80-200 mesh, Fisher, Pittsburgh-USA)/ alumina-impregnated heavy crude oil/ activated alumina in a 2.5 cm x 75 cm glass column. The elucidation of the fractions was based upon Snyder polarities (7). The solvents, followed in brackets by their polarities, and fractions were:

- (a) n-heptane (0,2)/ saturated hydrocarbons,
- (b) 75:25 n-heptane:toluene (0,75)/ aromatic hydrocarbons I;
- (c) Toluene (2,4)/ aromatic hydrocarbons II;
- (d) 94:6 toluene:MeOH (2,57)/ resins;
- (e) 13,3:26,7:60 MeOH: N,N Dimethyl formamide (DMF): CH<sub>3</sub>CN(5,9) / asphaltenes.

The separation between saturated hydrocarbons and aromatic hydrocarbons I was monitored using a UV-lamp. The aromatic hydrocarbons I was a light yellow fraction. The aromatic hydrocarbons II, resins and asphaltenes were orange, black and black-brown fractions, respectively.

### UV-Vis spectroscopy.

The UV-Vis spectra of the saturated hydrocarbons, aromatic hydrocarbons I, aromatic hydrocarbons II, resins, asphaltenes and vanadyl octaethylporphine (obtained from Strem Chemicals, Newburyport-USA; and used for quantification, see results and discussion below) in spectranalized CH<sub>2</sub>Cl<sub>2</sub> were determined in a double-beam ratio recording Perkin Elmer Lambda 3B Spectrophotometer.

### Atomic Absorption spectroscopy.

The Fe, Ni, and V contents of the resins, asphaltenes and standards of ferric chloride (Fisher, Pittsburgh-USA), metallic nickel (Fisher, Pittsburgh-USA), and ammonium

metavanadate (Strem Chemicals, Newburyport-USA) were determined with a Perkin Elmer Atomic Absorption 3100 Spectrophotometer.

## RESULTS AND DISCUSSION.

Table I shows the type of molecular fraction, the percentage of each fraction weight divided by the heavy crude oil weight (wt % original crude) and the Fe, Ni and V contents (in mg x Kg or ppm) of the last two fractions obtained using our chromatographic method. It also compares our results with those obtained from two standard chromatographic methods reported by ASTM (1) and Barwise and his co-worker (4).

TABLE I.  
THE MOLECULAR FRACTIONS FROM A TYPICAL HEAVY CRUDE OIL.

Method	Molecular Fraction*	Wt % of Original Crude	Fe (ppm)	Ni (ppm)	V (ppm)	V-P** (ppm)
ASTM (1)	S	10,1				
	AR	13,8				
	R	27,2	40,4	132,2	814,7	624,8
	A	29,3	177,4	373,2	2884,2	1120,9
BARWISE (4)	S	32,8				
	AR	12,8				
	R	1,4?				
	A	24,3	334,4	195,6	3580,9	2065,6
THIS WORK	S	19,3				
	ARI	21,3				
	ARII	15,3				
	R	25,1	42,6	208,8	1560,6	1045,6
	A	11,3	124,8	325,5	3748,4	1540,4

\* S: Saturated Hydrocarbons; AR: Aromatic Hydrocarbons, R: Resins; A: Asphaltenes.

\*\* V-P: Vanadium in Porphyrins.

It is important to point out that the ASTM method starts with a n-pentane extraction of the maltenes and asphaltenes. Then the maltenes are fractionated into saturated hydrocarbons (i.e., paraffins and naphthenes) with n-pentane, and polar compounds (i.e., *polar aromatics* and resins) with a 50:50 benzene:acetone solution in two parallel assembled columns packed with Attapulgas clay (30-60 mesh) and clay/silica gel. Aromatics are calculated by difference, or alternatively they can be recovered using toluene. The Barwise method starts with an extraction of the saturated hydrocarbons with n-heptane, and then follows it with the extraction of the aromatic hydrocarbons, *Ni-porphyrins*, *V-porphyrins* and a *residual polar fraction (resins?)* with 80:20 n-heptane:CH<sub>2</sub>Cl<sub>2</sub> solution, 50:50 n-heptane:CH<sub>2</sub>Cl<sub>2</sub>, CH<sub>2</sub>Cl<sub>2</sub>, 50:50 toluene:CH<sub>3</sub>OH solution, respectively in a column packed with silica. We consider that the Ni-porphyrins and V-porphyrins form basically the asphaltene fraction.

The addition of the wt % of the original crude values for each method in Table I gives the following total recovery sequence: this work (92,3%, of which 55,9% corresponds to saturated and aromatic hydrocarbons, and 36,4% to resins and asphaltenes) > ASTM (80,4%, 23,9%, 56,6%) > Barwise (71,3%, 45,6%, 25,7%). Similarly, the atomic absorption spectroscopic sequence for the total Fe, Ni and V contents for each method is: this work (6010,7 ppm, of which 5309 corresponds to V) > ASTM (4422,1 ppm, 3698,9 ppm) > Barwise (4110,9 ppm, 3580,9 ppm). The V content can be divided into porphyrinic vanadium (V-P) and non-porphyrinic vanadium (8) using the Soret band at 409 nm in the UV-Visible spectra of the collected fractions and the model vanadium compound. This procedure indicates that our method removed 2586 ppm and 2723 ppm of porphyrinic and non-porphyrinic vanadium, respectively. The Barwise and ASTM methods removed (2065,6 ppm, 1515,3 ppm) and (1745,7 ppm, 1953,2 ppm), respectively. Table I shows that the porphyrinic and non-porphyrinic vanadium is found in the resinic and asphaltenic fractions. The UV-Visible spectra of these fractions show basically a very strong and sharp band at ca. 234 nm, two strong and very broad overlapped bands at ca. 274 nm and ca. 300 nm and the already mentioned Soret band (see for example the UV-Visible spectra of Figure 1). The 234, 274 and 300-nm bands can be associated with condensed di-aromatic and poly-aromatic compounds that probably carry alkyl and alicyclic chains with heteroelements (i.e.

nitrogen, oxygen and sulfur). This indicates the intimate relationship between resins and asphaltenes, and the difficulty to obtain pure chromatographic fractions .

Finally, we had performed our chromatographic separation several times, and obtained very similar results to those reported above.

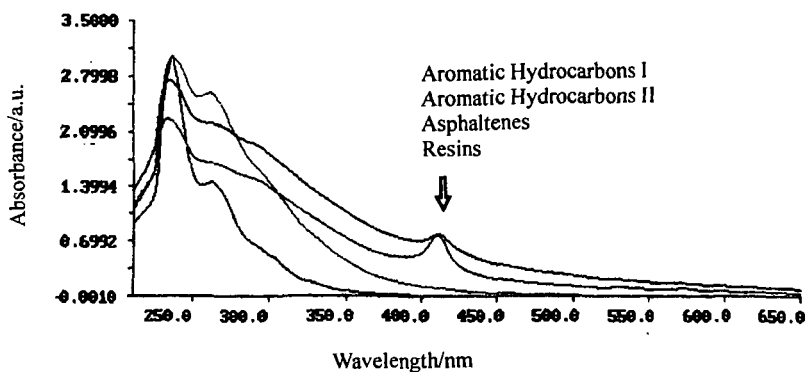


FIGURE I.  
The UV-Visible spectra of the molecular fractions of a heavy crude oil.

#### ACKNOWLEDGMENTS

The authors would like to thank CONDES and CONICIT for providing financial support for this research.

#### LITERATURE CITED

- (1) American Society for Testing and Materials, ASTM-D-2007-75, Annual Book of ASTM, Standard Part 37, 542 (1975).
- (2) Osorio, E., Angulo, E., Segovia, S., Ysambert, F, Márquez, N and De La Cruz, C., *Act. Cient. Venez.*, 45, 1 (1994).
- (3) Márquez, N., Gall, C., Tudares, C., Paredes, J. and De La Cruz, C., *A.C.S. Preprints, Div. Petrol. Chem.*, 34, 292 (1989).
- (4) Barwise, A. J.C. and Roberts, I., *Org. Geochem.*, 6, 167 (1984).
- (5) Speight, J. G., *A.C.S. Preprints, Div. Petrol. Chem.*, 34, 321 (1989).
- (6) Mitra-Kirtley, S., Mullins, O.C., Van Elp, J., George, S.J., Chen, J. and Cramer, S. P., *J. Amer. Chem. Soc.*, 115, 252 (1993).
- (7) Snyder, L. R., *J. Chromatogr. Sci.*, 16, 223 (1978).
- (8) Ysambert, F., Márquez, N., Rangel, B., Bauza, R. and De La Cruz, C., *Sep. Sci. Technol.* 30, 2539 (1995).

# ANALYSIS OF SULFUR X-RAY ABSORPTION NEAR-EDGE SPECTROSCOPY IN ASPHALTENES, RESINS, AND MALTENES OF TWO DIFFERENT CRUDE OILS

Sudipa Mitra-Kirtley\*, Oliver C. Mullins<sup>†</sup>, Corie Ralston<sup>‡</sup>, Dean Sellis\*, and Courtney Pareis\*

\*Rose-Hulman Institute of Technology, Terre Haute, IN 47803

<sup>†</sup>Schlumberger-Doll Research, Old Quarry Road, Ridgefield, CT 06877

<sup>‡</sup>University of California, Davis, CA 95616

Keywords: XANES, sulfur, asphaltenes, resins, maltenes

Sulfur chemical structures present in crude oil products such as petroleum asphaltenes, resins, and maltenes obtained from two different oils have been determined using X-ray absorption near-edge structure (XANES) spectroscopy. Maltenes are pentane soluble portions, resins are pentane insoluble and heptane soluble portions, and asphaltenes are heptane insoluble portions of crude oil. The sulfur forms in these six fossil fuel samples are predominately organic; of them thiophene, sulfide and sulfoxide are the main contributors. One of the crude oils is known to have a high sulfoxide content; results from this study showed that there is a considerable amount of sulfoxide present in its asphaltene, resin, and maltene fractions. In spite of the fact that asphaltenes are known to be more polar than the other two fractions, and also that sulfoxide is a very polar chemical moiety, this structure is present in considerable amounts also in the resin and the maltene fractions of this particular crude oil. The second oil, lower in oxygen content, showed consistently less amount of sulfoxide in all its asphaltene, resin, and maltene fractions. Furthermore, no evidence for higher oxides such as sulfones, sulfonates, and sulfates are found in the three fractions of either of the crude oils.

## INTRODUCTION

Asphaltenes, resins, and maltenes are some of the components of crude oil, and are of considerable interest.<sup>1,3</sup> The usual definition of these fractions are: maltenes are pentane soluble portions, resins are pentane insoluble and heptane soluble portions, and asphaltenes are heptane insoluble portions of crude oil. Asphaltenes are the heaviest, the next are resins, and the lightest parts of a crude oil are the maltenes. These fractions contain undesired heteroatoms; these heteroatoms are an issue in atmospheric pollution in the utilization of the resources. The study of heteroatoms, such as sulfur, in these components obtained from a particular crude oil is therefore of much interest, also in order to better understand the complex processes of crude oil formation.

Non-destructive and direct XANES spectroscopy methods have been very promising in analyzing the heteroatom structures of complex fossil-fuel samples. XANES spectroscopy has been recently employed to probe the chemical nature of sulfur in different fossil-fuel components<sup>3</sup> such as asphaltenes,<sup>4,6</sup> crude oils<sup>7</sup> and coal.<sup>8</sup> In asphaltenes the sulfur is found in mostly thiophenic and sulfidic forms, and the oxidized sulfur component in sulfoxide forms. In coal, sulfur exists in both organic and inorganic forms. Nitrogen XANES studies<sup>9</sup> on asphaltenes have shown that nitrogen occurs mostly in aromatic forms in pyrrolic and pyridinic forms.

In this study we present preliminary results of sulfur XANES spectroscopy on asphaltenes, resins, and maltenes obtained from two different crude oils. Several sulfur model compounds have been studied, and it is found that consistent with earlier results,<sup>7</sup> the *s*-*p* electronic transition peak in the XANES spectra vary in energies as the formal oxidation number of sulfur changes. The sulfoxide signature is well separated from the thiophenic signature, by about 3.00 eV. The organic sulfide peak also is separated from thiophenic peak by about 1.00 eV. The asphaltene fraction of one of the crude oils, CAL, is known to have a high sulfoxide content; the resin, and maltene fractions from this oil also consistently show much higher sulfoxide content than the three fractions from the other crude oil. In spite of the fact that asphaltenes are known to be more polar than the other two fractions, and also that sulfoxide is a very polar chemical moiety, this structure is present in considerable amounts also in the resin and the maltene fractions of this particular crude oil. Other forms of oxidized sulfur are not prominent in any of these samples.

## EXPERIMENTAL

Our sulfur data have been collected at beamline X-19A at National Synchrotron Light Source at Brookhaven National Laboratory. We used a double crystal monochromator of Si (111) crystals. The model samples were first diluted in boric acid, finely ground, and then smeared on sulfur-free Mylar film; the fossil fuel samples were either ground and mounted on the film, or diluted in CCl<sub>4</sub> and smeared to dry on the film.

All sulfur models were obtained from Aldrich Chemical Company; they were dibenzyl sulfide, dibenzothiophene, thianaphthene, dibenzyl sulfoxide, iron(II) sulfide, potassium sulfate, and sodium thiosulfate. The fossil-fuel samples were asphaltenes, resins, and maltenes, obtained from CAL and KUW crude oils.

## RESULTS AND DISCUSSIONS

Figure 1 plots the sulfur XANES of the asphaltene, maltene, and resin fractions obtained from CAL, KUW crude oils. Among the CAL suite, the most prominent region is around 2475.1 eV; the shoulder of this peak at around 2472.1 eV is quite prominent in all these samples. From the KUW suite, the most prominent feature occurs at 2472.1 eV, and the feature at 2475.1 eV is much less prominent. Thus from raw data it is evident that the structure with its s-p transition peak at 2475.1 eV is more abundant in the CAL suite than in the KUW suite. This trend is present in all the three fractions belonging to the same oil.

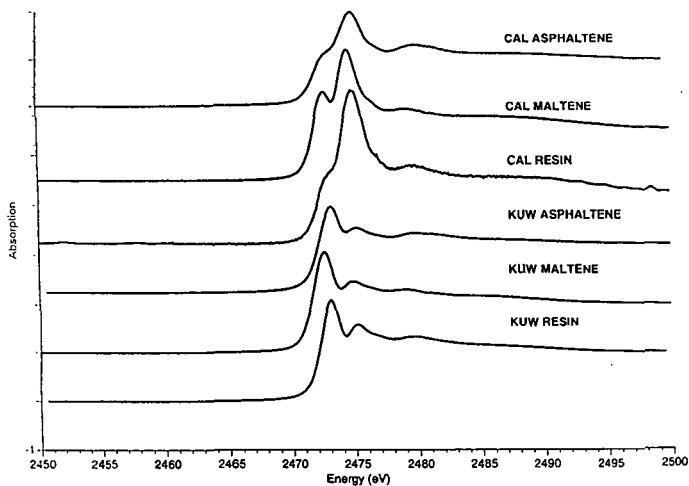


Figure 1: Sulfur XANES spectra of the asphaltene, maltene and resin fractions of CAL and KUW crude oils.

Figure 2 shows the XANES plots of several sulfur model compounds, studied by Waldo et al.<sup>7</sup> As mentioned earlier, the most prominent peak of a structure represents the s-p electronic transition peak. This figure shows that the different sulfur structures have s-p peaks located at different energies; these peaks shift to higher energies as the formal oxidation number of sulfur in the structure increases. As the formal oxidation number of sulfur in a structure increases, the electronics in the atom are more tightly bound to the nucleus, and it takes a larger energy to make the s-p transition. Our calibration procedure has resulted in a shift from these data by a few eV, but both the data sets show the same relative energy differences between the different sulfur structures. Dibenzyl sulfide, which has a formal oxidation number of zero, shows its prominent peak at 2474 eV (2471.1 eV in our case). Thiophene also has a formal oxidation number of zero, but the signature peak is shifted slightly from that of the sulfide, and occurs at 2475 eV (2472 eV in our case). The sulfoxide structure has a formal oxidation number of +2, and shows its signature peak much separated from the other two, at 2478 eV (2475.1 eV in our case).

XANES spectra of a maltene from the two different oils are shown in Figure 3. It is seen that the first peak of the KUW maltene appears at 2472.1 eV, the same energy as the main peak of our dibenzothiophene spectrum, and this feature appears only as a shoulder in the spectrum of CAL asphaltene. This leads one to the obvious conclusion that sulfoxide is present in larger percentage in CAL asphaltene than in the KUW sample.

A least-squares fitting program has been used in order to quantitatively analyze all the sulfur data. All the spectra of models and the fossil-fuels were first normalized with respect to the respective step heights, and then fit to a sum of several Lorentzian peaks and an arctangent step. The peaks specify bound to bound electronic transitions, whereas the step signifies electronic transition to the continuum. In order to be consistent, we held the width and the position of the step function constant

till the very end of the fitting procedure. We subtracted from the fossil-fuel spectra any secondary contribution from a structure appearing at the same energy as the s-p transition from a different structure.

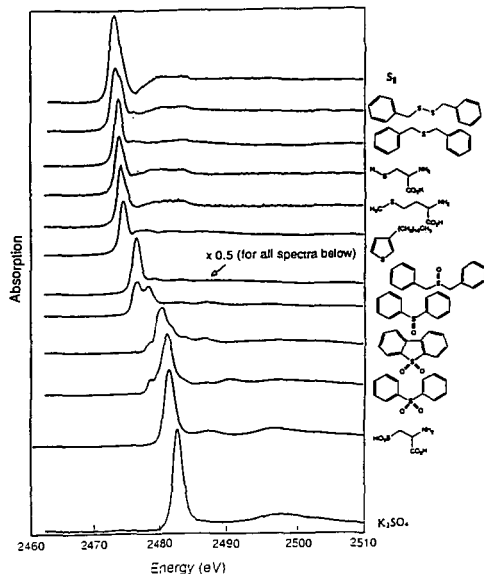


Figure 2. Sulfur XANES spectra of several model compounds. The s-p transition peaks are blue shifted as the formal oxidation number of the structure increases.

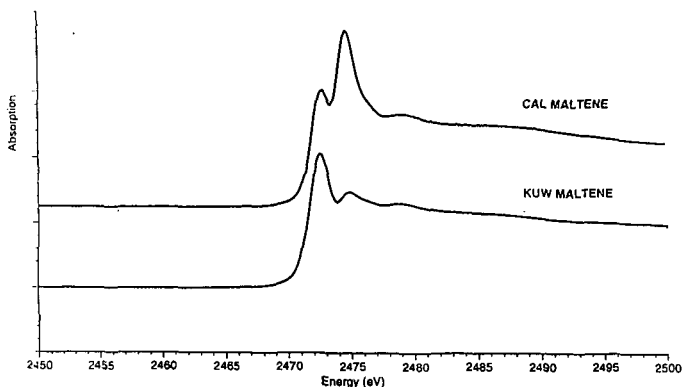


Figure 3. Sulfur XANES spectra of the maltene fractions from CAL and KUW. The differences in the resonance structures are very prominent.

Preliminary results of the sulfidic, thiophenic, and sulfoxide content of the asphaltenes, resins, and maltenes obtained from CAL and KUW crude oils show that the sulfoxide percentage in the CAL samples are higher not just in its asphaltene fraction, but also in the resin and maltene fractions. Asphaltene is known to be more polar than resin and maltene, and sulfoxide also has a very polar structure. It is interesting to note that in spite of this, all the CAL fractions showed higher sulfoxide percentages. Presence of high oxides, such as sulfone, and sulfate, in any of these samples was insignificant. There was no evidence of any inorganic sulfur structures in these samples.

## CONCLUSIONS

Sulfur XANES spectroscopy is a very powerful way to ascertain the different chemical structures present in a complex material both qualitatively and quantitatively. Asphaltene, maltene, and resin extracted from CAL, which has a high sulfoxide content, all show consistently high sulfoxide percentages. Higher oxides of sulfur, such as sulfones, and sulfates are not present in significant quantities in any of these samples.

## REFERENCES

1. G. V. Chilingarian, T. F. Yen, Editors, "Bitumens, Asphalts, and Tar Sands," Elsevier Scientific Publishing Co., New York (1978).
2. J. G. Speight, "The Chemistry and Technology of Petroleum," Marcel Dekker, Inc., New York (1980).
3. O. C. Mullins, Chapter 2, "Alphaltenes, Fundamentals and Applications," E. Y. Sheu, O. C. Mullins, Editors, Plenum Publishing Co., New York (1995).
4. G. N. George, M. L. Gorbaty, *J. Am. Chem. Soc.*, 111, 3182 (1989).
5. M. L. Gorbaty, G. N. George, S. R. Kelemen, *Fuel*, 69, 945 (1990).
6. G. S. Waldo, O. C. Mullins, J. E. Penner-Hahn, and S. P. Cramer, *Fuel*, 71, 53 (1992).
7. G. S. Waldo, R. M. K. Carlson, J. M. Moldowan, K. E. Peters, J. E. Penner-Hahn, *Geochimica et Cosmochimica Acta*, 55, 801 (1991).
8. G. P. Huffman, S. Mitra-Kirtley, F. E. Huggins, N. Shah, S. Vaidya, and F. Lu, *Energy and Fuels*, 5, 574 (1991).
9. S. Mitra-Kirtley, O. C. Mullins, J. vanElp, S. J. George, J. Chen, and S. P. Cramer, *J. Am. Chem. Soc.*, 115, 1, 252 (1993).

# MAYA PETROLEUM ASPHALTENE IMAGING BY SCANNING TUNNELING MICROSCOPY: VERIFICATION OF STRUCTURE FROM $^{13}\text{C}$ AND PROTON NUCLEAR MAGNETIC RESONANCE

G. W. Zajac\*, Amoco Corporation, N. K. Sethi and J. T. Joseph, Amoco Petroleum Products, P. O. Box 3011, Naperville, IL 60566.

Keywords: scanning tunneling microscopy, NMR structure, Maya asphaltene

## Introduction

Petroleum resids are generally upgraded to higher value products by hydroprocessing. This process, however, is very demanding because of the highly aromatic nature of the constituent molecules, high metal and heteroatom content. Most of the problems associated with resid upgrading are attributed to the presence of asphaltenes. Asphaltenes are generally believed to be the precursors of coke formation during resid processing, limiting the kinetics and economics of the process.

Asphaltene structure has been extensively investigated in the past (Speight, 1980; Strausz et al., 1992; Herzog et al., 1988; Ravey et al., 1988; Sheu et al., 1992; Storm, 1991). These studies have provided a global picture of asphaltene structure, which explains general asphaltene reactivity under thermal and catalytic conditions. Because of the dependence of the asphaltene structure on the origin of the crude oil, we performed a detailed study of this particular Maya asphaltene. This work describes a study focused on Maya asphaltenes, using carbon-13 and proton NMR and scanning tunneling microscopy.

## NMR - STM Analysis - Experimental, Results & Discussion

The asphaltene sample used in this study was obtained by heptane precipitation from Maya vacuum resid and its preparation has been discussed in detail previously (Zajac, Sethi and Joseph 1994). The virgin asphaltene sample was analyzed by carbon-13 and H-1 NMR in solution on a Varian VXR-300 spectrometer operating at 300 Mhz proton frequency. Deuterated chloroform was used as the solvent. The asphaltene sample was completely soluble in chloroform. The solubility was confirmed by filtration through a 1  $\mu\text{m}$  millipore filter that left no residue. The details of the analysis are discussed in our previous work (Zajac, Sethi and Joseph, 1994).

The average aromatic cluster parameters for virgin Maya asphaltene (heptane insolubles) were estimated from combined high resolution H-1 and C-13 NMR and atomic H/C data. Possible structural features of the virgin asphaltene molecule that include cyclic and linear aliphatic carbon atoms are illustrated in Figure 1. Three possible structural units of the virgin asphaltene are shown where the aliphatic sidechains repeat units range from  $n=1-5$ . Though no direct evidence of the precise structure groups that contain heteroatoms, N, S, O etc., is available, these are assumed to be part of the ring structure, e.g., thiophenic functional groups for S. These NMR derived structural models form the basis of input for the scanning tunneling microscopy study.

The precipitated virgin asphaltene was diluted in THF to a concentration of 1-5  $\mu\text{g/ml}$  which at the average molecular weight for the asphaltenes corresponds to a submonolayer coverage on an appropriate substrate if agglomeration does not occur. We have employed freshly cleaved highly oriented pyrolytic graphite (HOPG) as a substrate. Several microliters of the dilute solution are micropipetted on the surface and dried in dry nitrogen. A Digital Instruments Nanoscope II equipped with a side viewing stereo microscope is employed. The tunneling tips are electrochemically AC etched tungsten (250  $\mu\text{m}$ ) in 1 M KOH which are subsequently rinsed in distilled water and stored in alcohol. The tunneling conditions were typically 100-600 mV bias voltage and 0.5-2.0 nA tunneling current.

Scanning tunneling microscopy is a direct real space probe of structure. The structure of adsorbates on model surfaces resolved at the molecular level has been applied to a number of systems (see e.g. Chiang, 1992). In an ambient environment, STM studies of the adsorption geometry of alkylcyanobiphenyl on graphite has resolved the individual aromatic groups and alkyl chains (Smith et al., 1990; Mizutani et al., 1990). Previous STM imaging of Rawati asphaltenes (Watson and Barteau, 1994) at high concentrations (1, 5  $\times 10^{-2}$  wt%) in pyridine has indicated the self-assembly nature of the alkyl sidechains with large regions of self-assembled asphaltenes.

A typical 140  $\text{\AA}$  image of a cluster of asphaltenes is shown in Figure 2. The atomically resolved graphite substrate is visible and a group of asphaltenes are observed as the higher contrast regions. The dimensions are measured as full widths of the observed current perturbations. In Fig. 2, a typical measurement sets the scale of such features  $\sim 13 \text{\AA}$ . Another view of 102  $\text{\AA}$  STM

image of a similar cluster of several asphaltenes is presented in Figure 3, the highlighted feature is of order  $\sim 12$  Å. Because of the heterogeneous nature of this material it is difficult to distinguish aggregates versus individual structural units. Despite this difficulty we attempted a detailed measurement over twenty-four separate entities which were clearly isolated structures in approximately ten individual images yielding an average full width dimension of  $10.4 \text{ Å} \pm 1.9 \text{ Å}$ . A comparison is made to a random set of ten measurements from the possible NMR-derived asphaltene structural units shown in Figure 1, excluding the aliphatic sidechains. The measurements were made by calibration of the C-C bond length at  $1.42 \text{ Å}$  and making several measurements across the condensed ring portion of the three structural units presented. The average NMR dimension derived in this manner is  $11.1 \text{ Å} \pm 1.4 \text{ Å}$  for the condensed ring portion of the possible structural models. The reasonable agreement obtained between the NMR structural models and the STM observation argues in favor of the NMR molecular models.

An example of the heterogeneity in the distribution that we observe by STM is shown in Figures 4 & 5 where we find small structures in the presence of much larger structures. The larger structure shown in Fig. 4 of a  $62 \text{ Å}$  field of view is interesting for it appears to be comprised of three separate structural units which are individually  $< 20\text{-}30 \text{ Å}$ . It is not clear if the large structure is an aggregate of three smaller units or a single structure connected by aliphatic linkages. Although we do not have evidence for the existence of aliphatic sidechains, there is weak fine structure existing in the vicinity of many of the structures that we observe. At low bias voltages aromatic structures would be emphasized and aliphatic regions suppressed, hence we might be biasing our observations toward the aromatic structures.

### Summary and Conclusions

The C-13 and proton NMR analysis predicts small 6-9 ring condensed aromatic ring structural units with aliphatic sidechains for the virgin Maya asphaltene. The comparison of NMR structural models and STM direct observation reveals an agreement between the distribution of aromatic cluster sizes predicted and observed. The broad distribution ranges from several condensed rings to large macromolecular structures in excess of  $30\text{-}50 \text{ Å}$ . This study works in a very dilute limit ( $1\text{-}5 \times 10^{-3}$  wt%). During hydroprocessing NMR has shown condensation reactions to occur and that the average aromatic cluster size grows in size and number. One is tempted to extrapolate to the high concentration regime where very large aggregates and self-assemblies might dominate and form the basis of coke precipitation during the hydroprocessing process.

### References

- Chiang, S. Molecular Imaging by STM in *Scanning Tunneling Microscopy II*, H. J. Guntherodt and R. Wiesendanger (Eds.) Springer-Verlag, New York, 1992, 181.
- Herzog, P.; Tchoubar, D. and Espinat, D. Macrostructure of asphaltene dispersions by small angle x-ray scattering. *Fuel* 1988, **67**, 245.
- Mizutani, W; Shigeno, M.; Ono, M. and Kajimura, K. Voltage-dependent scanning tunneling microscopy images of liquid crystals on graphite. *Appl. Phys. Lett.* 1990, **56**, 1974.
- Ravey, J. C.; Ducouret, G. and Espinat, D. Asphaltene macrostructure by small angle neutron scattering. *Fuel* 1988, **67**, 1560.
- Sheu, E. Y.; DeTar M. M.; Storm, D. A. and DeCanio, S. J. Aggregation and kinetics of asphaltenes in organic solvents. *Fuel* 1992, **71**, 299.
- Smith, D. P. E.; Horber J. K. H.; Binnig, G. and Nejh, G. Structure, registry and imaging mechanism of alkylcyanobiphenyl molecules by tunneling microscopy. *Nature* 1990, **344**, 641.
- Speight, J. G. *The Chemistry and Technology of Petroleum* Marcel Dekker, New York, 1980.
- Storm, D. A.; Barresi, R. J.; DeCanio, S. J. Colloidal nature of vacuum residue. *Fuel* 1991, **70**, 779.
- Strausz, O. P.; Mojelsky, T. J.; Lown, E. M. The molecular structure of asphaltene: an unfolding story. *Fuel* 1992, **71**, 1355.
- Watson, B. A. and Barteau, M. A. Imaging Petroleum Asphaltenes using Scanning Tunneling Microscopy. *Industrial and Engineering Chemistry Research*, 1994 **33**, 2358.
- Zajac, G. W.; Sethi, N. K. and Joseph, J. T., Molecular Imaging of Petroleum Asphaltenes by Scanning Tunneling Microscopy: Verification of Structure from  $^{13}\text{C}$  and Proton Nuclear Magnetic Resonance Data, *Scanning Microscopy*, 1994, **8**, 463-470.

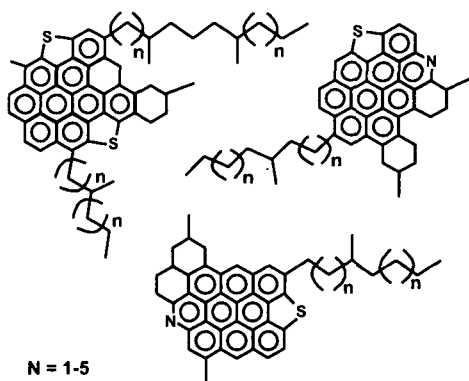


**Figure 1**  
The  $^{13}\text{C}$  and proton NMR derived average structural units in Maya asphaltenes.

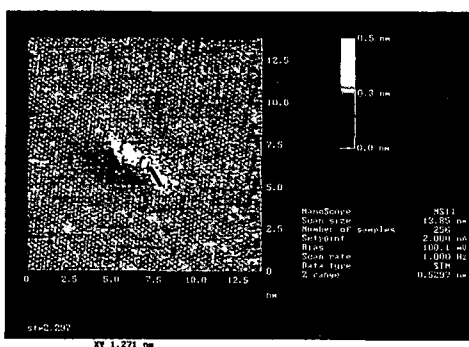


**Figure 2**  
A constant current STM 140Å view of graphite at atomic resolution with a cluster of asphaltenes appearing as bright current spots ( $V_F=100\text{mV}$ ,  $I_F=2.0\text{ nA}$ ). The white line marker indicated at bottom measures  $\sim 13\text{Å}$ .

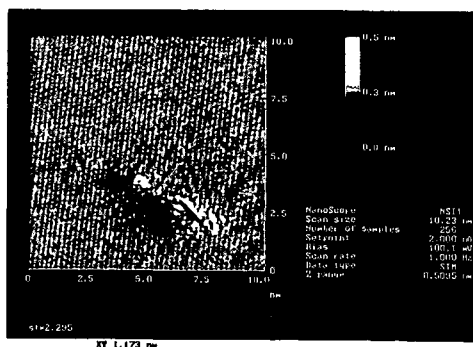


**Figure 3**  
A constant current STM 102Å view of graphite at atomic resolution with a cluster of asphaltenes, ( $V_F=100\text{mV}$ ,  $I_F=2.0\text{ nA}$ ). The marker indicates a dimension of  $\sim 12\text{Å}$ .

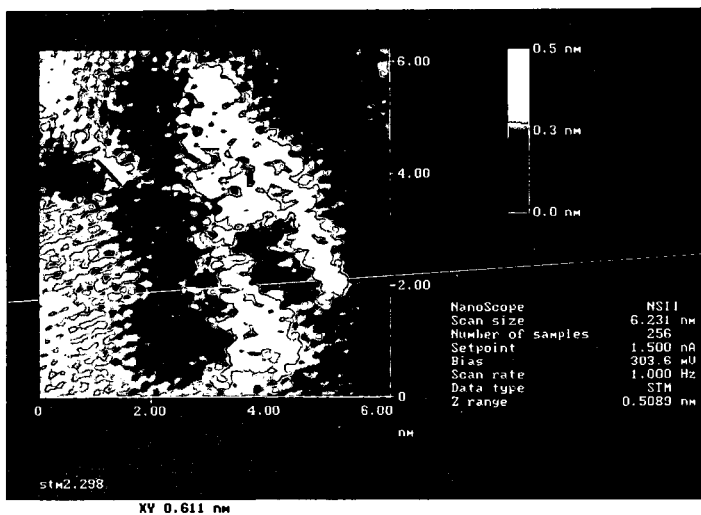


**Figure 4**  
 A constant current STM 62Å view of a large aggregated cluster of asphaltenes, ( $V_F=304\text{mV}$ ,  $I_F=1.5\text{ nA}$ ). The marker indicates an isolated structure of  $\sim 6\text{Å}$ .

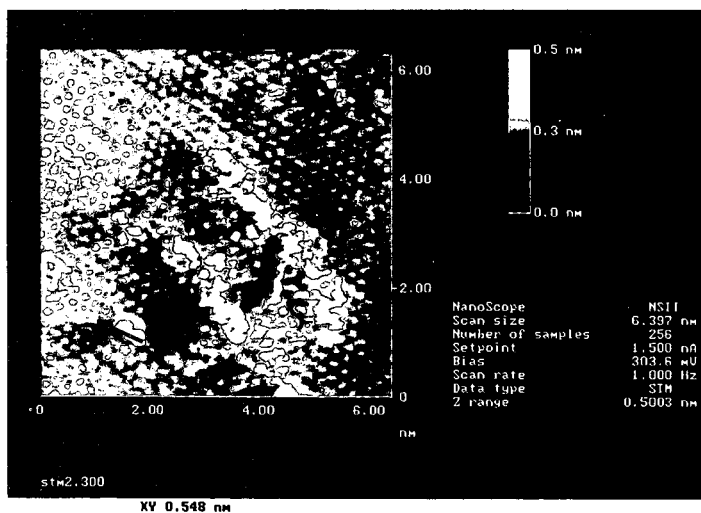


**Figure 5**  
 A constant current STM image of 64Å field of view on graphite of another asphaltene cluster, ( $V_F=304\text{mV}$ ,  $I_F=1.5\text{ nA}$ ). The marker measures an isolated structure of  $\sim 5.5\text{Å}$ .

## CHARACTERIZATION OF ASPHALTENES FROM PROCESSED RESIDS

Jerry E. Hunt and Randall E. Winans  
Argonne National Laboratory, Chemistry Division  
Argonne, IL 60439 USA  
Jeffrey T. Miller  
Amoco Corporation, Naperville, IL 60566

Keywords: asphaltene, ring size, molecular weight

### Introduction

The current and future trend for petroleum processing is towards conversion of heavier and heavier fractions into useful products such as gasoline and diesel. Asphaltenes, the heptane insoluble fraction of heavy oils, are a solubility class and not a specific boiling range. They tend to be the hardest fraction to process in the refinery because of their high molecular mass, aromaticity and heteroatom and metal (S, N, Ni, V) content. Molecular characterization of asphaltenes is important since a more thorough understanding of the chemical nature of the constituents should lead to more efficient processing schemes.

A major hurdle in the accurate representation of the molecular structure of asphaltenes has been the determination of the molecular weight. The main problem is the formation of molecular aggregates depending upon factors such as polarity of the solvent, temperature, concentration and others. Over the past 15 years or so, the apparent molecular weight of asphaltenes has dropped significantly lower as the cause and effect of aggregation on molecular weight was determined. Molecular weights as high as 500,000 have been reported for some asphaltenes in the past with weights as low as 600 appearing in the literature recently depending on the analytical method used.[1-2]

The problem of molecular aggregation has been studied by a number of techniques [5-11] including SAXS and SANS. Using SANS, Thiyagarajan, *et al.* [12] found that at room temperature that asphaltenes are highly ordered rod like species with lengths up to 500Å. As asphaltene samples are heated up, these large aggregates are broken up into smaller rod like species with average lengths of less than 100Å at temperatures of above 50°C. Further shrinkage of the aggregates occurs when the asphaltene is heated to 340-400°C resulting in spherical particles with radii of about 12Å. Returning the sample to 20°C resulted in a low intensity signal implying irreversible thermochemistry. Espinat, *et al.* [14] also using SANS, found that the size of the colloidal asphaltene particles decreased with increasing temperature or with increasing dilution with resin material and increased with the addition of *n*-hexane. Finally, Storm, *et al.* [13] found by SAXS that for asphaltenes from several sources at 93°C that the colloidal particles had an average radii of 30-60 Å. They also found that the average particle size was independent of the heteroatom content of the asphaltene. The exact mechanism by which aggregation occurs has not been established.

Recently mass spectrometry has been used to determine a limiting lower value for the molecular weight for asphaltenes. This technique found that the upper limit for the molecular weight of Ratawi asphaltene was 814 versus 2360 from VPO. The upper limit for an asphaltene from the Alaskan North Slope was determined to be less than 1270 versus 3248 from VPO. High resolution mass spectrometry (HRMS) is a well-established technique for determination of composition of petroleum distillates by compound types. HRMS provides exact mass measurement of molecular and fragment ions, allowing distinction of molecular of equal nominal mass but of different double bond equivalents. The exact mass measurements also allow classification of hydrocarbon (saturated and unsaturated) and sub-classification into heteroatom-containing (e.g., nitrogen, oxygen and sulfur) molecules. In this paper we use high resolution sector field mass spectrometry to determine the comparative speciation of the composition of the asphaltenes from resid subjected to processing conditions.

### Experimental

The resid was obtained by vacuum distillation of an asphaltene rich Maya crude oil. Asphaltenes were isolated by addition of a 40:1 excess of *n*-heptane to the Maya resid in toluene at 50 °C. The suspension was stirred overnight and filtered. The *n*-heptane was distilled from the filtrate to obtain the deasphalted oil (DAO). The yield of DAO was 83% of the resid. The precipitate was dissolved in a minimum of toluene and re-precipitated with a 40:1 excess of *n*-heptane. This precipitate was filtered, washed with *n*-pentane, and vacuum dried at 100 °C. The yield of asphaltene was 27% of the resid. The resid was processed under hydrotreating conditions at 425°C with 2000 psi H<sub>2</sub> with 0.05 weight per cent organic Mo catalyst. The extent of the reaction was monitored by GC methods.

A Kratos three-sector MS-50 mass spectrometer was used to obtain high resolution mass spectra of asphaltenes. The full-scan high-resolution (dynamic resolution of 10,000-40,000) electron

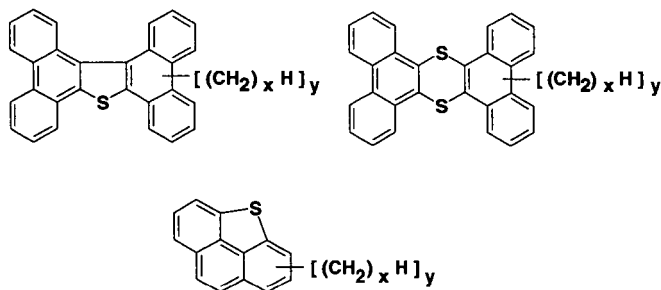
ionization (EI) mass spectra were acquired with a Kratos MS50TA triple sector tandem mass spectrometer of EBE design. High boiling perfluorokerosene was introduced via a heated inlet. Calibration to mass 900 was routinely achieved at a scan rate of 10 s/decade. The source temperature was 250 °C. Ionization method was the electron impact (70 eV). The samples were inserted into the source on a high-temperature probe. The accelerating voltage was a nominal 8 kV. The spectra were collected and recorded on the MACH 3X data system. Group analysis for all scans with ions above background was averaged and only those which occur a minimum of at least four times was saved. Formulae which fit within  $\pm 3.5$  millimass units are assigned for each averaged ion peak. The formulae are sorted by hydrogen deficiency and heteroatom content. Absolute response factors for each type of compound are not available, equal molar ionization sensitivities are assumed for all homologs in the analysis.

## Results

The mass spectra from the asphaltene fraction generally show ion intensity from 100 to almost 850 amu. The average mass of the observed spectra is about 400 amu. While this does not represent the average molecular mass when one takes into consideration that fragmentation occurs under electron impact conditions, for very aromatic species electron impact is a good indicator for molecular distributions. When the fact that asphaltenes are highly aromatic ( $C_{ar}$ -60%) is taken in account, the distributions may be only 50 to 100 amu higher. The elemental analysis calculated from the high resolution mass spectral data are in good agreement with those from traditional techniques, with aromaticity values slightly lower for the mass spectral data. This means that the mass spectral data is representative of the actual sample. Furthermore, at least 90% of the asphaltene is volatilized in to the mass spectrometer.

In the high resolution mass spectrum thousands of peaks can be measured. This number of peaks makes reducing the data into a more manageable form necessary. The double bond equivalent (dbe) and the heteroatom content can be calculated from the exact mass data without any assumptions. Sulfur combinations may be misrepresented, but oxygen and nitrogen should not have a high probability of misrepresentation. However, the elemental analysis data extracted from the mass data show that these errors are minimal. Detailed distributions of asphaltene sulfur and nitrogen organic molecules as a function of double bond equivalent for three processing levels (35%, 70% and 85%) are shown in Figure 1.

Several features are readily apparent. First, the mass limit of the ions (~800 amu) suggests that the ring size may be as high as 10 rings. Second, the sulfur containing species are processed fairly efficiently. Heteroatomic sulfur in benzothiophenes (dbe=6) is particularly well removed by processing as almost no db=6 is observable in the most processed sample (compare Fig. 1A and Fig. 1C). Likewise those sulfur species of db=9, of which dibenzothiophenes are a possibility, are processed efficiently. However, the larger S-containing species in the range of 12-35 db are unchanged or even concentrated under these processing conditions. Based on the mass spectral exact mass formulae, the following structures are suggested:



The  $y$  in the structures means that multiple substitution is observed in the mass spectrum and the  $x$  means that the chain length can vary.

The number of isomers of each species is quite high and mass spectrometry alone cannot discern them. A two-sulfur structure consistent with mass spectral data is also shown.

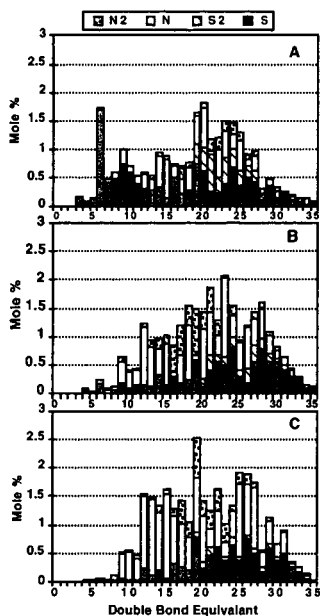


Figure 1. Sulfur and Nitrogen containing species for asphaltenes from processed resids. A, asphaltenes from 30% conversion; B, 70% conversion; C, 85% conversion.

Figure 2 shows the mass spectra for the three conversion levels of processing for a double-bond equivalent of 9. Although this class of molecules make up a small fraction of the total of the samples (~ 0.15 mole %), we can follow the processing on a molecular class basis. The asphaltenes in the 35% processed resid sample (Fig. 2A) show species from  $m/z$  300 to 700, in addition to fragment and molecular species in the 180 to 250 range. These high mass species correspond to dibenzothiophenic structures with either multiple alkyl substitutions or chain lengths or combinations of both.

Chromatographic separation or tandem mass spectrometry could identify which combinations of chain length and substitution are present. Further processing as shown in Fig. 2 tends to shorten the chain length of the molecule leaving only few short chains on the molecule. We suggest that the most resistant molecules are probably those that are substituted at positions adjacent to the sulfur.

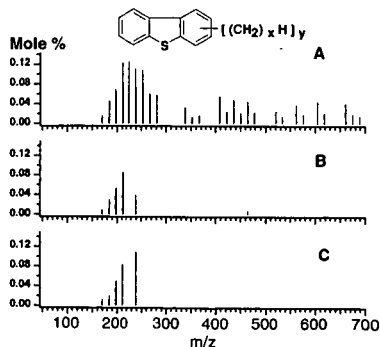
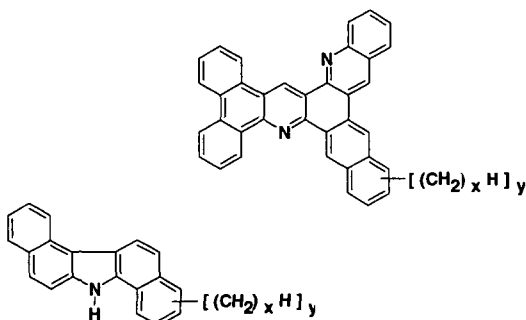


Figure 2. The mass distribution of sulfur-containing, double-bond equivalent=9 species. A, asphaltenes from 35% conversion; B, 70%; C, 85% conversion.

Nitrogen-containing species show a similar pattern to the sulfur pattern, but with one notable exception. The nitrogen species are much more resistant to processing. They are essentially untouched and perhaps concentrated. A similar pattern of multiple-alkyl substitution is found. Multiple nitrogens in rings systems are also present. Examples of suggested structures for the nitrogen-containing species follow:



Such structures differ markedly from those published elsewhere. Others have shown more condensed structures. Our data do not support more condensed ring systems, but rather more open ring systems.

Hydrocarbon molecules are also found in the processed asphaltenes. As processing severity increases the mass intensity shifts to larger aromatic rings systems. The existence of hydrocarbons, while surprising may be explained in terms of the separation and aggregation properties of the asphaltenes. Asphaltenes are separated only by precipitation. As the asphaltenes precipitate they form aggregates which may trap hydrocarbons. In addition, if the asphaltenes aggregate under processing conditions, some of the aggregate may escape aromatic treating, leaving sources of large aromatic hydrocarbons in the asphaltene fraction.

### Conclusion

Our mass spectral studies of asphaltenes from hydrotreated resid have shown them to be highly aromatic and present as extended open ring systems as high as 11 rings. Sulfur containing species with ring sizes smaller than 5 rings are effectively processed, while larger ring systems are more resistant to processing. The heteroatom containing species in the asphaltenes are multisubstituted with alkyl chains. Processing tends to remove the alkyl chains and/or reduce their, leaving the core ring system.

### Acknowledgment

This work was performed under the auspices of the U. S. Department of Energy, under contract number W-31-109-ENG-38. This work was supported by a CRADA agreement between Amoco Corporation and Argonne National Laboratory under the U. S. Department of Energy-Bartlesville, Fossil Energy Project.

### References

1. Dickie, J. P. and Yen, T. F.; *Anal. Chem.*, **39**, 1847 (1967).
2. Speight, D. A.; Wernick, D. L.; Gould, K. A.; Overfield, R. E.; Rao, B. M. L.; and Savage, D. W.; *Rev. Inst. Fr. Pet.*, **40**, 51 (1985).
3. Moschopedis, S. E.; Fryer, J. F.; Speight, J. G.; *Fuel*, **55**, 227 (1976).
4. Speight, J. G.; *Amer. Chem. Soc., Div. Fuel Chem., Prepr.*, **25**, 155 (1980).
5. Pfeiffer, J. P.; Saal, R. N.; *J. Phys. Chem.*, **44**, 139 (1940).
6. Ray, B. R.; Witherspoon, P. A.; Grim, R. E.; *J. Phys. Chem.*, **61**, 1296 (1957).
7. Dwiggins, C. W. Jr.; *J. Phys. Chem.*, **69**, 3500, (1964).
8. Dickie, J. P.; Yen, T. F.; *Anal. Chem.*, **39**, 1847 (1967).
9. Overfield, R. E.; Sheu, E. Y.; Sinha, S. K.; Liang, K. S.; *Fuel Sci. Technol. Int.*, **7**, 611 (1989).
10. Sheu, E. Y.; DeTar, M. M.; Storm, D. A.; DeCanio, S. J.; *Fuel*, **71**, 299 (1989).
11. Anderson, S. I.; Birdi, K. S.; *J. Colloid Interface Sci.*, **142**, 496 (1991).
12. Thiagarajan, P.; Hunt, J. E.; Winans, R. E.; Anderson, K. E.; and Miller, J. T.; *Energy and Fuel*, **9**, 829 (1995).
13. Storm, D. A.; Sheu, E. Y.; DeTar, M. M.; *Fuel*, **72**, 977 (1993).
14. Espinat, D.; Ravey, J. C.; Guille, V.; Lambard, J. Zemb, T.; Cotton, J. P.; *J. De Phys. IV*, **3**, 181 (1993).

# TLC-FID IN QUANTITATIVE HYDROCARBON GROUP TYPE ANALYSIS (HGTA) OF ASPHALTENES AND OTHER HEAVY FOSSIL FUELS

Vicente L. Cebolla, Jesús Vela, Luis Membrado, and Ana C. Ferrando

Departamento de Procesos Químicos

Instituto de Carboquímica, CSIC

P.O. Box 589, 50080 Zaragoza, Spain

Keywords: TLC-FID, petroleum asphaltenes and other heavy fossil fuels, TLC-scanning UV

## INTRODUCTION

Thin-Layer Chromatography with Flame Ionization Detection (TLC-FID) is mostly used in fossil fuel chemistry for quantitative hydrocarbon group type analysis (HGTA) (1-3). From an instrumental point of view, polemics about quantitative results have been reported with regard to different detector designs and sample application systems (4). Moreover, inadequate sample selection with respect to volatility properties have caused some confusing results. In order to validate TLC-FID, results should be confirmed using other techniques. On the other hand, quantitation in Chromatography is performed by previous calibration because evolution of responses of different compounds with sample load depends on each detector. Calibration becomes difficult because of the complexity of fossil fuels. Thus, the most used absolute calibration method is time-consuming, and new rapid and quantitative procedures should be developed.

In this work, instrumental performances of a modern TLC-FID system were first tested on pure *n*-alkanes and several polycyclic aromatic compounds (PACs). Detector linearity was evaluated in function of sample load and scan speed, as well as absolute response factors of the standards. Thus, criteria were developed for accurate application of TLC-FID with regard to sample volatility. Likewise, measurements of chromarod and flame temperatures permit the evaluation of whether an evaporation of compounds outside the H<sub>2</sub> flame can take place. In a second step of the research, TLC-FID results *from absolute calibration* (comparing Medium Pressure Liquid Chromatography MPLC, and other alternative methods for fraction isolation: preparative TLC and Solid Phase Extraction, SPE), and *from an alternative, fast calibration* procedure (based on a variety of the internal normalization method, VINM) were compared for different fossil fuels including asphaltenes. Repeatability and ranges for VINM application for each type of sample are reported. Finally, results from TLC-FID were validated using TLC-dual wavelength scanning UV.

## EXPERIMENTAL

**Standards and products analyzed.** Several *n*-alkanes, polycyclic aromatic hydrocarbons (PAHs, from 3 to 6 rings), heteronuclear-PACs, and hydroxy-PACs were used as standards (Across Chimica, Belgium). The studied fossil fuels were: a heavy oil (450°C+ vacuum Brent residue); several petroleum asphaltenes: a raw one (RAsph), their derived *n*-butylated asphaltene (BuAsph) and that treated with C<sub>6</sub>H<sub>5</sub>-CH<sub>2</sub> radical (PhCH<sub>2</sub>Asph), using reductive alkylation; a coal-derived product, obtained from hydroliquefaction of a Spanish coal at 430°C for 30 min, under a N<sub>2</sub>/H<sub>2</sub> atmosphere, without solvent, and subsequently extracted with DCM.

**TLC-FID runs.** Procedure details have been reported in previous works (2, 5). Sample application (0.2-2 μL) was carried out using a 3202/IS-02 automatic sample spotter, (SES, Germany). Chromatographic separation was performed on S-III chromarods (silicagel, 5 μm particle size, 60 Å pore diameter). Quantification of peaks was carried out using an Iatron Mark 5 TLC-FID apparatus (Iatron Labs). Acquisition and treatment of data were carried out as reported elsewhere (5). Samples were solubilized in DCM (15 mg mL<sup>-1</sup>). Chromarods were developed after sample application, using two different elution sequences:

- 1) in the case of the studied heavy oil, *n*-hexane (38 min), toluene (3 min), DCM/methanol 95/5 v/v (30 sec). The following peaks were separated (± 0.01 min): saturates (retention time, r.t.: 0.18 min), aromatics (r.t.: 0.29 min), polars (r.t.: 0.39 min), and uneluted (r.t.: 0.47 min), and
- 2) in the case of the studied coal hydroliquefaction product and petroleum asphaltenes, *n*-hexane (38 min), toluene (20 min), and DCM/methanol 95/5 v/v (5 min). Peaks from sequence 2 were (± 0.01 min): saturates (r.t.: 0.14 min), aromatics (r.t.: 0.24 min), polars (r.t.: 0.36 min), and uneluted (r.t.: 0.48 min).

The amounts (μg) of the studied PACs reported throughout the text correspond to the mass effectively injected. The response of a given standard is defined as its corresponding area counts (μV s<sup>-1</sup>), *A*. The response factor of each standard is defined as *A* per mass unit, *m* (μg). Only absolute response factors are used throughout this paper.

**Flame and chromarod temperature measurements.** These were made using a data acquisition system consisting of two thermocouples (Thermocoax, type K, 0.5 mm diameter, for the flame, and Thermocoax, type S, 1 mm diameter, for the chromarods), a Fluke Hydra 2620 multichannel data

acquisition unit, and an HP-95 handheld computer to receive and store the data. A serial RS-232-C connection was used to send the data from the data acquisition unit to the computer.

**Isolation of fractions for absolute calibration.** Preparative TLC was carried out on a silicagel aluminium sheet (20 x 20 cm, 0.2 mm layer). Aromatic fraction was developed using toluene, and polar fraction using DCM/methanol 95/5, v/v. Solid Phase Extraction (SPE) was carried out on silicagel. Samples were preadsorbed in CaCO<sub>3</sub> using DCM. This solvent was further removed at 50°C under vacuum (15 mbar). The powder was placed on the top of a polypropylene syringe which contained 5 g of silicagel. Subsequently, 20 ml of toluene, and 40 ml of DCM were consecutively eluted through.

Purity of fractions were monitored using either TLC-FID or TLC-scanning UV.

**TLC-scanning UV.** Silicagel plates were also used. Eluants used for development were the same as in the case of TLC-FID. UV scanning was carried out using a Shimadzu CS9301PC densitometer, and its corresponding data acquisition and treatment software. Wavelength working range was 200-700 nm. Linear scanning in reflectance mode was used.

## RESULTS AND DISCUSSION

### TLC-FID instrumental performances with regard to quantitation

Given that one of the aims of this work was to evaluate the performance of TLC-FID technique without interferences related to the inherent volatility of the solutes, rubrene (5,6,11,12-tetraphenyl-naphthacene) was chosen to allow an in-depth study of FID linearity, apart from the above-mentioned standards. Rubrene has a high Molecular Weight (MW= 532) and low volatility (i.e., 6.373\*10<sup>-6</sup> mm Hg at 171°C). Repeatability of absolute response factors (as RSD %, which was measured at 5 µg of sample load) was, in general, lower than 5 for all the standards, regardless of their volatilities.

Linearity was evaluated with regard to sample load and scan speed (Tables 1 and 2, Figure 1). Responses of standards were adequately fitted to logarithmic regressions in the whole mass range studied (0.1-12 µg) because deviations from linearity were found at sample loads lower than 1 µg. For the lowest mass range (< 1 µg), repeatabilities were worse (11% RSD) than those obtained at higher sample loads (< 5% RSD), and this should be considered when a quantitative analysis is to be done. For sample loads higher than 1 µg, linear regressions provide adequate regression coefficients and intercepts, with low relative errors.

A particular possibility of TLC-FID is to vary the scan speed. Fitting of responses at different scan speed showed the same pattern that those previously mentioned. As scan speed decreases: i) FID response also decreases, and ii) a greater deviation from the linearity for sample loads lower than 1 µg was found. Similar response factors were obtained using 30 or 35 s scan<sup>-1</sup>. In the case of the slowest speeds (i.e., 60 s scan<sup>-1</sup>), smaller, although linear, signals were obtained. This could be used in order to inject higher sample loads in cases in which a given mass saturates the detector.

Preliminary results, obtained from the measurements of chromarod and flame temperatures seems to indicate that volatilization of rubrene prior to combustion should not take place.

Criteria about sample volatility limits for TLC-FID analysis can be developed using pure standards. Although the absolute response factors vary for different petroleum fractions (saturates, aromatics, and polars), and for different homologous series of pure compounds, they are reasonably uniform for alkanes longer than C<sub>26</sub>, and aromatics with 4 or more rings. In the case of alkanes studied, the response factor of *n*-C<sub>24</sub> (0.1 mm Hg vapor pressure at 150°C) was 0.718, and that of a saturate fraction (C<sub>32+</sub>) from a heavy oil was 0.801. *n*-Alkanes shorter than C<sub>24</sub> (vapor pressures higher than 0.3 mm Hg at 150°C) showed significantly lower response factors. In the case of PAHs, response factors were near to unity for four or more-ringed standards, and for an aromatic fraction obtained from a heavy oil.

### Calibration methods and quantitative TLC-FID results

The absolute calibration method is usually performed when a quantitative HGTA of fossil fuels is required. Thus, fractions isolated from the fossil fuel itself are used as external standards for each peak. MPLC is mostly used for fraction isolation. This is time-consuming although it is convenient when further characterization of peaks must be done using other external techniques. As well, linearity of responses for each standard is not a necessary condition for the application of this method.

A fast calibration method based on a variety of the internal normalization (VINM) was applied to several coal and petroleum products, in previous works (2, 5, 6). Its basis is as follows: if the FID response of each peak in a given sample versus the mass of whole sample can be linearized (with forced zero intercept), then this calibration procedure is theoretically equivalent to the absolute calibration. Therefore, area percentage from the chromatogram is equal to mass percentage in the problem sample within the linear zone. VINM is a quantitative, quality-control oriented procedure and no useful when preparative amounts of fractions are required. However, the tedious pre-fractionation required in the absolute calibration of fossil fuels is substituted for a rapid TLC-FID screening of several different masses of the whole sample, which can be done in 1 or 2 Iatroscan runs

(2-3 hours, and milliliters of eluants).

The agreement between both calibration methods for the studied asphaltenes is presented in Table 3. In this case, the isolation of fractions for absolute calibration was carried out using preparative TLC, instead of MPLC. Table 4 also shows an agreement between both calibration procedures for another type of sample: a coal hydroliquefaction product. Likewise, the use of either preparative TLC or SPE for absolute calibration gave similar results. These techniques save time when compared to that of MPLC (hours vs days) when absolute calibration is necessary.

#### **Quantitative application of VINM for asphaltenes and other fossil fuels**

Table 5 shows the linearity ranges from VINM in the case of the studied asphaltenes, and, for comparative purposes, in the case of a heavy oil. In this table, repeatability is expressed as a mass range semi-interval ( $\pm$  wt.%) for 95 % confidence level. A previous work (2) demonstrated that mass range semi-intervals for each peak from a heavy oil were narrower than those tolerated using the ASTM D2007. Furthermore, TLC-FID experiments are fast, and ASTM D2007 consists of a time-consuming preparative MPLC with a previous removal of asphaltenes.

Linearity from VINM is usually accomplished in restricted mass intervals, and the analyst has to choose the range of application depending on the obtained regression coefficients. Likewise, the range of sample load for application of this procedure depends on the sample nature. It must be stressed that this linearity interval refers to the whole sample and not to the mass of each fraction. Although regression coefficients are not good for the studied asphaltenes, experimental results confirmed the equivalence between the two calibration procedures.

After performing the calibration and choosing the best linearity zone for each sample according to the regression coefficients, sufficient amount of sample must be applied onto the system in order to obtain quantitative results. Sample loads must be sufficiently high for the mass of each peak (taking into account its proportion) to be greater than 1  $\mu$ g. As previously reported, masses lower than 1  $\mu$ g present RSD % of nearly 11, and deviations from the linearity.

All the studied products present ranges more than sufficient for quantitative purposes in view of the small sample loads usually spotted using this technique.

#### **Validation of TLC-FID results using an external technique (TLC-scanning UV)**

As previously mentioned, TLC-FID is limited, to some extent, by volatility considerations. Although results from absolute calibration and VINM are in accordance, this would not necessarily imply that they are the true results. For this reason, results from TLC-FID were validated in this work using HPTLC-scanning UV with absolute calibration using the corresponding fractions as external standards. These were fractionated from the products using preparative TLC. Volatility is not a limitation for quantitative application of spectroscopic techniques, such as UV.

As samples used for validation must not contain alkanes, which do not absorb in the wavelength range used, one product without alkanes was chosen for validation test. Table 4 presents the agreement between the results from TLC-FID using both absolute calibration and VINM, and from HPTLC-scanning UV.

#### **ACKNOWLEDGEMENTS**

The authors are grateful to Spanish DGICYT (Project PB93-0100) and ECSC (European Steel & Coal Community, Project 7220-EC/765) for their financial support, and also Dr. R. Bacaud (CNRS, Villeurbanne) for fruitful discussions, and Dr. R. Gruber for providing asphaltene samples.

#### **REFERENCES**

1. Selucky, M.L. *Anal. Chem.* **1983**, *55*, 141.
2. Vela, J.; Cebolla, V.L.; Membrado, L.; Andrés, J.M. *J. Chromatogr. Sci.* **1995**, *33*, 417.
3. Barman, B.N. *J. Chromatogr. Sci.* **1996**, *34*, 219.
4. Shanta, N.C. *J. Chromatogr.* **1992**, *624*, 21.
5. Cebolla, V.L.; Vela, J.; Membrado, L.; Ferrando, A.C. *Chromatographia* **1996**, *42*, 295.
6. Cebolla, V.L.; Membrado, L.; Vela, J.; Bacaud, R.; Rouleau, L. *Energy & Fuels* **1995**, *9*, 901.

**Table 1.-** Linearity of FID detector with sample load.

Sample	Linear Regression	Logarithmic regression
n-Tetracosane	A = 663.4 * m - 19.26 (r = 0.9977)	Log A = 0.9363 * Log m + 2.849 (r = 0.9973)
Phenanthrene	A = 677.5 * m - 228.7 (r = 0.9977)	Log A = 1.105 * Log m + 2.719 (r = 0.9990)
Benzo-a-pyrene	A = 975.9 * m - 111.5 (r = 0.9986)	Log A = 1.0747 * Log m + 2.927 (r = 0.9973)
Fluorene	A = 573.0 * m - 102.0 (r = 0.9934)	Log A = 1.144 * Log m + 2.629 (r = 0.9972)
Fluoranthene	A = 886.0 * m - 390.5 (r = 0.9977)	Log A = 1.148 * Log m + 2.796 (r = 0.9991)
Pyrene	A = 761.2 * m + 205.4 (r = 0.9905)	Log A = 1.0747 * Log m + 2.895 (r = 0.9925)
Rubrene	A = 1074 * m - 53.79 (r = 0.9990)	Log A = 1.084 * Log m + 2.976 (r = 0.9979)

**Table 2.-** Error percentage<sup>1</sup> of linear and logarithmic regression in the case of rubrene for different scan speeds and sample loads.

Linear Regression					
Scan Speed (s scan <sup>-1</sup> )					
Masa	25	30	35	50	60
0.6	-4.69	-11.93	-36.94	-61.55	-48.67
1.8	1.32	0.48	-0.72	-3.7	-5.2
2.9	0.14	-2.95	-4.65	-1.54	-7.36
4.1	5.22	1.64	3.23	-3.45	-7.73
5.3	-3.59	-0.06	-0.32	3.02	-6.54
Reg. Coef <sup>2</sup>	0.9979	0.9996	0.9984	0.9974	0.9923
Logarithmic Regression					
0.6	-0.16	-0.45	-1.23	-2.08	-2.08
1.8	0.16	0.8	1.88	2.8	3.07
2.9	-0.06	-0.13	0.05	0.86	0.44
4.1	0.55	0.1	0.12	-0.81	-1.17
5.3	-0.51	-0.35	-0.96	-1.09	-0.6
Reg. Coef	0.9993	0.9993	0.9967	0.9942	0.9946

<sup>1</sup> Error % between the corresponding experimental value and that predicted from the corresponding fitting curve.

<sup>2</sup> Regression coefficient obtained in the mass range 0 - 5.3 µg.

**Table 3.-** Absolute and VINM calibration of petroleum asphaltens using TLC-FID.

	Calibration method	Aromatics	Polars	Uneluted
<b>RA<sub>sp</sub></b>	VINM	1.5	30.7	67.8
	Absolute Calibration	1.8	33.8	64.4
<b>BuAs<sub>ph</sub></b>	VINM	11.5	69.9	18.9
	Absolute Calibration	13.0	68.0	19.1
<b>PhCH<sub>2</sub>As<sub>ph</sub></b>	VINM	23.4	64.7	11.9
	Absolute Calibration	20.9	67.1	12.0

**Table 4.-** Validation of results for a coal hydroliquefaction product.

		TLC-FID		
Absolute calibration	Isolation method	Aromatics	Polars	Uneluted
	TLC	29.0	62.6	8.4
	SPE	30.6	60.4	9.0
VINM		31.2	60.7	8.1
		TLC-UVVIS		
Absolute Calibration	Isolation method	Aromatics	Polars	Uneluted
	TLC	30.1	62.2	7.7

**Table 5.-** Linearity intervals and repeatability from VINM (TLC-FID) of the studied asphaltenes and a heavy oil.

Sample	Average of Area percentage (n=5)	95 % Confidence interval (wt%±)	Usable linearity Interval (µg)	Regression Coefficient (r)
<b>RA<sub>sp</sub></b>				
Saturates	---	---		---
Aromatics	1.5	1	1 - 11.2 µg	0.8837
Polars	30.7	0.8		0.9935
Uneluted	67.8	1.2		0.9968
<b>BuAsph</b>				
Saturates	---	---		---
Aromatics	11.5	2.3	1 - 14.2 µg	0.9298
Polars	69.9	1.8		0.9824
Uneluted	18.9	1.2		0.9954
<b>PhCH<sub>2</sub>Asph</b>				
Saturates	---	---		---
Aromatics	23.4	2.6	1 - 9.1 µg	0.9161
Polars	64.7	4.7		0.9993
Uneluted	11.9	2.9		0.9748
<b>Heavy Oil</b>				
Saturates	33.2	0.63		0.9994
Aromatics	57.4	0.74	1 - 20.6 µg	0.9931
Polars	12.9	0.19		0.9758
Uneluted	0.5	0.09		0.9697

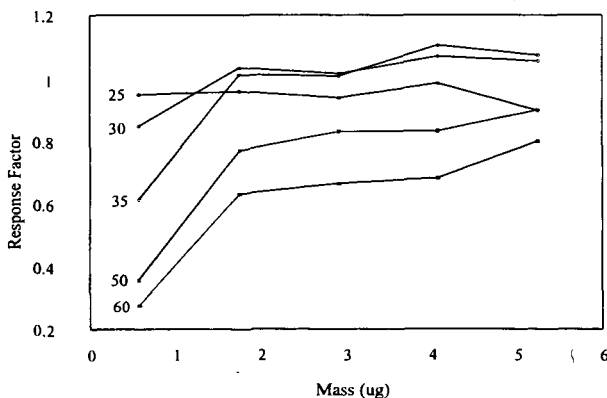


**Figure 1.-**Response factors (A/m) in the case of rubrene for different scan speeds and sample loads.

# ASPHALENE SELF-ASSOCIATION - A COMPUTER SIMULATION STUDY

P.S. Subramanian and Eric Y. Sheu  
Fuels and Lubricants Technology Department,  
Texaco Inc., P.O. Box 509, Beacon, NY 12508

Key Words: Asphaltene, Molecular dynamic simulation, Aggregation

## INTRODUCTION

Self-association of asphaltenes and the resulting colloidal-like particle structure, polydispersity, and other physical properties have drawn great scientific attention in the past decade. They are relevant to oil production, transportation and refining. One key question is yet to be answered is the energies that are involved in the self-association process. From thermodynamical point of view, the conventional micellization process is mainly driven by the hydrophilicity-hydrophobicity imbalance. Other energies, such as packing, double layer interacting, etc., often play minor roles only. The self-association of asphaltenes appear to be very different. Asphaltenes are defined based on the solubility. Their molecular structures are not unique. The molecules often consist of various degree of polynuclear aromaticity. No distinctive hydrophilic and hydrophobic portions in the molecules can be identified. Additionally, asphaltenes only self-associate in the organic environment with low permittivities. This amounts to saying that the hydrophilicity-hydrophobicity imbalance should not be the governing factor, and that the interactions between molecules are short ranged. In the past decade, experiments, theories and computer simulations have been reported on this issue [1-3]. Good progress has been made, however, the fundamental understanding of the self-association mechanism is still lacking.

In this study, we performed a molecular dynamic simulation to study the self-association process. The aim is to identify the governing energy in this association process. One difficulty in this simulation is to mimic the real systems. It requires in-depth knowledge of the system. In our case, we chose the Ratawi vacuum residue (VR) derived asphaltene as the system. Ratawi VR asphaltene have been well studied in our laboratory. Data regarding its elemental analysis, chemical properties, and physical properties are readily available for us to construct the molecular structures, distribution and the initial configuration of the simulation.

## COMPUTATIONAL DETAIL

The simulation consists of 64 asphaltene molecules ranging in size from 3 rings to 11 rings structure. The ring distribution was based on the Gaussian distribution with the peak at the 7 ring structure [4]. Two systems were modeled. One at a concentration of 0.015 wt % (below the critical micelle concentration, CMC) and the other at 5 wt % (above CMC). The size of the cell was chosen to represent the system at the desired densities. With the above concentrations, the corresponding cell dimensions are 743.0 Å and 108.8 Å respectively. The molecular dynamic (MD) simulation was performed using CERIU2 [5]. The molecules were placed randomly in the cell using the amorphous cell module in the Cerius2 package to define the initial configuration. This was followed by energy minimization. During the energy minimization process, the Dreiding force field was used to account for

both inter- and intra-molecular interactions except the electrostatic ones [6]. A dielectric continuum of 3.5 was used to model the solvent. Dreiding Force field was not used to compute the electrostatic interactions because it calculates the monopole-monopole interactions only. One can still use the Dreiding Force field for computing electrostatic interactions, provided the monopole-monopole interactions calculated can represent a good estimate of the intramolecular dipole moments. We tested several computation packages on this issue. We used charge equilibration, MOPAC6 [7], and CHARMM [8] to compute the electrostatic interactions, then evaluate the dipole moments estimated and compared with the experimental values. Single ring and double ring molecules as the test cases. MOPAC6 was found to be far superior to the other two packages as far as dipole moment representation is concerned. We thus calculated the electrostatic charges using MOPAC6. The MD simulation was lasted for 250 picoseconds (ps) where the system energy starts to be stable.

## RESULTS AND CONCLUSION

Figure 1 and 2 show the simulation results for the 0.015 wt % and 5 wt % respectively. As one can see, the 0.015 wt % does not show significant self-association. Dimers do exist, but no large aggregates are observed. On the other hand, the 5 wt % shows aggregates of various sizes. F (see figure 2) is a small aggregate while B, C, D and E are large ones of different shapes. Their common feature is the short range stacking phenomenon. The maximum stack observed contains approximately 7 asphaltene molecules. This was predicted by Yen based on the solid phase compounds. In solvent, these stacks appears to preserve. However, the stacks are loose and somewhat irregular (see D in figure 2). Aggregate B is a good example. It consists of many short range stacks linked loosely together. As a result the aggregate does not show well defined cylindrical shape. It appears more like a sphere. This is also true for aggregate A, C and E. Aggregate D is more like a cylinder although the stacking direction changes after 7th molecules. We also found a monomer in this simulation (unmarked molecule in Figure 2) which may or may not be significant. In order to evaluate the importance of the dipole-dipole interaction, we used the charges obtained from charge equilibration method to compute the electrostatic contribution, which under estimate the dipole moments for simple molecules. The result shows a collapse of the molecules into a single huge aggregate. Since experimental data from small angle neutron scattering (SANS) and small angle X-ray scattering (SAXS) [1,9] have indicated the average size of the aggregates to be approximately 30  $\text{\AA}$ , the occurrence of a collapse single aggregate phase should not be the case. This indicates, at least indirectly, that dipole-dipole interaction must play an important role in controlling the self-association process.

From the nucleation process point of view a system can undergo nucleation only when the dipole moment of the system is zero. If a non-zero dipole moment is introduced, the nucleation process would be terminated at a some point and the nucleation process would not be complete. This seems to be the case in asphaltene self-association process. The self-association of asphaltenes can be viewed as a nucleation process. It is initiated when concentration exceeds the CMC [9]. At the beginning stage, the molecules stack to form cylindrical-like aggregates. This process is then terminated partially due to non-homogeneous molecular structures which makes the

stacks loose, but mainly due to non-zero dipole-dipole interactions. As a result, the phase separation occurs only at microscopic length scale, similar to a micelle solution, though the energies involved are completely different. The dipole moments can arise from the structural arrangement of the atoms in the molecules and the heteroatoms (Nitrogen, sulfur, nickel, vanadium etc.) that are commonly found in asphaltenes.

[1] For reference, see *Asphaltene and Asphalts, Developments in Petroleum Sciences*, edited by T. F. Yen and G. V. Ghilingarian, Elsevier, Amsterdam, (1994).

[2] J. G. Speight, *The Chemistry and Technology of Petroleum*, 2nd ed.; Marcel Dekker, New York, (1991).

[3] I. Kowalewski, M. Vandenbroucke, A. Y. Huc, M. J. Taylor, and J. L. Faulon, *Energy & Fuels*, 10, 97 (1996).

[4] C. Y. Ralston, S. Mitra-Kirtley and O. C. Mullins, *Energy & Fuels*, 10, 623 (1996).

[5] Cerius2 is marketed by BIOSYM/Molecular Simulations Inc., 9685 Scarnton Road, San Diego, California, USA.

[6] Mayo, S. L.; Olafson, B. D.; Goddard III, W. A. *J. Phys. Chem.* 1990, 94, 8897.

[7] MOPAC6 is a semi empirical package available from Quantum Chemistry Program Exchange (QCPE), Indiana University.

[8] CHARMM (Brooks, B. R.; Bruccoleri, R. E; Olafson, B. D.; States, D. J. ; Swaminathan, S.; Karplus, M., *J. Comput. Chem.*, 1983, 4, 187).

[9] E. Y. Sheu, *J. Phys. : Condens. Matter* 8, A125 (1996).



Figure 1. MD simulation for 0.015 wt % Ratawi Aphaltene in solvent.



Figure 2. MD simulation for 5.0 wt % Ratawi Aphaltene in solvent.

## HYDROCARBON BACKBONE OF POLAR FRACTIONS

R. A. Wolny<sup>(\*)</sup>, L. A. Green, J. G. Bendoraitis, L. B. Alemany<sup>(\*\*)</sup>  
Mobil Technology Company, Paulsboro, NJ 08066

<sup>(\*)</sup> Current address: Saudi Aramco, LR&DC, Dhahran 31311, Kingdom of Saudi Arabia

<sup>(\*\*)</sup> Current address: Rice University, Department of Chemistry, Houston TX 77005

Keywords: Polar, Hydrocarbon, Structure

### SUMMARY

The quantity and composition of polar materials present in heavy process streams have an impact on the strategy used for their processing and the resulting yield structure. A chemical procedure was employed to deoxygenate the polar material which were later separated into aliphatic, aromatic, and residual polar fractions. These fractions were analyzed to determine their compositions. It was found that the deoxygenated hydrocarbon backbones of aliphatic and aromatic fractions derived from polar material are very similar in composition to the corresponding fractions separated from the original feed. However, structures that undergo easier oxidation are concentrated in the derived backbone fractions. The main components of the residual polar fractions obtained after deoxygenation are basic nitrogen compounds, polyheteroatom molecules, aliphatic sulfones, etc., that are resistant towards chemical processing.

### INTRODUCTION

Most of the results published in the open literature concentrate on the analysis of polar compounds with a single functional group. For example, the carboxylic acids have been widely investigated (1-4). Seifert identified carboxylic acids associated with a variety of aliphatic, aromatic and heterocyclic (S- and N-containing) backbones (1,2). Cason isolated and identified isoprenoidal acids from California crudes (3,4). Sulfoxides represent another large group of polar compounds particularly in crudes that have a high total sulfur content. Strausz et al. described a method for converting polar sulfoxide molecules to low polarity sulfides that can later be separated from the polar matrix by chromatographic techniques (5). Basic nitrogen compounds represent the majority of nitrogen in the polar fraction (6-11). However, neutral and acidic nitrogen compounds with polar functional groups (e.g. carbonyl) are also present in the polar fraction (1). In this work we attempted to analyze the polar fraction of a crude and account for all polar functionalities and the hydrocarbon backbone with which these polar functionalities are associated.

### EXPERIMENTAL PART

#### Reagents.

All solvents used were reagent or HPLC grade. Silica gel, mesh 100-200, Grade 923, supplied by Davison Chemical, was activated in an oven at 500°F for 24 hours. Alumina was purchased from ICN Biochemicals.

#### Instruments.

The GC/MS chromatograms were collected on Finnigan TSQ-70 and Kratos MS 80 instruments. The gas chromatographs on both instruments were equipped with J&W Scientific DB-5 columns, 30 m, 0.25 mm ID, 0.25  $\mu$ m film thickness. Kratos MS 80 instrument was used to acquire field ionization mass spectra.

Simultaneous chromatograms (GC/FID, GC/FPD-sulfur) were recorded on a Varian 3400 instrument, using a J&W DB-5 column, 30 m, 0.53 mm ID, 1.5  $\mu$ m film thickness.

The FTIR spectra were recorded on a Mattson Sirius 100 instrument.

#### PROCEDURE DESCRIPTION.

The polar fraction, 2.5 weight percent of the original material, was separated from the 550°F-1050°F fraction of a crude on silica gel. A sequence of hexane and toluene were used to elute aliphatic and aromatic fractions. The polar fraction was eluted with 50/50 vol% methanol/toluene and 50/50 vol% methylene chloride/acetone. The chemical procedure used to deoxygenate the polar fraction is similar to that described by Seifert et. al. (2). The sequence of LAH reduction, tosylation, and LAH reduction on the polar fraction gave an overall yield of 90.1 weight percent. Mass loss is expected due to removal of functional groups; however, some loss may be due to sample handling.

The chemically processed material was separated on silica gel into an aliphatic (Aliphatic Backbone), an aromatic (Aromatic Backbone), and a residual polar (Polar Backbone) fractions. The Aliphatic Backbone fraction was eluted with hexane, the Aromatic Backbone fraction was eluted with toluene, and the Polar Backbone fraction was eluted with 50/50 vol% methanol/toluene and 50/50 vol% methylene chloride/acetone. The aromatic fraction derived from the chemically processed polar fraction was further separated on alumina impregnated with 4% of silver nitrate (12). Aromatic Backbone Fraction-1 (ABF-1) and Aromatic Backbone Fraction-2 (ABF-2) were eluted with toluene, Aromatic Backbone Fraction-3 (ABF-3) with 5/95 vol% methanol/toluene, and Backbone Fraction-4 (ABF-4) with 30/70 vol% methanol/toluene and 50/50 vol% methanol/toluene. Residual silver nitrate was removed from ABF-3 and ABF-4 by extraction with distilled water.

#### RESULTS AND DISCUSSION

Selective reactions, outlined in the Experimental Part, remove reactive functional groups responsible for the polarity of molecules present in the polar fraction. Lithium aluminum hydride (LAH) reduces functional groups such as carboxylic acids, aldehydes, esters, ketones, acid anhydrides, and amides to hydroxyl groups (13). Then, hydroxyl groups are converted to the corresponding tosylates, which are later reduced with LAH to the hydrocarbon backbone (2).

The polar functional group can be associated with an aliphatic or an aromatic structure or attached to an aliphatic fragment of the aromatic molecule (naphthenic ring or alkyl side chain of an aromatic molecule). Also, a polar functional group can be attached to structures bearing a heteroatom.

Sulfoxides, another large group of polar compounds, are reduced to sulfides during the first reduction with LAH (5). Sulfides remain intact during tosylation and the second reduction with LAH.

Sulfones of thiophenes are easily reduced with LAH; however, sulfones of sulfides are difficult to convert back to sulfides. Reduction reactions of various functional groups with LAH are summarized by Hudlicky (13).

#### Infra-red

Infrared spectroscopy was used to quantify the contribution of various functional groups using average absorption coefficients reported in the literature (14,15). The result of this quantitative analysis is as follows: carboxylic acids and other carbonyls 8 weight percent; sulfoxides 47 weight percent; phenols and alcohols 12 weight percent.

#### Separations

The Aliphatic Backbone fraction represents only 4.5 weight percent of the chemically

processed material (Table 1). Table 2 shows the group type distribution of the Aliphatic Backbone fraction and of the aliphatic fraction separated from the original crude fraction by a similar method. The Aliphatic Backbone derived from the polar fraction has a strong paraffinic character and absence of sulfur compounds (Figure 1). It is apparent from these data that the character of both aliphatic materials is similar.

The chemically processed polar fraction contains 65.2 weight percent as the Aromatic Backbone fraction (Table 1). This material contained high concentration of sulfides (Figure 1). This group of compounds was further separated from the rest of the aromatic matrix, as outlined in the Experimental Part.

The first two fractions eluted with toluene, were relatively small. The weight percent distributions and elemental analyses for ABF-1 and ABF-2 are shown in Table 1. ABF-1 and ABF-2 consist of aromatic hydrocarbons, thiophenic compounds, and nitrogen compounds having a pyrrolic ring that originated from the polar precursors. Pyrrolic nitrogen compounds are significant contributors to ABF-1 and ABF-2. Calculated from the average molecular weight and nitrogen content, determined by field ionization mass spectrometry (FIMS), ABF-1 and ABF-2 contain 43 and 63 weight percent of pyrrolic compounds, respectively. Mononaphthenocarbazole is the most abundant in this series.

Thiophenic compounds were identified in ABF-1 and ABF-2. Thiophenes could have originated from the corresponding sulfones or from thiophenes that had functional groups (R) reducible with LAH to hydroxyl. Based on sulfur measurements and average molecular weight from FIMS, ABF-1 and ABF-2 contain 6 and 11 weight percent of thiophenes, respectively.

ABF-3 and ABF-4 derived from the polar fraction constitute a majority of the total Aromatic Backbone fraction (Table 1). These two fractions contain predominantly sulfides and a small amount of pyrroles. Sulfides present in the ABF-3 and ABF-4 are very similar to the sulfides found in the corresponding fractions separated, by similar method, from the original crude fraction. Based on molecular weight from FIMS and nitrogen content, ABF-3 and ABF-4 contain 16 and 5 weight percent of pyrrolic nitrogen, respectively.

It is remarkable that the chemically processed polar fraction contains 46.6 weight percent of material defined as sulfides. This high concentration of sulfides is in very good agreement with 47 weight percent of sulfoxides quantified by IR. Pyrroles, aromatic hydrocarbons, and thiophenic compounds represent 12.9, 0.9, and 4.8 weight percent of the total polar fraction, respectively.

The residual polar material, Polar Backbone, represents 29.3 weight percent of the chemically processed polar fraction and contains 3.26 weight percent sulfur and 2.57 weight percent nitrogen (Table 1 and Figure 1). The Polar Backbone has substantial aromatic character (32% aromatic C and 9% aromatic H). Sulfur present in this fraction may exist in structures with polyheteroatoms, or sulfones and sulfoxides that are resistant towards reduction with LAH. Nitrogen is present mainly in the form of basic nitrogen compounds or polyheteroatom structures (8-13). Limited information was obtained from these data due to the high complexity of this fraction. More research is needed to characterize basic nitrogen and polyheteroatom compounds.

## CONCLUSIONS

Removal of oxygen-bearing functional groups from the polar fraction produced non-aromatic and aromatic hydrocarbons (including those containing heteroatoms), and sulfides.

The low level of Aliphatic Backbone in the polar fraction results from minimal

biodegradation of the original crude. Sulfoxides represent almost half of the polar fraction. It is suspected that sulfoxides may result from the oxidation during sample handling; however, indigenous sulfoxides can not be excluded. Pyrrolic nitrogen molecules that bear a polar group represent a significant part of the polar fraction. Pyrrolic molecules that contain naphthenic ring(s) are concentrated in the polar fraction.

Polar fraction bear a striking resemblance to non-polar material of the original crude. That is, polar fraction differ in functionality, but its backbone is consistent with compounds from the non-polar material. We believe that this observation can be applied to the polar materials from other petroleum feeds and products.

#### ACKNOWLEDGMENTS

Authors thank C.A. Simpson for acquiring the IR spectra, D.L. Parisi for assistance in acquiring FIMS spectra and P.P. Durand for his help in processing FIMS data.

#### REFERENCES

1. Seifert, W. K., *Progress in the Chemistry of Organic Natural Products*, **1972**, Vol. 32, pp. 1-49. Look also for citations in this publication.
2. Seifert, W. K., Teeter, R. M., Howells, W. G., Cantow, M. J., *Analytical Chemistry*, **1969**, Vol. 41, pp. 1638-1647.
3. Cason, J., Graham, D. W., *Tetrahedron*, **1965**, Vol. 21, pp. 471-483.
4. Cason, J., Khodair, A.I., *J. Org. Chem.*, **1967**, Vol. 32, pp. 3430-3439.
5. Payzant, J. D., Montgomery, D. S., Strausz, O. P., *Tetrahedron Letters*, **1983**, Vol. 24, No. 7, pp. 651-654.
6. Ignatiadis, I., Schmitter, J. M., Arpino, P. J., *Journal of Chromatography*, **1985**, Vol. 324, pp. 87-111.
7. Schmitter, J. M., Ignatiadis, I., Arpino, P. J., *Geochimica et Cosmochimica Acta*, **1983**, Vol. 47, pp. 1975-1984.
8. Schmitter, J. M., Collin, H., Excoffier, J. L., Arpino, P. J., *Analytical Chemistry*, **1982**, Vol. 54, pp. 769-772.
9. Shive, B., Roberts, S. M., Mahan, R. I., Bailey, J. R., *J. Am. Chem. Soc.*, **1942**, Vol. 64, pp. 909-912.
10. Schenck, L. M., Bailey, R. J., *J. Am. Chem. Soc.*, **1941**, Vol. 63, pp. 1364-1365 and 1365-1367.
11. Bakel, A. J., Philp, R. P., *Organic Geochemistry*, **1990**, Vol. 16, No. 1-3, pp. 353-367.
12. Felsky, G., US Patent 4,430,205.
13. *Reductions in Organic Chemistry*, M. Hudlicky, published by Ellis Horwood Limited, 1984.
14. Petersen, J.C., *Transportation Research Record* 1096.
15. Petersen, J.C., *Analytical Chemistry*, **1975**, Vol. 47, No. 1, pp. 112-117.

TABLE 1. MASS, SULFUR, AND NITROGEN BALANCES FOR CHEMICALLY PROCESSED POLAR FRACTION.

	Mass Wt %	Sulfur in Sample wt% (*)	Sulfur in Total Polars wt%	Nitrogen in Sample wt% (**)	Nitrogen in Total Polars wt%
Starting Material (***)	100	3.97	3.97	1.28	1.28
Aliphatic Backbone	4.5	0.00	0.00	0.00	0.00
Aromatic Backbone	65.2	NM	3.09	NM	0.69
Total			(****)		
Aromatic Backbone Fraction 1 (ABF-1)	7.6	0.59	0.05	1.96	0.15
Aromatic Backbone Fraction 2 (ABF-2)	3.8	1.03	0.07	2.99	0.11
Aromatic Backbone Fraction 3 (ABF-3)	39.3	4.96	1.95	0.99	0.39
Aromatic Backbone Fraction 4 (ABF-4)	14.5	7.04	1.02	0.32	0.04
Polar Backbone	29.3	3.26	0.95	2.57	0.75
Balance	99.0		4.04		1.44

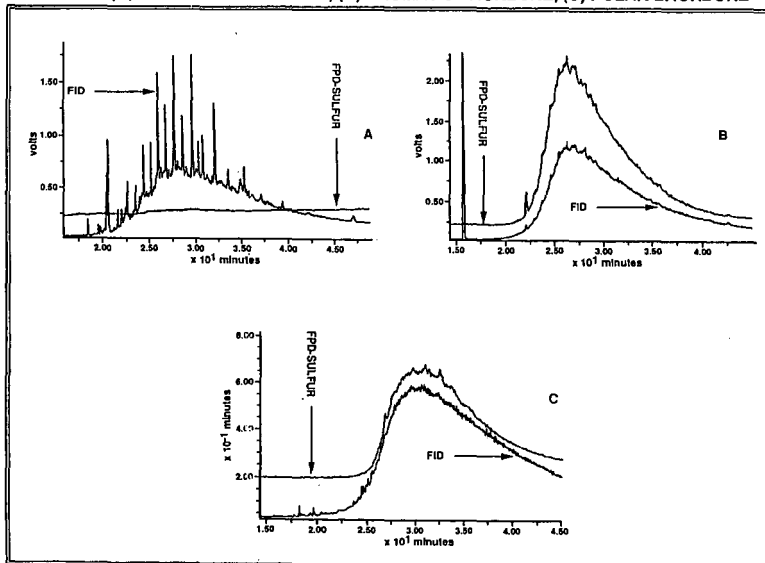
(\*) Measured by D 1552  
 (\*\*) Estimated from FIMS

(\*\*\*) Charge to LC column after reactions  
 (\*\*\*\*) Sum of ABF-1, ABF-2, ABF-3, and ABF-4

TABLE 2. GROUP TYPE DISTRIBUTION IN ALIPHATIC BACKBONE FRACTION AND ALIPHATIC FRACTION SEPARATED FROM ORIGINAL MATERIAL.

Compounds	Aliphatic Backbones	Aliphatics-original material
Paraffins	46.5	50.5
Mononaphthenes	17.4	15.1
Dinaphthenes	11.3	13.0
Trinaphthenes	6.6	7.6
Tetranaphthenes	7.9	6.3
Pentanaphthenes	7.8	5.0
Hexanaphthenes	0.0	1.7

FIGURE 1. GC TRACES (FID & FPD-SULFUR) FOR CHEMICALLY PROCESSED POLAR FRACTION. (A) ALIPHATIC BACKBONE, (B) AROMATIC BACKBONE, (C) POLAR BACKBONE



## THE NATURE OF RESINS AND ASPHALTENES

Felix Unger, Institute of Petroleum Chemistry,  
Russian Academy of Sciences, Siberian Division,  
3 Akademicheskyy Ave., Tomsk, 634055, Russia

Keywords: asphaltene, resin, paramagnetic resonance, electrolytic dissociation

In 1944, Zavoisky [1] discovered electronic paramagnetic resonance (EPR), a tool for direct detection of unpaired electrons in molecular systems, which gave rise to a new avalanche of studies on radical reactions and paramagnetic phenomena, and in 1957 Garif'yanov and Kozyrev [2] found unpaired electrons in petroleum-like systems and thus proved the presence of free radicals in these systems. Thereafter, the role of radicals in petroleum-like systems was discussed rather [for example 3, 4]. However, it could not be evaluated adequately because of the absence of any methodical basis for correct determination of the number of unpaired electrons in the petroleum-like system under investigation. Thus, Flinn et al. [5], based on the published estimate for the paramagnetism of asphaltenes  $10^{18}$  spins/g, arrived at the conclusion that for every 100 molecules there is one free radical. This estimate gave rise to the wide-spread opinion that the role of paramagnetics in asphaltene structures is insignificant. However, once a method for rigorous quantitative estimation of the fraction of paramagnetic molecules has been developed [6], the paramagnetism of petroleum-like systems is estimated as  $10^{15}$  (for gasolines),  $10^{17}$  -  $10^{18}$  (for oils),  $10^{19}$  -  $10^{21}$  (for asphaltenes), and  $10^{20}$  -  $10^{22}$  spins/g (for carbenes-carboids, some cokes, and insoluble carbonic materials). Even for some petroleum (e.g., Archinskoe petroleum of Tomsk region), the paramagnetism is abnormally high  $10^{21}$  spins/g, which is a direct indication of the specific role played by paramagnetic molecules in petroleum-like systems.

Other evaluations of asphaltenic-resin systems are the following.

a. Those systems have no FREE IONS, namely the dissociation of molecules by action of the kinetic energy movement does not go through the heterolytic mechanism, but through the homolytic mechanism.

b. The experiments show that organic acids and bases concentrate not in asphaltenes, but into maltenes with minimum of their contents into the resins (carbon radioactive label), namely the oil systems (with the asphaltenes and resins) contain minimum (or zero) amount of polar molecules. This is confirmed by the value of dielectric constant of oil systems, which is close to benzene.

c. The quantummechanic calculations show, that the potential energy of attraction between the molecules of compounds in oil systems maybe the following:

1. Ion-ion. ATTRACTION. However, the ions are absent.

2. Radical+radical. ATTRACTION. Radical existing in the system and those formed as a result of homolytic reactions, recombine or transition into the singlet state or associate depending on volume restrictions.

3. Radical+charge-polarised molecules. ACIDATION. Therefore organic acids and bases concentrate into the maltene parts, but only minimum of their amount is found in resins.

4. Radical+charge and spin-neutral molecules. ACIDATION. Therefore, the radicals are rejected from the saturated carbon hydrogenates and other compounds with large dielectric constants. Under industrial conditions this process is entitled "DEASPHALTISATION".

5. Radicals+spin-polarised molecules. ATTRACTION. On this basis colloid particles of oil systems are built with radicals in the centre of a particle, surrounded with aromatic and heteroorganic molecules.

6. Spin-polarised+spin-polarised molecules. The DIFFERENT DEGREE OF THE ENERGIES of ATTRACTION. On this basis circumference stratum of colloid particles are built.

7. Spin-polarised+spin-neutral molecules. LITTLE, TILL TO ZERO ENERGIES OF ATTRACTION. On this basis the combination of the circumference stratum of colloid particles with encircling medium is built (with the paraffin-naphthene saturate hydrocarbons, in particular with maltenes in oil systems). A universal theoretical picture the common equation of potential energies may be given for interaction between molecules:

$$V = K_0 e^{-kr} + K_1 r^{-1} + K_2 r^{-2} + K_3 r^{-3} + K_4 r^{-4} + K_5 r^{-5} + K_6 r^{-6} \quad (1)$$

where: k, K - coefficients, e - natural logarithm, r - distance between the interaction centres. The coefficient "K" may be either "+" or "-". The latter denotes attraction.

The Zero member beats reflects exchangeable interactions between radicals, the first - charge between ions, the second - between ions and charge-polarised molecules, the third - between radicales and spin-polarised molecules, the fourth and fifth - between breakwater molecules with different degree of spin and charge polarization (multipole members), and the sixth - between neutral molecules (Van-der-Vaals member).

d. From quantum mechanics considerations the virial-theorem for compound-mixtures must be followed:

$$\langle T \rangle = 1/2n \langle V \rangle \quad (2),$$

where "n" is the number of grade on the variable "r" in formula (1) with allowance for the sign of grade, and "T" - kinetic energy. The brackets  $\langle \rangle$  denote the middle meanings of energies.

Out of formula follows the strict necessity of coordination of acts for the alteration of potential energies of attraction-acidation between molecules and of the kinetic energies of their movement with distance between interacting molecules in physical-chemical processes, into this numerals homolytise, heating, cooling, in chemical reactions and etc.

e. Molecules with unpaired spin will not give NMR-spectra (coordinately with quantum mechanics considerations). The oil samples with high number of spins give weak (low intensity) NMR-spectra, what is attributed from the few contribution of diamagnetic molecules (some of asphaltenes will not give NMR-spectra at all), that is well coordinated with theory. The theoretical and experimental results allow estimation and understanding of the nature of resins and asphaltenes in oil dispersed systems.

The contradictory explanation of the colloidal structures of petroleum systems in terms of charge phenomena (electrolytic dissociation, donor-acceptor interactions, hydrogen charge-dipole interactions, etc.) called for both a new theoretical base and a complex comprehensive interpretation of the information obtained by chemical and instrumental methods for analyzing petroleum, petroleum products, resins, asphaltenes, and other petroleum-like materials, which has been reduced to several basic principles that are in excellent agreement with all available experimental data. These principles are discussed here.

There is no doubt that, the process of excitation and/or homolytic dissociation is a process actually identifiable with the use of instruments intended for physical investigations; second, from theoretical (quantum mechanical) reasonings it should be stated that this process fails not to occur, and, third, this process does occur on introduction of a solvent into a disperse petroleum system and/or its heating. Therefore, the statement is valid that the study of the interaction of the molecules of the solvent introduced with the molecules of associative combinations under varied conditions may be of primary importance for the technology of raw petroleum transformation in the near future.

In view of the importance of these results for the chemistry of solvents, in particular, petroleum, we present below the fundamental aspects of the chemistry of petroleum-like systems inherent in any non-water solutions and in some low-polarity water solutions.

1. Asphaltenes (being a type of powder) are not involved as components in petroleum (petroleum-like) systems, but they are formed in the process of action of a solvent on the system as associative combination of molecules having a higher density than the solution and separated from the system to form a precipitate.
2. The reason for the appearance and existence of asphaltenes is the presence of paramagnetic molecules that have positive potential energies of interaction with respect to saturated hydrocarbon molecules (repulsion) or other type molecules with sigma-bound atoms.
3. The possibility for the prolonged existence of paramagnetic molecules in the medium of diamagnetic molecules is provided by a shell preventing radicals from recombination. The shell is formed by the same principles as the solvate shells in electrolytic solutions, but the forces therewith are quantum (exchange) rather than charge in nature. Low-activity radicals may have thin shells or none at all. Active radicals will have heavy shells; in their nearest vicinity there will be accumulated molecules with a high energy of interaction with paramagnetic molecules, and the interaction energy will decrease in going to the periphery of the associative combination of molecules. If the associate density is comparable with the medium density, no separation will

occur, and the paramagnetic molecule will be able to exist for an infinitely long time in the center of the associate and will not recombine notwithstanding its high activity.

4. Diamagnetic molecules which go into the triplet state or dissociate into radicals under minor energy actions (e.g., on the order of a dozen of kilojoules per mole) are the basic molecules consisting resins. Owing to the kinetic energy of molecules, paramagnetic molecules are always present in small amounts in resins, that appear and due in equilibrium homolysis-recombination reactions. The range of energies required for a molecule to go into the triplet state or to dissociate into radicals may be rather large in view of the variety of molecules; so asphaltenes (precipitates) may occur from resins under the action of saturated solvents at elevated temperatures in substantial amounts. However, the molecules of such precipitates, when the original low-temperature conditions are reverted, recombine to transform again into the resin diamagnetic molecules.

5. Resins are a potential source for asphaltenes owing to the high probability of homolytic processes; asphaltenes are a potential source for resins owing to the molecules present in the nearest surrounding of radicals in associative combinations.

6. The properties of resins and asphaltenes are fundamentally independent of the atomic composition but depends on the energy of the interaction of atoms in molecules and molecules with one another. The varied element composition of resins and asphaltenes from various raw materials imparts them some specific properties, but the principles of appearance and existence of these associative combinations are almost independent of the composition.

7. All properties of resins and asphaltenes are well explained by the quantum mechanical principles of the formation of homopolar interactions and fail to be explained in terms of heteropolar interactions.

8. The properties of asphaltenes and resins are inherent in all types of viscous and liquid homopolar systems (petroleums, tars, homopolar schistose resins, homopolar carbonic hydrogenation products, etc.) and have an universal nature.

9. The properties of homolytes and the regularities of the formation of associative combination in them dictate some rules for the application of instrumental techniques whose violation may result in artifacts.

-Spectral characteristics (intensities of peaks and their positions on the frequency or angle axis) should be calculated (measured) with respect to quantitative references.

-The references should not be introduced they may change (sometimes substantially) the system properties. For solid systems no changes of this type were noticed, with the exception of asphaltenes being concentrates of paramagnetic molecules with variable paramagnetism.

-To obtain the spectral characteristic of a material, it is necessary to use a complete referenced spectrum. If a partial spectrum is used, even with referencing it is impossible to estimate the contribution of a given parameter into the properties in total. If this contribution is small and this has been overlooked, an artifact is unavoidable.

10. The paramagnetic nature of disperse homolytes, the peculiarities of the physical chemistry of the prohibited singlet-triplet and triplet-singlet transitions (diamagnetic-to-paramagnetic and reverse transitions of molecules) in petroleum-like systems, as well as, the quantum mechanical prohibitions for the filling of phase spaces by bosons, fermions, and paulions offer the possibility to predict certain types of chemical interactions in such systems.

-The presence of molecules with a high degree of spin polarization and with unpaired electrons is responsible for the amphoteric nature of the properties of petroleum-like systems. Thus, the compounds precipitated on acid impregnates behave like the compounds precipitated on base impregnates. In a detailed analysis it is generally revealed that these are the same compounds which are precipitated in a way inherent in the precipitation of the high-polarity molecules whose high polarity is due to the readiness of forced charge polarization. Note that for this type of compounds both the ionization potential and the electron affinity are low.

-In petroleum-like liquid mixtures, molecules with pronounced charge polarization or electrolytic dissociative ions are practically absent. All electrophoretic and electrical conductance phenomena in these systems are the consequence of the field-assisted charge polarization of various spin-polarized molecules and radicals. Therefore, both the cathode and the anode masses strongly vary qualitatively and quantitatively with electric field to the extent that the direction of

precipitation is changed which requires significant potentials, some orders of magnitude higher than those required for electrolytic dissociation.

-All reactions with petroleum-like media are homolytic in nature, and the touch of heterogeneity in them is conditioned by the pronounced charge properties of specially used electrolytic reagents. However, the propositions of the ionic mechanism are often not justified even for ferric chloride, sulfuric acid, and the like. A study of catalytic reactions should also be performed with due account of the regularities revealed.

11. As leads for further research, besides pending studies of already raised problems, it is noteworthy to develop adequate quantum mechanical and physicochemical models to describe:

- the DPS states;
- homolytic processes and the possibility of affecting their passage by fields;
- the thermolytic reactions in the existing chemical works;
- the catalytic reactions in the existing and predicted chemical works;
- the mechanism of action of additives for stabilization, inhibition, inflammation, quenching, ignition, etc;
- the DPS compounds showing the properties of radicals, biradicals, and spin-polarized particles with high and low degrees of spin polarization and the places of these compounds in the DPS.

12. The most important line of studies, going far beyond petroleum chemistry, is research in the field of theory of liquids. It is for the first time since the impressive studies on electrolytic dissociation performed by Arrhenius that we may say that homolytic dissociation has equally attracted the attention of researchers and the possibility has appeared to develop a unified theory of dissociation based on the available and future achievements in quantum mechanics with the goal to gain an understanding of the structure of liquid systems of any origin.

In conclusion, we present several figures illustrating some experimental results to confirm the above fundamental inferences on the paramagnetic nature of the dispersions in petroleum-like systems.

#### References

- [1] E.K. Zavoisky, *J. Phys.* (1945) v.9, N 3.
- [2] I.S. Garif'yanov and B.M. Kozyrev, *Zh. Eksper. Teor. Fiz.* (1956) v.30, N.2 p.255.
- [3] E.C. Tynan and T.F. Yen, *Fuel*, (1969) v.48, n.2, p.191.
- [4] T.F. Yen, J.C. Erdman, and A.J. Saraceno, *Ann. Chem.*, (1962) v.34, n.6, p.694.
- [5] R.A. Flinn et al., *Petrol. Refiner*, (1955) v.40, n.4, p.139.
- [6] F.G.Unger, L.N.Andreeva. *Fundamental aspects of the oil chemistry. Nature of the resins and asphaltenes.* Novosibirsk, Nauka, Siberian Publishing Firm RAN (1995).